Paramagnetic tools for the structural analysis of high molecular weight proteins

Dissertation for the award of the degree
"Doctor rerum naturalium"
of the Georg-August-Universität Göttingen

within the doctoral program
Biomolecules: Structure - Function - Dynamics
of the Georg-August University School of Science (GAUSS)

Submitted by
Aldo Román Camacho Zarco
From Mexico City, Mexico

Göttingen, 2014

Thesis committee:

Supervisor: Prof. Dr. Markus Zweckstetter
Department of NMR-based Structural Biology,
Max Planck Institute for Biophysical Chemistry, Göttingen

Prof. Dr. Ralph Kehlenbach
Department of Biochemistry
Georg-August-Universität, Göttingen

Prof. Dr. Marina Bennati
Electro Spin Resonance Spectroscopy Group,
Max Planck Institute for Biophysical Chemistry, Göttingen

Members of the Examination Board:

Prof. Dr. Markus Zweckstetter
Department of NMR-based Structural Biology,
Max Planck Institute for Biophysical Chemistry, Göttingen

Prof. Dr. Marina Bennati
Electro Spin Resonance Spectroscopy Group,
Max Planck Institute for Biophysical Chemistry, Göttingen

Prof. Dr. Ralph Kehlenbach
Department of Biochemistry, Georg-August-Universität, Göttingen

Dr. Claudia Höbartner
Department of Chemistry, Georg-August-Universität, Göttingen

Dr. Wolfgang Wintermeyer
Physical Biochemistry Department,
Max Planck Institute for Biophysical Chemistry, Göttingen.

Prof. Dr. Christian Griesinger
NMR-based structural Department,
Max Planck Institute for Biophysical Chemistry, Göttingen.

Date of oral examination:

19/January/2015

Affidavit

I hereby declare that this dissertation has been written independently and with no other sources and aids than quoted.

…………………………………

Aldo Román Camacho Zarco

Göttingen, 2014

Abstract

Paramagnetic effects provide important structural and dynamic information of biomolecules. However, the attachment of lanthanides through small chelating organic molecules to proteins (the most common way to obtain paramagnetic effects) requires single cysteine mutants, optimization of the tagging reaction and previous knowledge of the three-dimensional structure of the target to select proper attachment sites. In this work was developed a new method that relieves most of these disadvantages: the lanthanide is not directly attached to the target protein, but instead to a "reporter" protein that binds and transmits paramagnetic information to the target protein.

In this thesis is shown that the attachment of a lanthanide in different locations on the surface of the reporter protein PDZ allows measuring residual dipolar couplings and pseudo contact shifts from several independent molecular alignments on any target. This is shown for ubiquitin and the maltose binding protein. The fusion of a 7-residue PDZ recognition peptide to the C-terminus of the target proteins is the only necessary modification to obtain the paramagnetic restraints. Therefore, this method allows recording a large amount of paramagnetic information from orientationally independent molecular alignments in proteins. Moreover, it is not necessary to have previous knowledge of the three-dimensional structure of the targets.

To my family

Acknowledgements

It is my pleasure to express my most sincere thanks to all the people that made this thesis possible:

- I am very grateful to Prof. Dr. Markus Zweckstetter, for his guidance and the amazing opportunity that has been to work in this project.

- Thanks a lot to the members of my thesis committee, Prof. Dr. Marina Bennati and Prof. Dr. Ralph Kehlenbach, for their useful discussions.

- Thanks a lot to Prof. Dr. Griesinger. I feel very grateful and proud for having the opportunity to be part of NMR-2.

- I would like to express my gratitude to Dr. Francesca Munari, who introduced me to the acquisition and analysis of NMR data.

- My sincere thanks to Dr. Stefan Becker and Melanie Wegstroth. It would be very difficult to imagine this thesis without their support.

- I feel very lucky for the amazing people that have been around me at NMR-2, like Luis, Fran, Martin, Yao, Hessam, Hari, Sheng-Qi, Ragav, JP, Elias, Frederik, Rakhi, Guowei, Piotr, Javier, Yunior, Saskia, Timo, Filippo, the twins, JP, Hannes, Mitch, Supriya, Gerhard, Petra, Davood, Dirk, Karin, and all the NMR-II people.

- Thanks a lot to Almudena Ponce Salvatierra, for her encouragement through all this work.

An important part of the present thesis is based on the following publication:

Camacho-Zarco AR, Munari F, Wegstroth M, Liu MW, Ubbink M, Becker S, Zweckstetter M. Multiple Paramagnetic Effects Through a Tagged Reporter Protein. Angew Chem Int Ed Engl. 2014 Oct 7. doi: 10.1002/anie.201408615

Index

1. Introduction

1.1 Classic NMR restraints and the emergence of paramagnetic NMR.

NMR spectroscopy is the only technique besides X-ray crystallography that can solve the structure of a biomolecule at atomic resolution (Wüthrich K, 2003). Moreover, NMR can also study the dynamic behavior of biomolecules, which is intrinsically linked to their function (Boehr DD et al. 2006; Henzler-Wildman K et al. 2007). As a result, the scientific community is constantly challenging the limits of NMR spectroscopy in several ways. For example, there are efforts to increase the magnetic field of the spectrometers, to decrease the acquisition times through alternative sampling methods, to automate the assignment of signals for high-throughput protein structure elucidation, to develop methods to isotopically (^{2}H, ^{13}C, ^{15}N) enrich the proteins, etc (Billeter M et al. 2008).

Regarding the traditional distance and angular restraints obtained by NMR spectroscopy, these are often not enough to study large, multi domain or membrane proteins because they provide just "local" information. For instance, NOE-based distance restraints (based on the Nuclear Overhauser Effect) are short-range interactions that appear when two nuclei (usually hydrogen atoms) are closer than 6 Å (figure 1.1). As soon as the density of NOEs decreases and this network of short-range restraints is interrupted, the spatial correlation of remote regions of the protein becomes problematic, producing structures that have regions correctly determined but overly

incorrect (Kay LE et al. 1997). In the case of multi domain proteins, it is often difficult to record enough inter-domain NOEs and therefore to determine their location relative to each other (Hass M et al. 2014). Another complication for the measurement of NOE-based distance restraints comes from "perdeuteration" of proteins; a special method applied to big proteins in order to improve the sensitivity of many NMR experiments. This methodology decreases the amount of protons in the protein (they are replaced by deuterium), so a smaller amount of NOE-based restraints can be recorded. Actually, when a protein is fully perdeuterated, NOEs can just be recorded between exchangeable protons, mainly amide protons.
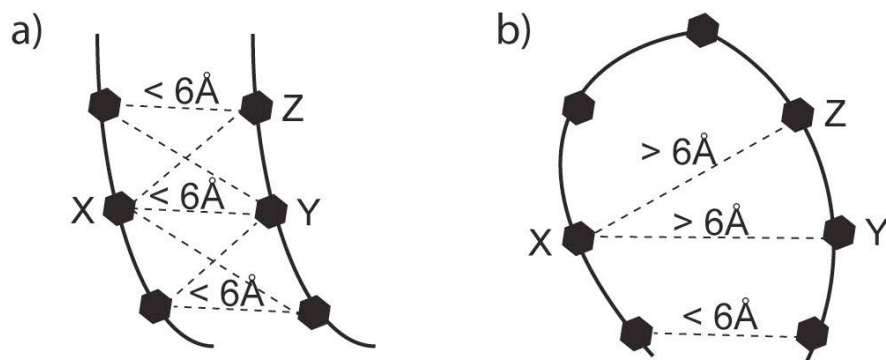
Figure 1.1 (a) Restraints produced by the nuclear Overhauser effect (NOE) can be measured easily for example in the core of a globular protein, but not (b) in long and extended structures like loops.

Concerning angular information, the measurement of scalar J couplings is the traditional way to acquire it by NMR spectroscopy. Scalar J couplings are through-bond interactions between spins. They are very important because the magnitude of the coupling (via three covalent bonds) depends directly on the dihedral angles. This information, as in the case of NOEs, comes just from neighboring atoms, so the information provided by J

couplings is also "local" structural information (O'Connell MR et al. 2009).

Because of the short-range nature of classic NMR restraints, in the last years paramagnetic NMR has attracted a lot of attention because it provides long-range distance and orientation restraints that can complement the traditional ones (Otting G. 2010). The three main paramagnetic effects are paramagnetic relaxation enhancement (PRE), residual dipolar couplings (RDC) and pseudocontact shifts (PCS). This type of NMR restraints can be observed just when an ion with unpaired electrons, like a lanthanide ion, is rigidly attached to a biomolecule. RDC for example, provide orientation information relative to a common axis system for all the inter-nuclear vectors of a molecule. Therefore, RDCs provide global information, something that distinguishes the paramagnetic effects from NOEs and J couplings.

In fact, there are already reports were paramagnetic restraints have been able to complement, or even substituted traditional restraints. For example, distance restraints derived from PRE have been used to determine the backbone of a barnase without the addition of any other restraint (Gaponenko V et al. 2000). PCS were enough to calculate the fold of the chaperone ERp29 (Yagi et al. 2013). RDC are normally used in refinement protocols nowadays, however they have been shown to be sufficient (together with chemical shifts) to calculate the structure for proteins up to 25 KDa through computational methods (Raman S et al. 2010). Paramagnetic NMR restraints can provide very valuable structural information, however the first requirement to obtain them is the rigid attachment of a lanthanide ion to

the target protein. In the present thesis is developed a strategy to obtain several datasets of paramagnetic restraints through a new method to attach a lanthanide to a target protein. Therefore, the traditional methods to attach a lanthanide will be review in the following section.

1.2 Strategies to introduce a lanthanide ion into a protein.

Historically paramagnetic centers were conceived as something undesired due to the signal broadening that they produce, so NMR spectroscopists used to invest time to remove them from their samples. However, the scientific community has realized the unique characteristics of the paramagnetic restraints, and has started to exploit this information since almost 20 years ago in protein structure determination. Paramagnetic effects were discovered a long time ago. PCSs produced by lanthanides were used in 1971 to obtain structural information of nucleotides (Barry CD et al. 1971) and RDCs were measured for the first time in a protein in 1995, when the group of James Prestegard measured them on Cyanometmyoglobin, a protein that has a paramagnetic iron in its heme group (Tolman JR et al, 1995).

The use of paramagnetic centers in the structure determination of proteins was stopped for several years among other reasons by the inability to attach the paramagnetic center to proteins in a rigid and site-specific fashion (Koehler J et al. 2011). The paramagnetic center must be attached rigidly to the target biomolecule; otherwise the molecular alignment that

leads to the observation of RDCs and PCS wouldn't be transmitted quantitatively. It is the main goal of this thesis to develop an innovative strategy to attach a lanthanide into a target protein to transmit paramagnetic effects. Therefore, it is important to review the main strategists to introduce a paramagnetic center rigidly (a lanthanide) into a target protein.

1.2.1 The case of metalloproteins.

Generally speaking, the sidechains of Asn, Thr, Ser, Gln, Glu, Asp; as well as the carbonyl groups of the backbone, are usually the chemical moieties that bind metal ions in metalloproteins. However, metalloproteins that naturally bind a paramagnetic center like a lanthanide are strange because they do not have any biological role in nature. As a consequence, it is necessary to replace the "natural occurring metal" (like Mg^{2+}, Ca^{2+} or Mn^{2+}) from the binding site for a lanthanide ion. It is rational to conjecture that this replacement will not perturb the structure of the protein, or at most the coordination sphere (Bertini I et al. 2005). It is important to mention that the magnetic properties of lanthanides are unaffected by changes in the coordination sphere, in contrast to other paramagnetic centers like Fe^{3+}. This replacement is possible in many cases because their ionic radius is similar; for instance the ionic radius of Mg^{2+} is 86 pm and the one of Tm^{3+} is 88 pm. In some cases this replacement is not possible due differences in the charge and coordination number, but this can be overcome by the introduction through mutagenesis of additional charged residues in the binding site

(Bertini I et al. 2003).
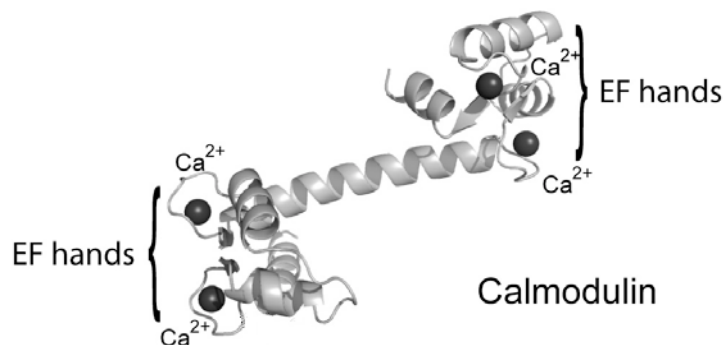
Figure 1.2 Calmodulin is a protein that naturally binds Ca^{2+}, but this ion can be replaced by lanthanide ions like Tb^{3+} (PDB: 1CLL).

An early example of this strategy came from the group of James Feeney (Biekofsky RR et al. 1999). In this work they partially replaced the diamagnetic Ca^{2+} in the protein Calmodulin by the paramagnetic Tb^{3+}. Calmodulin is a calcium biding protein that binds up to four Ca^{2+} ions, and is composed by two resembling domains connected by a flexible linker. Each domain has two calcium binding motifs called EF-hands, which explains why each domain can bind two Ca^{2+} ions (figure 1.2). The displacement of Ca^{2+} by Tb^{3+} produced big ^{15}N-^{1}H RDCs of up to 17 Hz and PCS were observed far away from the position of the lanthanide, even at 40 Å. An advantage of this strategy is that the big magnitude of the PCSs reduces the experimental error of the data; unfortunately it also complicates its analysis since re-assignment of the NMR signals is usually necessary for the same reason.

An interesting article from the laboratory of Ivano Bertini reported the replacement of all the lanthanides (except the radioactive Pm and isotropic Gd) in the metalloprotein Calbindin D_{9k} (Bertini I et al. 2001; Allegrozzi M et

al. 2000). It was shown that because of the different strength of their paramagnetic properties, different lanthanides are useful to provide restraints in different ranges from their position in the protein. For example, PCSs from Ce^{3+} were useful to refine the atomic position of atoms located from 5 to 15 Å from the paramagnetic center, Yb^{3+} from 9 to 25 Å and Dy^{3+} from 13 to 40 Å. It was also observed that the orientation of the alignment tensors induced by each lanthanide was basically the same one, confirming that all lanthanides bind a certain binding site with the same coordination geometry. This collinearity of the alignment tensors for different lanthanides in the same binding site has been observed in other metalloproteins (Pintacuda G et al. 2006).

A further disadvantage of this strategy is that many signals are commonly broadened beyond detection due to PRE because the paramagnetic center is very close in space to many residues. This tendency holds true specially whenever using a lanthanide with strong Curie relaxation like Dy^{3+} or Tb^{3+}. For example, in the case of Calbindin D_{9k}, it was possible to acquire 132 PCS for the weakly paramagnetic Sm^{3+}, but just 46 PCS were observed when Tb^{3+} was used due to signal disappearance (Allegrozzi M et al. 2000).

1.2.2 Fusion to lanthanide binding peptides or domains.

Other strategies are needed to introduce a paramagnetic center rigidly when a target protein doesn't have a natural binding site. Since there are peptides and domains in nature that bind lanthanides with high affinity, another strategy is to fuse them to the target protein to transfer their paramagnetic effects to the target (Allen KN et al. 2010). In the first attempts, the lanthanide binding peptides were fused to the N or C terminus of the target protein. In one of the first reports using this strategy, RDCs were observed (from -6 to 5 Hz at 750 MHz) in the membrane protein Vpu when an EF-hand motif (12 residues binding Dy^{3+}) was fused to its N-terminus (Ma C et al. 2000). Not only natural binding motifs like EF-hands and zinc fingers have been fused (Gaponenko V et al. 2000), but also artificial binding peptides obtained by combinatorial methods or designed. An advantage of artificial motifs is that smaller concentrations of lanthanide can be used due to their higher affinity (usually in the nm range), so the usual metal-induced precipitation of the samples is lower. Using an artificial binding peptide fused to the N-terminus of ubiquitin, the group of Harald Schwalbe reported RDCs in the range of -6.6 to 6.1 Hz for Dy^{3+} at 800 MHz (Wöhnert J et al. 2003).

A similar method to transfer an alignment from a lanthanide-binding motif to a target protein was reported by the group of P. Bayley (Feeney J et al. 2001). In this work, calmodulin loaded with four Tb^{3+} ions was used to produce a paramagnetic alignment, but it was not directly fused to the target protein (dihydrofolate reductase, DHFR). A peptide that is recognized with

high affinity by calmodulin was fused to the C-terminal of the target protein, with a linker of four flexible residues in between the target and the recognition sequence. This approach produced RDCs in the range of -7 to 4 Hz at 600 MHz, but when a longer flexible linker (14 residues) was added, no RDCs were observed. A relative advantage of this method is that PCSs were not excessively big, so it was not necessary to reassign the signals of the target, something that otherwise would be time consuming especially for a big proteins.

There have been clever approaches in order to increase the magnitude of the paramagnetic alignment (therefore the magnitude of RDCs and PCSs) transmitted by the lanthanide tag to the target. The group of Fuyuhiko Inagaki reported two to threefold bigger paramagnetic effects by using a binding peptide linked to the target protein in two points: an N-terminal fusion and a disulfide bridge to a cysteine residue close to this binding peptide (Saio T et al. 2009). In another interesting article, a lanthanide binding peptide was designed to bind two lanthanides at the same time. The theory says that the total strength of the alignment tensor would double if the axial components of both tensors were parallel; any deviation would reduce this increment. This "double" lanthanide binding peptide was fused to ubiquitin and produced bigger RDCs, in the range of -16 to 14 Hz at 800 MHz for Tm^{3+} (Martin LJ et al. 2007).
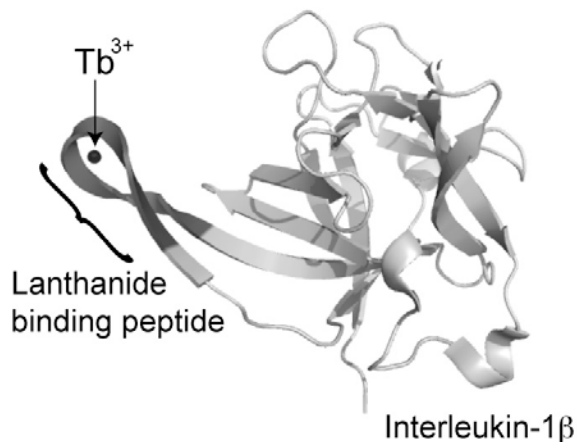
Figure 1.3 Lanthanide binding peptides can be inserted into loops among other positions in a protein (PDB: 3LTQ).

Lanthanide binding peptides have been fused not only to the N or C-terminal of proteins, but also to loops (figure 1.3). This strategy is interesting because a lanthanide binding peptide fused to a loop has two linking points to the target protein, something that rigidify the position of the lanthanide. In order to test this strategy, a lanthanide binding peptide was incorporated iteratively into the three loops of the protein interleukin-1β. This method produced also bigger RDCs compare to preceding reports in the range of -12 to 21 Hz when loaded with Tm^{3+} at 800 MHz (Barthelmes K et al. 2011). A disadvantage of this strategy is that it requires previous knowledge of the secondary structure of the target; otherwise it could be complicated to select a position to fuse the lanthanide binding peptide.

This strategy, which fuses lanthanide-binding peptides to a target is interesting since this kind of tags are usually rigid relative to the target because they are bulky, therefore steric hindrance plays a major role. There are two big drawbacks: the increase in the molecular weight of the target,

which is a factor that reduces the signal intensity on any molecule studied by NMR spectroscopy (Koehler J et al. 2011) and that it is not possible to generate multiple independent alignments with this strategy. One construct target/lanthanide-binding peptide will generate just one set of alignment tensors with the same orientation, even if different lanthanides are used (Wöhnert J et al. 2003). Therefore a different strategy has to be applied to obtain multiple independent alignment tensors for structure and dynamic analysis.

1.2.3 Attachment of small synthetic metal-chelating tags

The fusion of binding peptides restricts the location of the paramagnetic center to loops, the N or the C-terminal region of proteins. A powerful strategy that allows more freedom regarding the location of the lanthanide tag comes from chemical modification of the target by synthetic metal-chelating tags (Su XC et al. 2010). Synthetic tags use modified metal chelating agents such as ethylenediamine tetraacetic acid (EDTA) or tetraazacyclododecane tetraacetic acid (DOTA). The modifications consist on the addition of amine or cysteine-reactive groups, which are used to attach them on the surface of a target protein. There are two main points that have to be taken into account when designing a synthetic tag (Keizers PH et al. 2011). The first one is the potential formation of enantiomers upon metal binding, which produce diasteroisomers once attached to the chiral protein. This is important because the presence of diasteroisomers produces two sets

of signals in NMR spectra. It has been shown that a chiral tag can resolve this issue due to its preference for a determined chirality upon binding to a metal ion (Leonov A et al. 2005).

A second fundamental characteristic of any synthetic tag is the length of the linker, the atoms between the Cα of the protein and the coordination site of the lanthanide. It is important because long linkers are usually more flexible, resulting in barely measurable RDCs and PCSs. In addition, the flexibility makes more difficult to locate the position of the metal during the structure calculation process (Pintacuda G et al. 2004). An example of the impact of the linker's length comes from one of the first EDTA-derived synthetic tags (Dvoretsky A et al. 2002). This tag had a lot of mobility relative to the target protein (barnase), therefore the correlation between experimental and theoretical RDCs and PCSs was poor. Once the length of the linker was reduced, the quality of the paramagnetic data improved and now this cysteaminyl-EDTA tag (figure 1.4) is commercially available and widely used (Tang C et al. 2006).
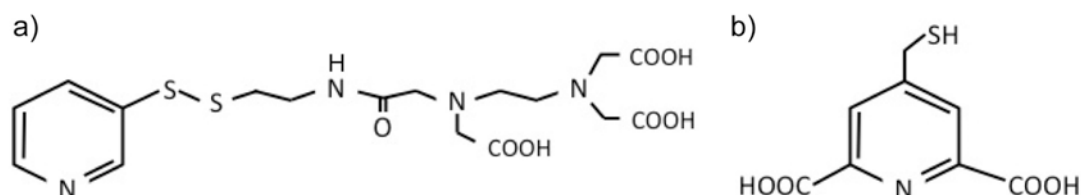
Figure 1.4 Some examples of small synthetic tags reported in the literature are (a) cysteaminyl-EDTA and (b) dipicolinic acid (DPA) tag.

Synthetic tags derived from DOTA are also very popular because they are bulkier, so the mobility relative to the target is even smaller compare to

EDTA-based tags (Häussinger D et al. 2009). Another strategy to increase the rigidity of a synthetic tag is to attach them to two sites (cysteine residues) in the target. This is the case of the "caged lanthanide complex" tag (CLaNP-5), which was attached to two cysteines that have their Cα atoms 8 Å apart in the protein pseudoazurin (Keizers PH et al. 2007). RDCs obtained with this tag loaded with Tm^{3+} are in the range of -18 to 25 Hz at 700 MHz (Keizers PH et al. 2008), on of the biggest reported in the literature.

It has been shown that alignment tensors with different orientations can be produced by attaching the same lanthanide tag on different sites on the surface of the protein (Gaponenko V et al. 2004; Su XC et al. 2006). However, this strategy requires several single or double cysteine mutants if the tag is mean to be attached to two sites. The design of these cysteine mutants could be time consuming and especially difficult for big proteins that contain several cysteine residues. In addition, some of the designed mutants could be unstable, or it might be difficult to tag them with high yields (Keizers PH et al. 2008). A method that could produce several independent paramagnetic datasets would be valuable in NMR spectroscopy and it is the objective of this thesis.

1.3 Paramagnetic centers

In order to observe paramagnetic effects in an NMR spectrum, a paramagnetic center has to be introduced into the target molecule. The paramagnetic effects have their origin in the unpaired electrons that are found in organic radicals and some metal ions, mainly lanthanides. The magnetic moment of unpaired electrons is 658 times bigger than the one of protons; this is the reason for the large effects that produce in NMR spectra. Chemically unreactive paramagnetic metal ions include Mn^{2+}, Fe^{2+}, Co^{2+}, Ni^{2+}, Cu^{2+} and the majority of the lanthanide ions (Koehler J et al. 2011). In the case of lanthanides, these electrons are in f orbitals, which are chemically unreactive inner orbitals. Concerning organic radicals, nitroxides are the most commonly used. It is important to mention that paramagnetic restraints are obtained after recording differences between an NMR spectrum of the target molecule in the presence of a paramagnetic center and a reference spectrum with a chemically similar but diamagnetic center, one that doesn't have unpaired electrons. As an example, for paramagnetic lanthanides the best diamagnetic references are Lutetium (Lu^{3+}) and Lanthanum (La^{3+}), which are also lanthanides and therefore have a similar ionic radius and coordination chemistry (Otting G et al. 2010).

There are two properties of a paramagnetic center that determine the effects that it produces on NMR spectra. The first one is the presence of magnetic susceptibility anisotropy (MSA), which yields an orientation-dependent interaction with the magnetic field. All paramagnetic centers

produce PRE, but if a certain center presents MSA, this anisotropic center will produce in addition PCS shifts on the NMR signals and induce an alignment of the molecule whenever located in a strong magnetic field that leads to the generation of RDC.

P. center	τ_e (10^{-12}s)	$\Delta\chi_{ax}$ (10^{-32} m^3)	$\Delta\chi_{rh}$ (10^{-32} m^3)	PCS (ppm)	RDC (Hz)
MTSL	100000.0	0.0		0.0	0.0
Gd^{3+}	10000.0	0.2		0.1	0.2
Cu^{2+}	3000.0	0.6		0.3	0.7
Tb^{3+}	0.2	42.1	11.2	22.3	46.7
Dy^{3+}	0.3	34.7	34.7	18.4	38.5
Tm^{3+}	0.4	-21.9	-20.1	-11.6	-24.3
Lu$^{3+,\ a}$	0.1	0.0		0.0	0.0

Table 1.1 Data taken from J. Koehler et al 2011. Parameters for calculations: r = 10 Å, f = 800 MHz, T = 298 K, θ = 0, 30 kDa protein with τ_r = 3.26 x 10^{-8}s using a viscosity η = 3.5 x 10^{-3} kg/sm and a density d = 1300 kg/m^3. [a]Diamagnetic.

The second property is the electronic relaxation time (τ_e) of the spin of the unpaired electron, which ranges from microseconds to picoseconds (table 1.1). Paramagnetic centers with slow electronic relaxation (μs to ns range) like Gd^{3+} and nitroxides produce stronger PRE. On the other hand, the paramagnetic centers with fast spin relaxation (ns to ps range), which includes all lanthanides but Gd^{3+} (like Dy^{3+}, Tb^{3+} and Tm^{3+}), produce smaller PRE. In general, paramagnetic centers that produce strong PRE present small MSA, therefore small (if any) RDC and PCS. Conversely, paramagnetic centers with high MSA generate big RDCs and PCSs, but smaller PRE (Keizers PH et al. 2011). These two groups of paramagnetic centers are different regarding their relaxation rates because different nuclear relaxation mechanisms dominate; this point will be addressed in the following section.

1.4 Paramagnetic relaxation enhancement (PRE)

The addition of a paramagnetic center produces an enhancement of the relaxation rates of close nuclear spins in a distance-dependent manner (figure 1.5); which can be exploited as structural distance restraints (Koehler J. et al 2011). PRE is observed in NMR spectra as a decrease in signal intensity (signal broadening) and in extreme cases the NMR signals can't be detected. In contrast to the classic NOE restraints, which are short-range (<6 Å), the effects produced by PRE can be observed up to 35 Å (electron-nucleus distance) depending on the paramagnetic center used (Iwahara J et al. 2003). Actually, the two types of restraints are clearly complementary because the signals that belong to nuclear spins that are too close to the paramagnetic center cannot be detected. PRE is produced mainly by one of two mechanisms depending on the paramagnetic center: Solomon relaxation is predominant in slowly relaxing centers (also called dipolar relaxation) and Curie relaxation is predominant in fast relaxing paramagnetic centers (table 1.1). In both mechanisms the magnitude of the PRE is directly proportional $1/r^6$ (the electron-nucleus distance) and on squared nuclear gyromagnetic ratio, which means that the relaxation for ^1H is 100 and 16 times more pronounced than the relaxation of ^{15}N and ^{13}C respectively (Clore GM et al. 2009).
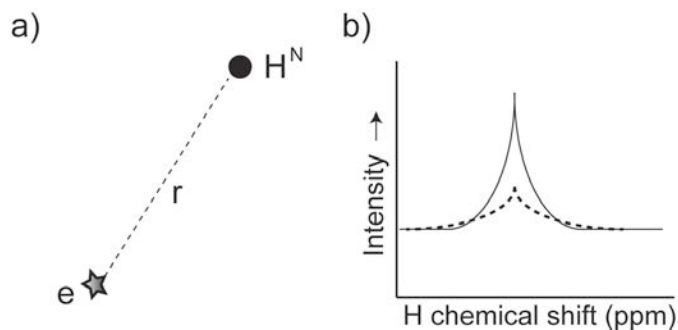
Figure 1.5 (a) Paramagnetic relaxation enhancement (PRE) depends on the nuclear spin - electron distance, r. (b) NMR signals affected by PRE are observed in NMR spectra more broadened (dash line) compare to a reference (continues line).

The PRE produced by the Solomon mechanism has its origin in the large dipole-dipole interaction that appears between the unpaired electron in the paramagnetic center and an NMR-active nucleus. Actually, this is the same type of interaction that is recorded when measuring NOEs in NMR spectroscopy, and double-electron-electron resonance (DEER) in electron paramagnetic resonance spectroscopy (EPR). If both dipolar moments are from nuclear spins, NOEs are measured, but if both spins are electron spins then DEER can be measured by EPR. In the case of PRE, the electron spin density interacts with the magnetic moment of the nucleus; therefore the nucleus senses the changes between the +1/2 and -1/2 electron spin energy levels. The paramagnetic enhancement on the transverse relaxation rate produced by the Solomon mechanism is described by the following equation (Solomon I, 1955; Keizers PH et al. 2011):

$$R_2^{Solomon} = 1/15\ (\mu_0/4\pi)^2\ [\gamma_i^2 g^2 \mu_B^2 S\ (S+1)/r^6_{MH}](4\tau_r+(3\tau_c/1+\omega_I^2\tau_c^2)$$

where r_{MH} is the distance between the paramagnetic center and the NMR active nucleus, μ_0 is the permeability of free space, γ_i is the gyromagnetic ratio, g is the electron g-factor, μ_B is the Bohr magneton, S is the total electron spin momentum quantum number, τ_c is the total correlation time of the molecule and ω_I is the Larmor frequency. This equation is only valid for slowly relaxing paramagnetic centers that do not present MSA like nitroxides and Gd^{3+} (Koehler J et al. 2011). The total correlation time (τ_c) is defined in the following way:

$$1/\tau_c = 1/\tau_e + 1/\tau_r + 1/\tau_M$$

τ_e is the electron relaxation rate, τ_r is the rotational correlation time of the biomolecule and τ_M is the chemical exchange term (if it exits). If studying a protein (commonly the $\tau_r > 5$ ns) with a slowly relaxing paramagnetic center (μs-ns range), then the biggest contribution will most probably come from the electron relaxation rate τ_e.

For fast relaxing paramagnetic centers (mainly lanthanides) the Curie mechanism is the dominant source of PRE. In this case, it is the external magnetic field (produced by the NMR spectrometer) the one that produces a magnetic moment in the electrons because of the difference that exists between their -1/2 and +1/2 energy levels. Molecular tumbling affects this induced magnetic moment, something that is perceived by the nucleus

producing Curie relaxation (Clore GM et al. 2009). The PRE produced by the Curie mechanism is described by the following equation:

$$R_2^{Curie} = 1/5 \; (\mu_0/4\pi)^2 \; [\gamma_i^2 B_0^2 g_j^4 \mu_B^4 J^2 \; (J+1)^2/(3kT)^2 r^6_{MH}](4\tau_c+(3\tau_c/1+\omega_I^2\tau_c^2)$$

in this case B_0 is the external magnetic field, g_j is the Landé g-factor, J is the total angular momentum quantum number, k is Boltzmann's constant and T is the temperature. In contrast to the Solomon mechanism, in Curie the total correlation time is usually dominated by the rotational correlation time of the molecule, because the electron relaxation rate of fast relaxing centers is in the picoseconds range, so all electron spin states are averaged. As a result of the dominance of the rotational correlation time, Curie relaxation is stronger for big biomolecules (Otting G et al. 2010). The temperature and the strength of the external magnetic field also modulate this relaxation mechanism. Temperature has an influence because the rotational correlation time is inversely proportional to the temperature. It is influenced by the strength of the magnetic field because it raises the population difference between the -1/2 and +1/2 energy levels.

Regarding the interpretation of PRE data, it is much easier when it is dominated by Solomon relaxation. The first reason for so is that when Curie relaxation dominates, there is also an important cross-correlation with other relaxation mechanisms (Pintacuda G et al. 2004), something that cannot be eliminated experimentally. The second reason is that PCS are usually also

present in this kind of paramagnetic centers. The problem is that the exchange contributions produced by molecular interactions could be quite different in the paramagnetic and in the reference diamagnetic state. For isotropic systems in which there isn't MSA and the Solomon mechanism dominates, these inconveniences are not present, so the interpretation of PRE data is straightforward (Clore GM et al. 2009).

1.5 Residual dipolar couplings (RDC)

The magnetic moments of two or even more nuclear spins can interact in a through-space fashion producing dipolar couplings. These dipolar couplings appear because the interacting magnetic moments can have a parallel or antiparallel orientation relative to each other while they are in an external magnetic field (Koehler J et al. 2011). Unfortunately, the approximately isotropic (random) tumbling of a protein in solution results in these dipolar couplings being averaged to zero. However, paramagnetic centers that present magnetic susceptibility anisotropy (MSA) align weakly with the external magnetic field (Keizers PH et al. 2011). Therefore, if a target biomolecule has rigidly attached a paramagnetic center that presents MSA, this alignment can be transmitted to the biomolecule, and as a result residual dipolar couplings can be observed in NMR spectra (PCS also depend in this molecular alignment produced by MSA, and will be reviewed in the next section). The magnetic susceptibility is called anisotropic if the magnetic moment of the paramagnetic center depends on its orientation relative to the

magnetic field. This can be represented with a second rank tensor called magnetic susceptibility tensor (χ) that extends over three axes (χ_X, χ_Y and χ_Z) that are fixed to the molecule (figure 1.6):
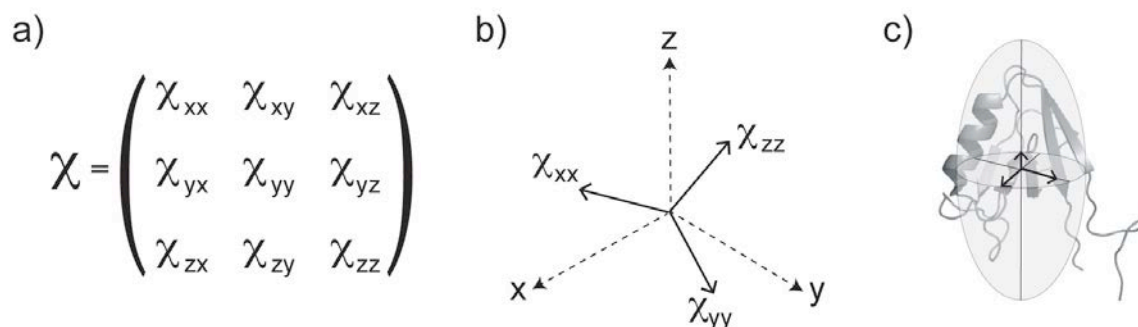
Figure 1.6 (a) Magnetic susceptibility anisotropy can be described by a second rank tensor. (b) The axes of the tensor are defined in a way that $|\chi_{zz}| > |\chi_{yy}| > |\chi_{xx}|$. (c) If there isn't internal mobility, each internuclear vector has a fixed orientation relative to the tensor frame.

The paramagnetic alignment just depends in the deviation of the magnetic susceptibility tensor from spherical symmetry, the anisotropic component (Koehler J et al. 2011). The anisotropic component of the magnetic susceptibility tensor, also called $\Delta\chi$ tensor or alignment tensor, is described by a rhombic ($\Delta\chi_{rh}$) and an axial ($\Delta\chi_{ax}$) component:

$$\Delta\chi_{rh} = \chi_{XX} - \chi_{YY}$$

$$\Delta\chi_{ax} = \chi_{ZZ} - (\chi_{XX} + \chi_{YY})/2$$

The $\Delta\chi$ tensor is by definition anisotropic, so it disappears when its axis have the same magnitude, $\chi_X = \chi_Y = \chi_Z$. Both tensors, the χ and the $\Delta\chi$ tensor, have the same coordinate system. The RDC (in Hz) between two spins, A and B is given by:

$$RDC_{AB} = (hB_0{}^2\gamma_A\gamma_B)/(240\pi^3kTr^3{}_{AB})\{ \Delta\chi_{ax} (3\cos^2 \theta\text{-}1) + 3/2\ \Delta\chi_{rh} \sin^2 \theta \cos 2\phi\}$$

Where D_{AB} is the residual dipolar coupling observed between nuclei A and B, r_{AB} is the distance between them, θ and ϕ are angles that determine the orientation of the A–B inter-nuclear vector relative to the $\Delta\chi$ tensor (figure 1.7), B_0 is the strength of the external magnetic field and h is Planck's constant.
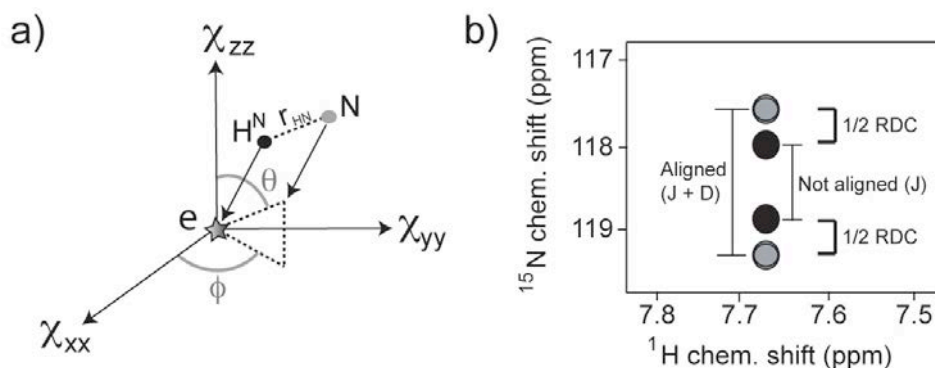
Figure 1.7 (a) RDCs depend on the orientation of the internuclear vector relative to the frame of the Dc tensor. (b) A certain RDC can be observed in 15N-HSQC spectra without decoupling as an addition to the J-coupling.

RDC provide long-range orientation restraints that can overcome the usual limitations of the classic restraints because they are independent of the distance to the paramagnetic center. This type of angular restraints can be obtained for all of the inter-nuclear vectors of a protein, and all of them refer to the same molecule-fixed coordinate system (Prestegard JH et al. 2004). Something that is clear from the last equation is that the magnitude of the RDC depends on the magnitude of the alignment induced by the paramagnetic center. If there weren't alignment, then the rhombic and axial

component of the $\Delta\chi$ tensor would tend to zero and with them the RDCs too. It is worth to mention that there are other methods in addition to the "attachment of a paramagnetic center" to align weakly a biomolecule, but the equation that is presented above can only be used when the alignment is completely produced by the presence of MSA (Clore GM et al. 2009).

1.6 Pseudocontact shits (PCS)

PCSs are observed as large chemical shift changes in NMR spectra. They are the result of an interaction between the nuclear spin and the unpaired electron of the paramagnetic centers. In this kind of interaction the nucleus perceives the dipolar magnetic field, and it is positive when the electron-nucleus vector is parallel relative to the magnetic field of the spectrometer and negative whenever it is perpendicular. The weak alignment produced by paramagnetic centers with MSA is important in order to observe PCS (Otting G et al. 2010). If there is no alignment, then the normal isotropic tumbling of molecules in liquid state cancels out these negative and positive contributions and the PCS would disappear too. A PCS for a certain nuclear spin is:

$$PCS = 1/12\pi r^3_{MA} \{\Delta\chi_{ax} (3\cos^2\theta - 1) + 3/2 \, \Delta\chi_{rh} \sin^2\theta \cos 2\phi\}$$

The equation presented above is quite similar to the one which describes the RDC, but in the PCS equation the factors r_{MA}, θ and ϕ refer to

the electron-nucleus vector and not an inter-nuclear vector (figure 1.8). PCS are not transmitted through-bonds, but rather through-space and can reach even further than PRE (up to 40 Å; Allegrozzi M *et al*, 2000) because the PCS distance-dependency (r^{-3}) is weaker than for PRE (r^{-6}) as observed above.
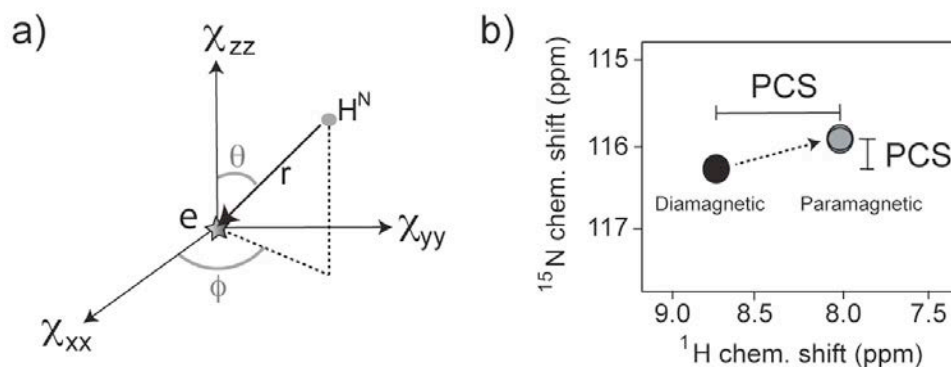
Figure 1.8 (a) PCSs depend on the θ and ϕ angles with respect to the $\Delta\chi$ tensor and the distance between the paramagnetic center and the nuclear spin. (b) PCSs are observed as large shifts in NMR spectra.

This difference in the distance dependency is important, because PCS can be measured for atoms that are far away from the paramagnetic center, where the signals are not broadened anymore due to PRE. Other conclusions can be obtained from this equation: the best paramagnetic centers to obtain PCS are those with a large anisotropic tensor (mainly fast-relaxing lanthanides; table 1.1) and that the magnitude of a PCS is independent of the strength of the external magnetic field.

1.7 The importance of paramagnetic datasets from independent alignments.

It could also be concluded from the equations that describe the RDCs and PCSs that in the absence of a 3D structure, a single RDC or PCS value could be interpreted by different sets of angles. The important point is that the number of solutions can be reduced by acquiring datasets of paramagnetic restraints produced by $\Delta\chi$ tensors with different orientations (Otting G, 2008). Actually, RDCs and PCSs measured from multiple independent alignments proved to be powerful tools not only in the structure calculation process (Bouvignies G *et al*, 2006), but also in the dynamic analysis of biomolecules (Lange OF *et al,* 2008). For instance, four different PCSs datasets of amide groups produced by orientationally independent $\Delta\chi$ alignment tensors are sufficient to determine the backbone structure of a protein (Su XC *et al*, 2008; Otting G, 2008). This is possible because the position of a certain nucleus involves 3 variables (x, y and z coordinates); therefore four independent datasets would provide an extra set of information that could be used to determine in addition the parameters of the $\Delta\chi$ tensor.

Regarding dynamic information, several datasets of RDCs measured from independent alignment tensors were able to provide dynamic information on the protein ubiquitin (Lange OF et al. 2008). This kind of analysis is possible because the value of a certain RDC depends on the θ and ϕ angles of the inter-nuclear vector; therefore any dynamic process will

affect the value of an RDC. As a matter of fact, any measured RDC value is an average of all the conformation sampled by the inter-nuclear vector. However, the only way to extract this dynamic information is by measuring at least 5 datasets of RDCs produced by independent alignment tensors (Lakomek NA et al. 2008).

For all these reasons, a major goal of paramagnetic NMR spectroscopy is to develop an easy and robust method that could enable the acquisition of multiple independent datasets for any target molecule. In the following section, the main strategies to attach rigidly a paramagnetic center in a target protein will be described, which is the main pre-requisite to measure paramagnetic restraints.

1.8 Aim and outline of this thesis

The paramagnetic effects produced by lanthanide ions have shown to provide a great amount of distance and/or orientational restraints, especially if it is possible to acquire multiple datasets from independent orientations. However, the traditional way to attach a lanthanide requires the covalent tagging of a small chelating molecule (lanthanide tag) to a unique surface reactive cysteine on the target protein. This is a condition that could be difficult to accomplish particularly in large proteins, which might have several cysteine residues. An additional challenge arises if the 3D structure of the protein is not available, because it could be difficult to select a surface-accessible tagging site without disturbing the structure of the target.

The main goal of this thesis is to develop a method that could alleviate many of the drawbacks mentioned before. The central idea is to attach the lanthanide tag to a reporter protein, which then binds to the target, hence transmits the paramagnetic effects to any target that is fused to a recognition peptide (figure 1.9). Moreover, if different reporter mutants are designed to attach the lanthanide on different locations onto its surface, then each mutant will transmit orientationally independent datasets of paramagnetic restraints.

The protein that was selected to work as a reporter is the erbin PDZ domain, which is known to bind the peptide TGWETWV when located in the C-terminal of another protein. The tag called CLaNP-5 was chosen to attach the lanthanide ion; it binds covalently to two cysteine residues; so several PDZ double cysteine mutants were designed. The proteins ubiquitin and

maltose binding protein (MBP) were chosen as targets to test if the proposed method works; therefore the peptide TGWETWV was fused to their C-terminal (ubiquitin^{TGWETWV} and MBP^{TGWETWV}) to mediate binding with PDZ.

The first part of this thesis is devoted to check if PDZ can actually bind the targets without disturbing their natural structure. Then, the designed PDZ mutants (PDZ-1 to PDZ-7) were tagged with CLaNP-5 loaded with a paramagnetic lanthanide (Tm^{3+}) or a reference ion (Lu^{3+}). These tagged PDZ reporters were added to both target proteins in order to test if they could transmit the paramagnetic effects (RDC, PCS and PRE) as expected. Finally, the impact of the flexible residues connecting PDZ and the targets on the magnitude of the paramagnetic effects were studied through an ubiquitin mutant with a shorter linker, ubiquitin^{WETWV}.
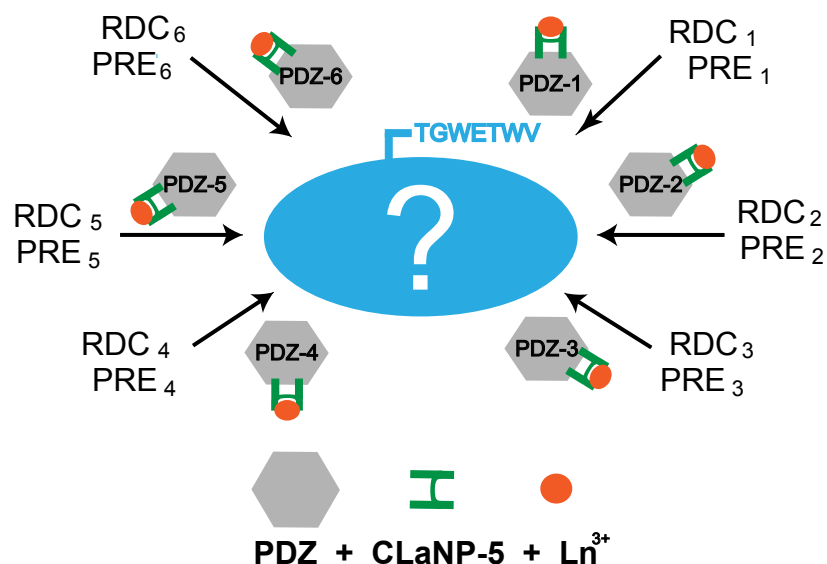
Figure 1.9 Schematic view of the method developed in this work.

28

1.9 The PDZ domain and the TGWETWV peptide: the reporter system.
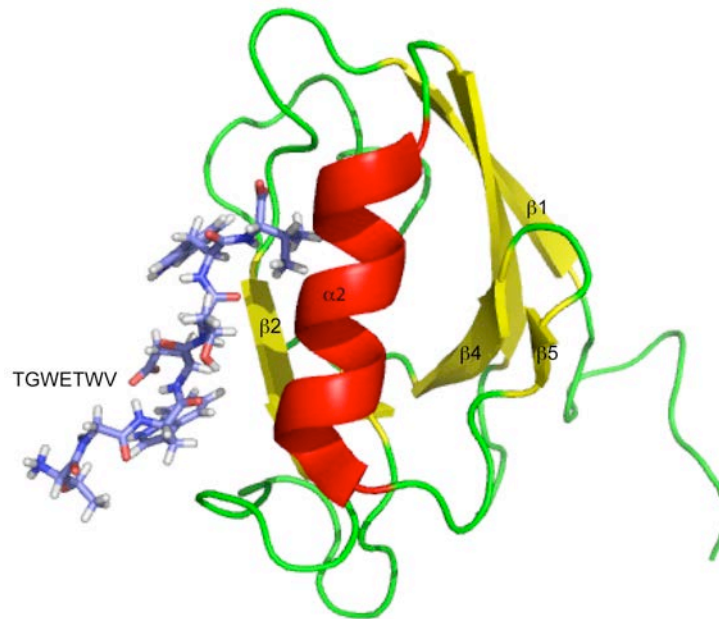
Figure 1.10 Erbin PDZ structure 1N7T in complex with the peptide TGWETWV (blue). α–helixes are shown in red, beta sheets in yellow and green for residues without secondary structure.

The PDZ domain proteins were observed for the first time in the post-synaptic density-95, discs large, and zonula occludens 1, where it is a usual component of such scaffold proteins. PDZ domains have around 90 residues that fold into a β-barrel capped by α-helices (Ye F et al. 2013). The main function of the different PDZ domains is to recognize and bind the C-terminal residues of another protein. The human Erbin PDZ domain (ERB-interacting protein; residues 1273-1371 of Erbin) was selected as reporter in the method developed in this thesis. It has six β-strands that are organized as two antiparallel β-sheets (figure 3.1). The β1, β4, β5 and β6 integrate the lower β-sheet while β2, β3 and β4 integrate the top sheet. The α2 helix covers the β2- β5 border of the sandwich. The following is the sequence of the Erbin PDZ domain:

```
1          10             20             30             40             50
GHELAKQEIRVRVEKDPELGFSISGGVGGRGNPFRPDDDGIFVTRVQPEG

      60        70        80        90        99
PASKLLQPGDKIIQANGYSFINIEHGQAVSLLKTFQNTVELIIVREVSS
```

Erbin PDZ is stable protein that binds with high affinity (IC_{50} = 0.15 μM) the peptide TGWETWV (Skelton NJ et al. 2003). This peptide was fused in this thesis to the target proteins in the C-terminal.
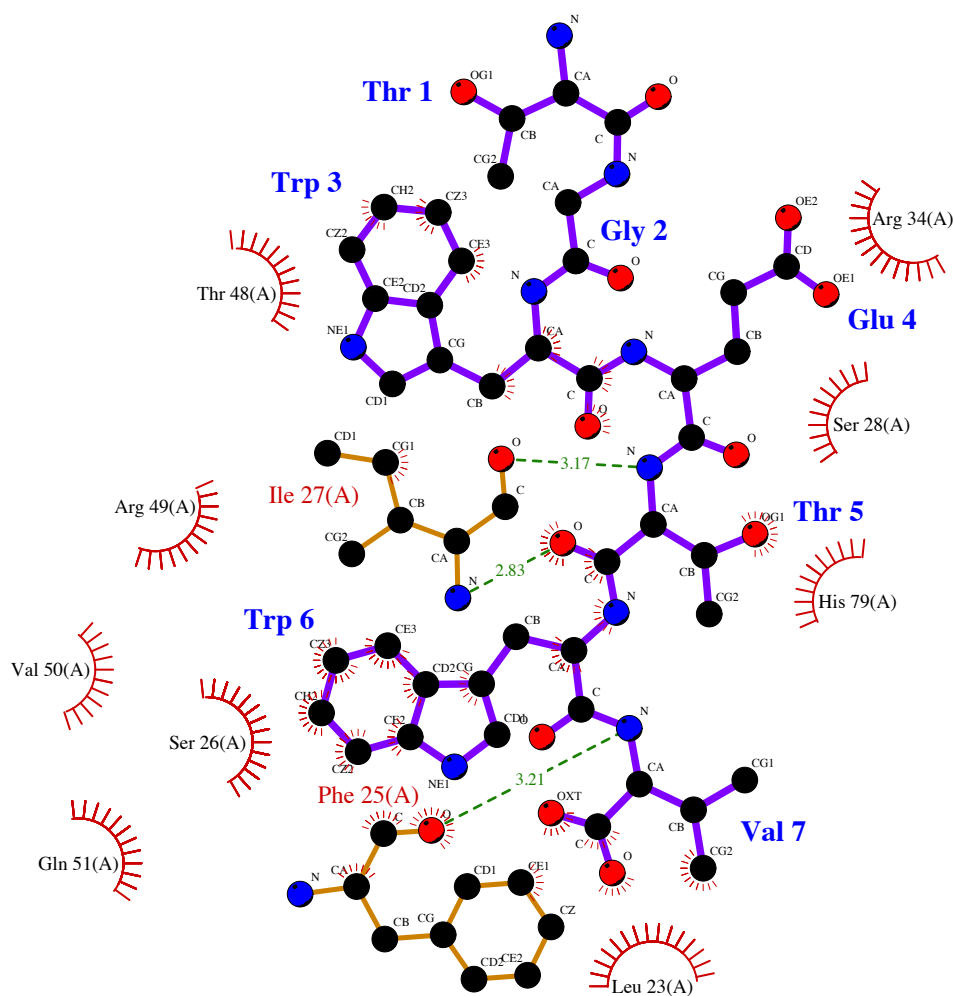
Figure 1.11 Schematic diagram of the interaction between Erbin PDZ and the peptide TGWETWV. The program LIGPLOT v.4.5.3 (Wallace AC et al. 1995) was used to show the interactions. Hydrogen bonds are shown as green dashed lines and hydrophobic contacts are shown as a yellow arc that radiates in the direction of the atoms it contacts. The information is based on NMR structure 1N7T.

1.10 Human ubiquitin as a target
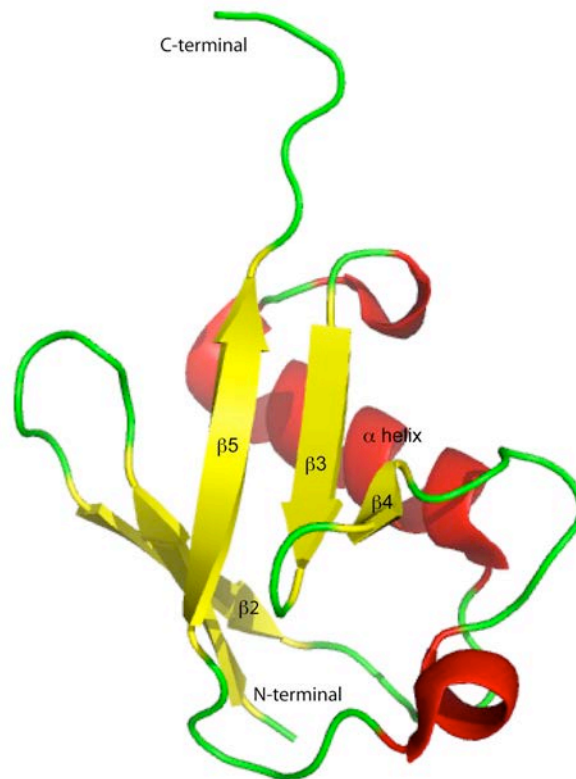
Figure 1.12 Ubiquitin structure 1D3Z. Alfa helixes are shown in red, beta sheets in yellow and green for residues without secondary structure.

Human ubiquitin is a highly conserve protein of 76 residues that has been found in almost all eukaryotic organisms. It is involved in a degradation pathway of proteins, where is attached to a substrate protein (Hershko A et al. 1998). Human ubiquitin is structurally well characterized (figure 3.4); there are already crystal (1UBQ) and NMR structures (1D3Z; BMRB 6457) of high resolution (Massi et al. 2005; Cornilescu G et al. 1998). This protein was chosen as one of the targets used to test the method that is developed in this thesis. The Erbin PDZ domain recognizes the peptide TGWETWV, so it was fused to the C-terminal of ubiquitin, just after its last

residue to produce the 83 residues protein ubiquitin^{TGWETWV}:

```
1           10          20          30
MQIFVKTLTGKTITLEVEPSDTIENVKAKI

            40          50          60
QDKEGIPPDQQRLIFAGKQLEDGRTLSDYN

             70      76 78   80
    IQKESTLHLVLRLRGGTGWETWV
```

A "shorter version" of ubiquitin^{TGWETWV} was produced; it has deleted the residue 76 and the first two residues of the TGWETWV peptide (residues 77 and 78). This shorter version of 80 residues is called ubiquitin^{WETWV}.

1.11   The maltose binding protein (MBP) as a target.

Figure 1.13 The maltose binding protein in complex with beta-cyclodextrin (blue); PDZ structure 1DMB. Alfa helixes are shown in red, beta sheets in yellow and green for residues without secondary structure.

The maltose binding protein (MBP) is a 42 kDa protein (370 residues) that works as a receptor in the maltose/maltodextrin system, which uptakes and transports maltodextrins across the cytoplasmic membrane of bacteria. The MBP protein of *Escherichia coli* has 370 residues (42 kDa) and is biochemically and structurally characterized (PDB 1DMB; Sharff AJ et al. 1993; Gardner KH et al. 1998). In addition, the chemical shift assignment of this protein has already been published (BMRB entry 4354). This protein was selected also as a target protein in addition to ubiquitin, for that reason the TGWETWV peptide was fused to its C-terminal. The following is the sequence of this MBP mutant:

```
1                         25                              50
MKIEEGKLVIWINGDKGYNGLAEVGKKFEKDTGIKVTVEHPDKLEEKFPQ
                          75                             100
VAATGDGPDIIFWAHDRFGGYAQSGLLAEITPDKAFQDKLYPFTWDAVRY
                         125                            150
NGKLIAYPIAVEALSLIYNKDLLPNPPKTWEEIPALDKELKAKGKSALMF
                         175                            200
NLQEPYFTWPLIAADGGYAFKYENGKYDIKDVGVDNAGAKAGLTFLVDLI
                         225                            250
KNKHMNADTDYSIAEAAFNKGETAMTINGPWAWSNIDTSKVNYGVTVLPT
                         275                            300
FKGQPSKPFVGVLSAGINAASPNKELAKEFLENYLLTDEGLEAVNKDKPL
                         325                            350
GAVALKSYEEELAKDPRIAATMENAQKGEIMPNIPQMSAFWYAVRTAVIN
```

AASGRQTVDEALKDAQTRITKTGWETWV

2. Materials and methods

2.1 Chemical reagents and laboratory products.

The group of Prof. Marcellus Ubbink, in the Leiden Institute of Chemistry (The Netherlands), Leiden University, provided the lanthanide tag CLaNP-5 (already chelating Lu^{3+} or Tm^{3+}) used in the current thesis (figure 2.2). Other special reagents and laboratory products were used in the current thesis: β-Cyclodextrin and TEMED (Tetramethylethylenediamine) were purchase from Sigma-Aldrich. 2,2'-Dipyridyl disulfide was purchased from Merck. Dithiothreitol (DTT) was purchased from GERBU Biotechnik GmbH. Ampicillin (sodium salt); Acrylamide gel (37.5:1) and Imidazol were from Carl Roth GmbH. Deuterium monoxide (D_2O, 99.9%) was purchased from Deutero GmbH.

Dialysis membranes (MW 3500) were purchased from Spectrum laboratories Inc. Ni-NTA (nickel-nitrilotriacetic acid) agarose was purchased from Qiagen. Vivaspin PES (polyethersulfone) sample concentrators were purchased from Sartorius AG.

2.2 Protein expression and purification methods

All the proteins used in this thesis were produced and then purified by Melanie Wegstroth, under the supervision of Dr. Stefan Becker at the NMR-based structural biology department (NMR-2), Max Planck Institute for Biophysical Chemistry.

2.2.1 Production and purification of the maltose binding protein (MBP^{TGWETWV})

The cDNA coding for MBP (*E. coli*) was amplified by PCR and cloned into the commercial T7 promotor expression vector pET32a (Novagen). The plasmid containing the desired sequence was transformed into the strain BL21 (DE3) of *E. Coli*. Liquid cultures were grown up in Luria-Bertani media (LB) complemented with Ampicillin. Once the culture reached an optical density of 0.7 (at 600 nm), the cells were induced with 0.5 mM IPTG. Seven hours after induction (OD$_{600}$ ~4.5), the cells were harvested through centrifugation. The cells were then re-suspended in a lysis buffer, containing 200 mM NaCl, 1 mM of EDTA, 0.5 mM of phenylmethylsulfonyl fluoride (PMSF, a protease inhibitor) and 20 mM Tris/HCl pH 7.4 to regulate the pH.

The cells were lysed through seven cycles of sonication. They then were centrifuged at 4°C for 45 minutes (48000 g). The supernatant was loaded onto an amylose resin column (50 mL, 4°C). After loading the column was washed with lysis buffer at a constant flow rate (1 mL/min) until a stable baseline was reached. The protein was released from the resin by using 10 mM of maltose in lysis buffer.

The eluted protein was dialysed against a buffer containing 25 mM NaCl and 20 mM Tris/HCl buffer pH 8.0 (buffer A) before its purification through ion exchange chromatography. For the ion-exchange step, the protein was loaded into a DEAE-FF Sepharose column (5 mL) and washed with 100 mL of buffer A at a flow rate of 2 mL/minute. In order to elute the protein, a gradient of NaCl was applied, from 25 to 500 mM. If fractions of 1 mL were collected, then the protein normally appeared between fractions 11 and 23. A further step of purification involved a MonoQ 10/10 column (anion exhange), using a 100 mL gradient from

25 to 500 mM of NaCl, again in buffer A. The last step in the purification process was molecular exclusion chromatography, already in measurement buffer: of 20 mM phosphate buffer pH 7.2, 50 mM NaCl.

NMR samples used to acquire paramagnetic data on MBP^{TGWETWV} contained 0.25 mM of ^{15}N,^{2}H-MBP^{TGWETWV}, 0.5 mM of CLaNP-5 tagged PDZ loaded with either Lu^{3+} of Tm^{3+} in a buffer composed of 20 mM phosphate buffer pH 7.2, 50 mM NaCl, supplemented with 2 mM β-cyclodextrin and 10% of D$_2$O. The sample used in the 3D HNCO-based experiment recorded at 700 MHz Bruker spectrometer contained a higher concentration of protein: 0.6 mM of ^{2}H,^{13}C,^{15}N-MBP^{TGWETWV} and 1.2 mM of CLaNP-5 tagged PDZ-1.

2.2.2 Production and purification of PDZ mutant proteins

The NMR structure with PDB code 1N7T is important in this thesis because the peptide TGWETWV appears in complex with the Erbin PDZ domain. The chemical shifts of Erbin PDZ can be accessed with the BMRB entry 5631. The peptide binds over an edge of the β-sandwich through contacts with the β2 strand (figure 3.2). PDZ residues important for binding (and shouldn't be mutated) were previously determined through an alanine and homolog scanning that is reported in the literature (Skelton NJ et al. 2003). All this information was used to select the residues that were mutated to cysteine in order to attach the lanthanide tag CLaNP-5. Seven double cysteine mutants (PDZ-1 to PDZ-7) were designed and produced by standard molecular biology methods in order to attach the lanthanide tag CLaNP-5 (figure 4.5). The mutated residues are located at the surface of PDZ; their Cα atoms are between 6-10 Å apart and their side chains point to the solvent as recommended in the literature (Keizers PH et al. 2008).

The PDZ mutants were cloned into the plasmid pET16b (Novagen) for easy purification. Plasmids encoding the desired protein were transformed into the *E. coli* strain BL21 (DE3). A colony of transformed cells were used to inoculate 2 mL of LB media supplemented with 50 μg/mL of ampicillin; this culture was let to grow for 6 hours. The 2 mL culture was used to inoculate a 50 mL culture of LB media supplemented with ampicillin; this culture was let to grow overnight. 20 mL of the overnight culture were used to inoculate 1 L of culture. Once the optical density (600 nm) reached 0.4, the culture was transferred to 25° Celsius. At an optical density between 0.6 - 0.7m the culture was induced with 0.5 mM of IPTG. The cells should be harvest after 12 hours of induction by centrifugation at 6000 rpm. The pellet of cells can be stored at -80° C.

The purification of PDZ starts using a Ni^{2+}-affinity chromatography column. This step uses the following buffers:

Lysis buffer: 50 mM phosphate buffer pH 8.0, 300 mM NaCl, 10 mM Imidazol, 2 mM of DTT and 0.5 mM of PMSF.

Wash buffer: 50 mM phosphate buffer pH 8.0, 300 mM NaCl, 20 mM Imidazol, 2 mM of DTT and 0.5 mM of PMSF.

Elution buffer: 50 mM phosphate buffer pH 8.0, 300 mM NaCl, 250 mM Imidazol, 2 mM of DTT and 0.5 mM of PMSF.

The first step involves re-suspending the pellet of cells in lysis buffer (aprox. 50 mL). Then the cells are sonicated and centrifuged for 45 minutes at 20 000 rpm (4° C). The supernatant is loaded into a HIS TRAP column (GE Healthcare) of 5 mL using a flow rate of 1.5 mL/minute. The column is washed with lysis buffer and then with wash buffer, using a flow rate of 2 mL/minute. In order to elute the protein, the elution buffer is flow through the column and the

protein is collected. The protein is then dialyzed against 50 mM Tris buffer pH 8.0, 0.5 mM of EDTA and 2 mM of DTT.

The His-tag of the protein was removed by using a TEV protease (Tobacco Etch Virus nuclear inclusion endopeptidase). For this step, 2 mg of the protease are added for each 100 mg of PDZ. This mixture is incubated overnight at room temperature. In order to separate the PDZ from the protease, a batch purification step is performed. In this purification step, the protein is centrifuge during 30 minutes at 20 000 rpm (4° C). Then 10 mM of imidazol are added to the supernatant; this solution is incubated with 2 mL of Ni-NTA agarose for 1 hour at 4° C. The suspension is applied to a disposable gravity column of 5 mL. The flow through is collected and dialyzed against 50 mM Tris buffer pH 8.0, 300 mM NaCl and 2 mM DTT.

Finally, a gel filtration step is performed using a Superdex 75 26/60 column (GE Healthcare), using the same buffer in the last dialysis step. In this purification step, the reduce protein is concentrated (VIVA spin sample concentrator) to 2.5 mL; this sample is loaded into the column using a 5 mL loop (column volume: 320 mL; flow rate 2.5 mL/min). The protein obtained after this purification step is ready to be tagged with CLaNP-5, it is just necessary a further step to eliminate the DTT.

2.2.3 Purification of tagged PDZ with activated Thiol Sepharose 4B.

Some PDZ mutants like PDZ-3 showed a relatively low yield of tagging with CLaNP-5 (table 4.1). Therefore, it was attempted to separate tagged (paramagnetic) from untagged PDZ (diamagnetic) through Thiol Sepharose 4B (GE Healthcare). This Sepharose reacts and forms covalent bonds with molecules containing thiol groups. If untagged PDZ had still reduced cysteine residues, then it would react and be immobilized by this resin (Egorov TA et al. 1975) and tagged PDZ protein should appear in the flow-through.

The first step is addition of the mixture of protein to binding buffer: 20 mM phosphate buffer pH 6.5 and 0.1 M NaCl (degassed). Then, the mixture of tagged and untagged protein was added to a column packed with activated Sepharose 4B. It is recommended to let the protein stay in contact with the resin for at least one hour, therefore the flow rate was slow: 0.4 mL/min. Protein started to elute after 45 mL (around 112 min after loading). The purity of eluted protein was checked through NMR spectroscopy.
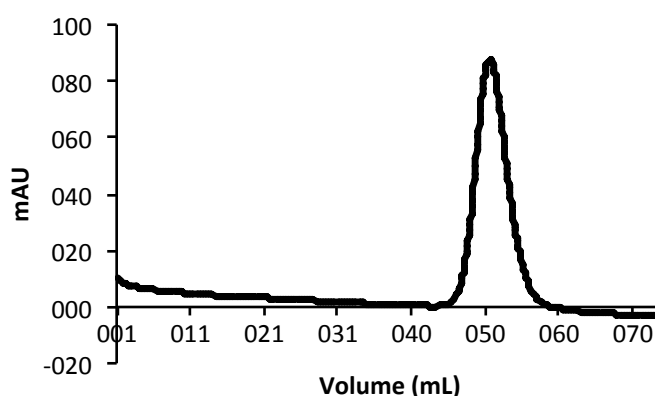
Figure 2.1 Elution profile of a mixture of tagged and untagged PDZ-3 measured at 280 nm on a column packed with activated thiol Sepharose 4B.

2.2.4 Production and purification of ubiquitin^{TGWETWV}

Recombinant human ubiquitin was overexpressed and purified according to a method reported in the literature (Vijay-Kumar et al. 1987). NMR samples used to measure paramagnetic effects had 0.25 mM ^{15}N-ubiquitin^{WETWV} or ^{15}N-ubiquitin^{TGWETWV}, 0.5 mM of a tagged PDZ mutant in 20 mM sodium phosphate buffer pH 6.5, 10% D$_2$O and 50 mM NaCl.

2.3 CLaNP-5 and the protocol to tag the PDZ reporter mutants

The first step to attach the lanthanide tag CLaNP-5 to a PDZ mutant is to make sure that the cysteine residues are in the reduced form. In order to reduce these residues, 5 mM of the reducing agent DTT was added to a 0.5 mM solution of PDZ in 20 mM sodium phosphate pH 7.2 supplemented with 50 mM NaCl. This solution was incubated on ice for 1 h. Once the incubation was finished, the DTT was removed through a gel filtration Superdex 75 (16/60) column (GE Healthcare). The reduced protein obtained after this column can be used in the tagging reaction.
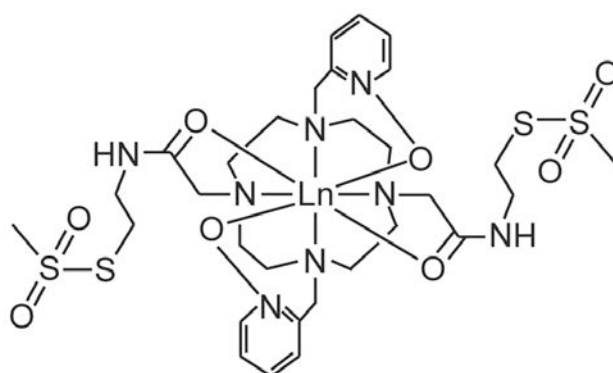
Figure 2.2 Structure of the synthetic lanthanide tag CLaNP-5 binding a lanthanide (Ln).

To tag PDZ, 10 equivalents of CLaNP-5 (already chelating Lu^{3+} or Tm^{3+}) were added to a 60 μM solution of reduced PDZ in degassed buffer containing 20

mM sodium phosphate pH 7.2 and 150 mM NaCl. This reaction mixture was stirred "side to side" in the cold room overnight. For example, an average reaction was a mixture of 8 mL of 60 μM PDZ and 40 μM of 120 mM CLaNP-5 loaded with Tm^{3+}. The PDZ that precipitates is eliminated by centrifugation at 6000g for 10 minutes. It is also necessary to eliminate the excess of lanthanide from the reaction mixture; therefore supernatant is added into a Viva Spin column (5 kDa cut off, GE healthcare) and concentrated until getting the adequate volume (0.5 – 1 mL) to inject it in a gel filtration column like the one used to remove the excess of TCEP. Alternatively, the excess of lanthanide can be removed by exchanging the buffer through 5 cycles of concentration/dilution (from 0.2 mL to 2 mL) in the same a Viva Spin column. The amount of tagged PDZ obtained after a tagging reaction was determined by the DC protein assay (Bio-Rad) and the tagging yield through HPLC-MS analysis.

2.4 Experiments to acquire paramagnetic data

The following experiments were recorded in order to obtain the paramagnetic restraints shown in this thesis:

Table 2.1 The following spectroscopic parameters are given: **pts** is the number of complex points in t1, t2 and t3; **ns** is the number of scans and the field strength (^{1}H Larmor precession).

Sample	Experiment	Parameters
0.25 mM ^{2}H, ^{15}N- MBP ^{TGWETWV} in presence of 0.5 mM PDZ-1 (Tm^{3+})	Interleaved HSQC-TROSY	512x512 pts. ns = 120 800 MHz
0.25 mM ^{2}H, ^{15}N- MBP ^{TGWETWV} in presence of 0.5 mM PDZ-1 (Lu^{3+})	Interleaved HSQC-TROSY	512x512 pts. ns = 60 800 MHz
0.25 mM ^{2}H, ^{15}N- MBP ^{TGWETWV} in presence of 0.5 mM PDZ-2 (Tm^{3+})	Interleaved HSQC-TROSY	512x512 pts. ns = 120 900 MHz
0.25 mM ^{2}H ^{15}N- MBP ^{TGWETWV} in presence of	Interleaved HSQC-TROSY	512x512 pts. ns = 80

0.5 mM PDZ-2 (Lu^{3+})		900 MHz
0.25 mM ^{2}H, ^{15}N- MBP ^{TGWETWV} in presence of 0.5 mM PDZ-3 (Tm^{3+})	Interleaved HSQC-TROSY	512x512 pts. ns = 112 800 MHz
0.3 mM ^{2}H, ^{15}N- MBP ^{TGWETWV} in presence of 0.6 mM PDZ-3 (Lu^{3+})	Interleaved HSQC-TROSY	512x512 pts. ns = 20 800 MHz
0.25 mM ^{2}H, ^{15}N- MBP ^{TGWETWV} in presence of 0.5 mM PDZ-5 (Tm^{3+})	Interleaved HSQC-TROSY	512x512 pts. ns = 72 900 MHz
0.25 mM ^{2}H, ^{15}N- MBP ^{TGWETWV} in presence of 0.5 mM PDZ-5 (Lu^{3+})	Interleaved HSQC-TROSY	512x512 pts. ns = 64 900 MHz
0.25 mM ^{2}H, ^{15}N- MBP ^{TGWETWV} in presence of 0.5 mM PDZ-6 (Tm^{3+})	Interleaved HSQC-TROSY	512x512 pts. ns = 104 900 MHz
0.25 mM ^{2}H, ^{15}N- MBP ^{TGWETWV} in presence of 0.5 mM PDZ-6 (Lu^{3+})	Interleaved HSQC-TROSY	512x512 pts. ns = 80 900 MHz
0.8 mM ^{15}N, ^{13}C PDZ-1 tagged with CLaNP-5 loaded with Lu^{3+}	Interleaved HSQC-TROSY	512x512 pts. ns = 64 900 MHz
0.8 mM ^{15}N, ^{13}C PDZ-1 tagged with CLaNP-5 loaded with Tm^{3+}	Interleaved HSQC-TROSY	512x512 pts. ns = 72 900 MHz
0.6 mM ^{2}H, ^{13}C, ^{15}N- MBP ^{TGWETWV} in presence of 1.2 mM PDZ-1 (Lu^{3+})	TROSY-HNCO	26x52x512 pts. ns = 16 700 MHz
0.6 mM ^{2}H, ^{13}C, ^{15}N- MBP ^{TGWETWV} in presence of 1.2 mM PDZ-1 (Tm^{3+})	TROSY-HNCO	26x52x512 pts. ns = 40 700 MHz
0.25 mM ^{15}N- ubiquitin ^{TGWETWV} in presence of 0.5 mM PDZ-1 (Tm^{3+})	BSD IPAP-HSQC	256x512 pts. ns = 256 900 MHz
0.25 mM ^{15}N- ubiquitin ^{TGWETWV} in presence of 0.5 mM PDZ-1 (Lu^{3+})	BSD IPAP-HSQC	256x512 pts. ns = 120 900 MHz Acquired twice
0.25 mM ^{15}N- ubiquitin ^{TGWETWV} in presence of 0.5 mM PDZ-1 (Tm^{3+})	BSD IPAP-HSQC	256x512 pts. ns = 120 600 MHz Acquired twice
0.25 mM ^{15}N- ubiquitin ^{TGWETWV} in presence of 0.5 mM PDZ-1 (Lu^{3+})	BSD IPAP-HSQC	256x512 pts. ns = 120 600 MHz
0.25 mM ^{15}N- ubiquitin ^{TGWETWV} in presence of 0.5 mM PDZ-2 (Tm^{3+})	BSD IPAP-HSQC	256x512 pts. ns = 268 900 MHz
0.25 mM ^{15}N- ubiquitin ^{TGWETWV} in presence of 0.5 mM PDZ-2 (Lu^{3+})	BSD IPAP-HSQC	256x512 pts. ns = 92 900 MHz
0.25 mM ^{15}N- ubiquitin	BSD IPAP-HSQC	256x512 pts.

^{TGWETWV} in presence of 0.5 mM PDZ-3 (Tm^{3+})		ns = 280 900 MHz
0.25 mM ^{15}N- ubiquitin ^{TGWETWV} in presence of 0.5 mM PDZ-3 (Lu^{3+})	BSD IPAP-HSQC	256x512 pts. ns = 100 900 MHz
0.25 mM ^{15}N- ubiquitin ^{TGWETWV} in presence of 0.5 mM PDZ-5 (Tm^{3+})	BSD IPAP-HSQC	256x512 pts. ns = 248 900 MHz
0.25 mM ^{15}N- ubiquitin ^{TGWETWV} in presence of 0.5 mM PDZ-5 (Lu^{3+})	BSD IPAP-HSQC	256x512 pts. ns = 120 900 MHz
0.25 mM ^{15}N- ubiquitin ^{TGWETWV} in presence of 0.5 mM PDZ-6 (Tm^{3+})	BSD IPAP-HSQC	256x512 pts. ns = 240 900 MHz
0.25 mM ^{15}N- ubiquitin ^{TGWETWV} in presence of 0.5 mM PDZ-6 (Lu^{3+})	BSD IPAP-HSQC	256x512 pts. ns = 116 900 MHz
0.25 mM ^{15}N- ubiquitin ^{TGWETWV} in presence of 0.5 mM PDZ-7 (Tm^{3+})	BSD IPAP-HSQC	256x512 pts. ns = 280 900 MHz
0.25 mM ^{15}N- ubiquitin ^{TGWETWV} in presence of 0.5 mM PDZ-7 (Lu^{3+})	BSD IPAP-HSQC	256x512 pts. ns = 80 900 MHz
0.25 mM ^{15}N- ubiquitin ^{WETWV} in presence of 0.5 mM PDZ-1 (Tm^{3+})	BSD IPAP-HSQC	256x512 pts. ns = 264 900 MHz
0.25 mM ^{15}N- ubiquitin ^{WETWV} in presence of 0.5 mM PDZ-1 (Lu^{3+})	BSD IPAP-HSQC	256x512 pts. ns = 108 900 MHz

2.4.1 RDC measurement and data analysis

The RDC between two nuclear spins adds to the scalar J coupling in an NMR spectrum (J_{NH} = $^{1}J_{NH}$ + D_{NH}), therefore the simplest method to measure amide RDCs (H^{N}-N) is to record a ^{1}H-^{15}N heteronuclear single quantum correlation (HSQC) spectrum without decoupling in t_1 or the t_2 evolution period. However, this simple technique doubles the amount of signals in the spectrum producing signal overlap, which is a big disadvantage. In the case of ubiquitin^{TGWEVWTV} and ubiquitin^{WETWV}, RDCs were measured in ubiquitin through an improved version of the original in-phase/antiphase technique (2D BSD-IPAP

HSQC; figure 2.3). This experiment reducing spectral overlapping and eliminates systematic errors due to the addition of ^{1}H-decoupling pulses (Ottiger M et al. 1998; Yao L et al. 2009).
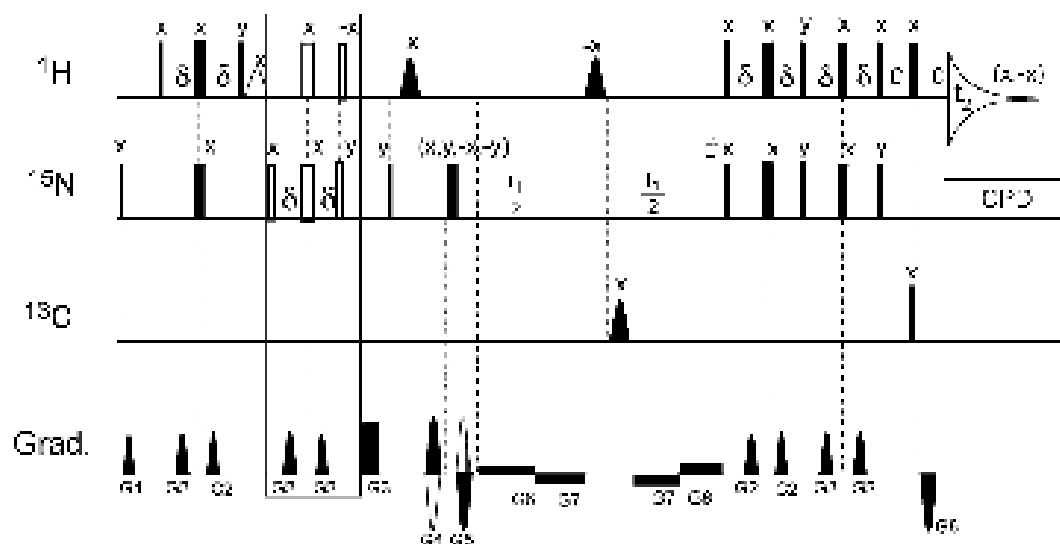
Figure 2.3 Pulse sequence of the improved IPAP experiment (2D BSD-IPAP HSQC). Modified from Yao L. et al. 2009. The antiphase (AP) spectrum is produced due to the pulses in the black box, so these pulses are skipped in order to produce the in-phase spectrum (IP). The ^{1}H solid (shaped) pulses are IBURP-2 (Green H et al. 1991). In this scheme, the narrow pulses represent 90° flip angles and wide pulses represent 180° flip angles.

In this technique, the two doublet components are separated into two different spectra: one just contains the upfield doublet component and the other the downfield component, avoiding spectral crowding. Spectra were recorded with 256X512 complex points for each spectrum and 256 transients for the paramagnetic sample or 128 for the diamagnetic one. Residual dipolar couplings were obtained as the difference in the splitting between the paramagnetic (Tm^{3+}) and diamagnetic sample (Lu^{3+}) in the ^{15}N dimension (figure 2.4).
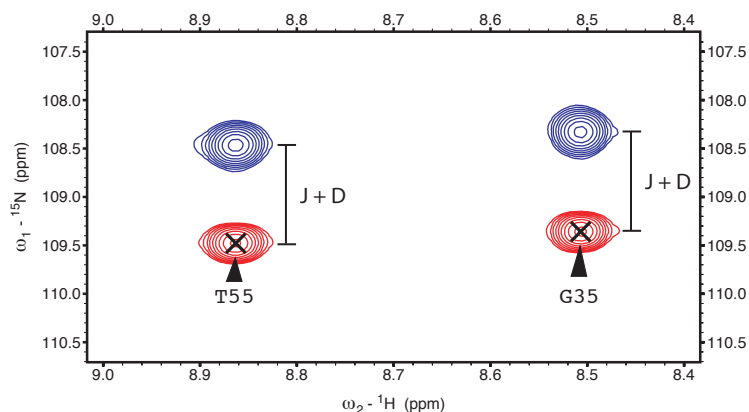
Figure 2.4 Superimposed downfield and upfield ^{1}H-^{15}N HSQC spectrum (zoom in to ubiquitin residues T55 and G35) measured using the BSD-IPAP HSQC experiment (Yao L. et al 2009). The RDC value (D) adds to the J coupling (J) in this type of experiment.

In the case of MBP^{TGWETWV}, amide RDCs (^{1}H-^{15}N) were measured as the frequency difference between a ^{1}H-^{15}N-HSQC and a ^{1}H-^{15}N-TROSY spectrum recorded in an interleaved fashion (Prestegard JH et al. 2004). From peak positions in the ^{15}N dimension, RDC (D) values were calculated according to:

$$D = 2 * (\omega_{N, HSQC} - \omega_{N, TROSY}) - {}^{1}J_{NH}$$

The $^{1}J_{NH}$ value was obtained through the same experiments but using a reference diamagnetic sample (PDZ tagged with CLaNP-5/Lu^{3+}). HSQC-TROSY interleave experiments (figure 2.5) increase the precision of the measurement especially at high magnetic fields, which are necessary for high molecular weight proteins like MBP in order to obtain more signal resolution.
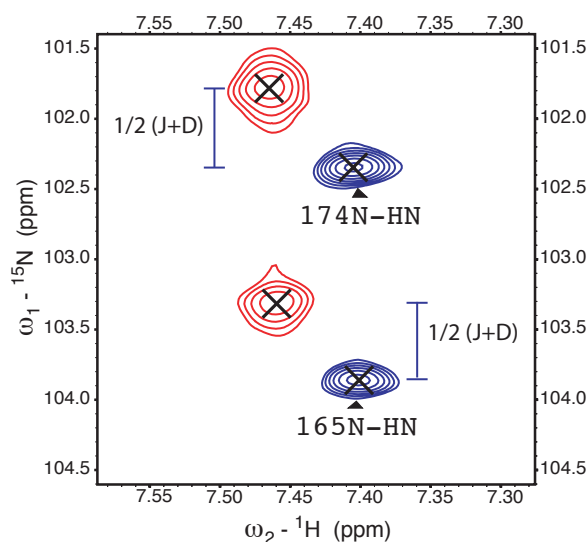
Figure 2.5 Superimposed ^{1}H-^{15}N HSQC (red) and ^{1}H-^{15}N TROSY (blue) spectrum (zoom in to MBP residues 174 and 165) measured using the HSQC-TROSY experiment (Prestegard JH et al 2004). The difference in the signal position is one half of J (diamagnetic) or J+D (paramagnetic).

To decrease signal overlap, a 3D HNCO-based experiment (Yang D et al. 1999) was recorded in addition using a 700 MHz Bruker spectrometer. The sample used in this experiment contained 0.6 mM of ^{2}H,^{13}C,^{15}N-MBP^{TGWETWV} and 1.2 mM of CLaNP-5 tagged PDZ-1. The experimental conditions were the same ones used in the 2D experiments. Recorded spectra were processed using the software NMRPipe and NMRDraw (Delaglio F et al. 1995) and analyzed using the softwares Sparky to determine the RDCs (Goddard TD et al.). The software PALES (Zweckstetter M. 2008) was used to determine the alignment tensors by singular value decomposition (Losonczi JA et al. 1999) and back-calculate theoretical RDC values using the reported structures of ubiquitin (1D3Z), MBP (1DMB) and PDZ (1N7T). To determine the uncertainty in the calculated alignment tensors, 1000 steps of the "structural noise Monte-Carlo method" were performed (Zweckstetter M et al. 2002). In short, this method consists in adding noise to the structure with a magnitude that matches the RMSD between observed and predicted RDCs. The extent of the alignment parameters obtained

from these noise-corrupted structures (when using the coupling constants back-calculated for the original structure) represents a good measure of the uncertainty in the derived tensor. All spectra were acquired at 310 K on Bruker 600, 700, 800 or 900 MHz spectrometers with cryogenic probes.

2.4.2 PCS measurement and data analysis

Pseudo contact shifts were measured as chemical shift differences in paramagnetic and diamagnetic spectra used to measured RDCs (figure 2.6; John M et al. 2007). The signal assignment of wild type MBP, ubiquitin and PDZ are already reported in the literature with the BMRB codes 4354, 6457 and 5631 respectively. Backbone chemical shifts of MBP^{TGWETWV} bound to wild-type PDZ were confirmed and completed using TROSY-based triple-resonance experiments recorded on a sample of 0.6 mM ^{2}H, ^{13}C, ^{15}N-MBP^{TGWETWV} in the presence of 1.2 mM wild-type PDZ. Backbone chemical shifts of ubiquitin^{TGWETWV} bound to wild-type PDZ were obtained using standard triple-resonance experiments recorded on a 1.3 mM sample of ^{13}C, ^{15}N-ubiquitin^{TGWETWV} in presence of wild-type PDZ at molar ratio of 1:2.
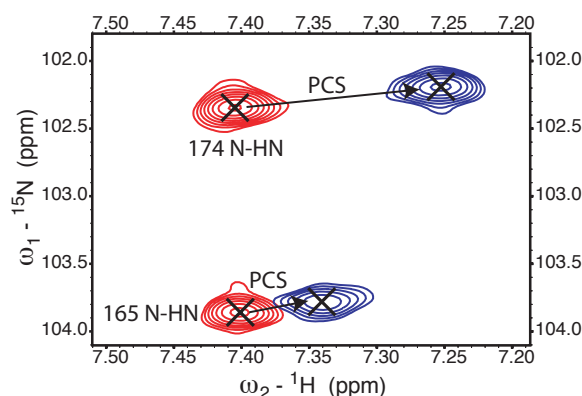
Figure 2.6 Superimposed diamagnetic (red) and paramagnetic (blue) ^{1}H-^{15}N TROSY spectrum (zoom in to MBP residues 174 and 165) measured using the HSQC-TROSY experiment for a diamagnetic and a paramagnetic sample (Prestegard JH et al 2004). The arrows indicate the ^{1}H PCS, which is the difference in the chemical shift between the

diamagnetic and paramagnetic signal (John M et al. 2007).

The transfer of assignments to the paramagnetic spectra was done manually, without running further experiments, as most of the pseudo contact shifts were smaller than 0.3 ppm. PCSs were fit to 3D structures using the software Numbat (Schmitz C et al. 2008).

2.4.3 PRE measurement and data analysis

Intensity ratios of the NMR signals reported by the program Sparky (paramagnetic/diamagnetic signal) were normalized by averaging the values of those residues that are far away from the C-terminal region according to the corresponding 3D structures. The signal to noise ratio of each signal (S/N) was used to estimate the error according to the following equation:

$$\text{Error} = I/I_o \{(1/(S/N^{Para}))^2 + (1/(S/N^{Dia}))^2\}^{1/2}$$

PRE distances were calculated from intensity ratios (assuming a Curie-spin relaxation mechanism) according to previously published procedures (Battiste JL et al. 2000). Briefly, normalized intensity ratios were converted into paramagnetic relaxation enhancements (R2^{sp}) by calculating the additional relaxation needed to decrease the intensity of the reference diamagnetic sample by the estimated ratio. Paramagnetic rate enhancements were turned into distances through the following equation:

$$r = [K/R2^{sp} \ (4\tau_c + (3\tau_c/(1 + \omega^2_h\tau_c^2)))]^{1/6}$$

r is the distance between the nuclear spin and the electron, τ_c is the correlation time (28.9 ns for MBP^{TGWETWV} bound to PDZ), ω_h is the ^{1}H Larmor frequency and K is a constant that according to Curie relaxation equals to:

$$K = (1/5) \ J \ (J+1)^2 \ \gamma^2 \ B_0^2 \ g_j^4 \ \beta^4$$

In these calculations, it was taken into account that Tm^{3+} has a total angular magnetic quantum number J of 6, its Landé g-factor (g_j) equals to 7/6, β is the Bohr magneton (9.274×10^{-24}), B_0 is the magnetic field and γ is the nuclear gyromagnetic ratio (Koehler J et al. 2011). The program HYCUD (Rezaei-Ghaleh N et al. 2013) was used to estimate the correlation time of $MBP^{TGWETWV}$ bound to PDZ.

2.5 R_2 and R_{1rho} relaxation measurements

The ^{15}N-R_2 spin relaxation rates of free and $MBP^{TGWETWV}$ bound to PDZ, wild type ubiquitin and PDZ-bound ubiquitin^{TGWETWV} were acquired using a CPMG (TROSY based) experiment (written by Dr. Saskia Villinger). The conditions were the following ones: temperature 310 K, at a ^1H Larmor frequency of 600 MHz. The samples of $MBP^{TGWETWV}$ had 0.4 mM of ^2H, ^{13}C, ^{15}N-$MBP^{TGWETWV}$, and 0.8 mM of PDZ (wild type) for the measurement of the complex. For ubiquitin, the experiments were recorded on a sample composed of 0.5 mM ^{15}N (wild type) ubiquitin or ^{15}N-ubiquitin^{TGWETWV} bound to 1 mM of unlabeled PDZ. The buffer conditions were: 20 mM sodium phosphate buffer pH 6.5, 10% D_2O and 100 mM NaCl. The following delay durations were used: of 4, 8, 12, 16, 28 and 36 ms ($MBP^{TGWETWV}$/PDZ complex). For free $MBP^{TGWETWV}$, 4, 12, 28, 40, 52 and 80 ms were used as relaxation delays. In the case of ubiquitin^{TGWETWV} in complex with PDZ, relaxation delays of 4, 20, 40, 80, 136 and 216 ms were employed. For (wild type) ubiquitin the delays following delays were used: 36, 67, 99, 182 and 269 ms.

R_{1rho} values (Palmer AG et al. 2006) of ^{15}N-ubiquitin^{TGWETWV} bound to wild-type PDZ were obtained using relaxation delays of 8, 24, 48, 80, 120, 150, and

210 ms at a ^{1}H-Larmor frequency of 600MHz (298 K). For this experiment, the concentration of ubiquitin^{TGWETWV} was 0.48 mM and the concentration of wild type PDZ was the double.

2.6 Assignment of ubiquitin^{TGWETWV} and MBP^{TGWETWV} bound to PDZ

The chemical shifts of the amide groups of wild type ubiquitin and MBP are reported in the literature. The chemical shift was apparently not affected in the target proteins bound to PDZ, however 3D experiments were acquired in order to check the assignment and confirm this observation. In addition, the tagging of CLaNP-5/Lu^{3+} produced small changes in the position of some signals; therefore it was necessary to corroborate its assignment.

Table 3.2 The following spectroscopic parameters are given: **pts** is the number of complex points in t1, t2 and t3; **ns** is the number of scans and the field strength (^{1}H Larmor precession). *Experiment recorded by Dr. Francesca Munari.

Sample	Experiment	Parameters
0.6 mM ^{2}H, ^{13}C, ^{15}N-MBP ^{TGWETWV} in presence of 1.2 mM wild type PDZ.	TROSY-HNCA	44x24x512 pts. ns = 24 800 MHz
0.75 mM ^{15}N,^{13}C-ubiquitin ^{TGWETWV} in presence of 1.5 mM wild type PDZ.	*HNCA	34x30x512 pts ns = 32 700 MHz
0.8 mM ^{15}N, ^{13}C PDZ-1 tagged with CLaNP-5 loaded with Lu^{3+}	HNCA	66x20x512 pts. ns = 32 700 MHz

2.7 Chemical shift perturbation analysis upon binding of PDZ

For chemical shift perturbation analysis, chemical shifts of ubiquitin[TGWETWV] or MBP[TGWETWV] bound to PDZ were compared to those reported of wild-type ubiquitin or MBP. Averaged, normalized $^1H/^{15}N$ chemical shift changes were calculated according to:

$$\Delta_{HN}=\{[(\Delta\delta_H)^2 + (\Delta\delta_N/5)^2]\}^{1/2}$$

where $\Delta\delta_H$ and $\Delta\delta_N$ are the chemical shift differences for the 15N and 1H dimensions respectively.

2.8 Isothermal titration calorimetry studies and NMR titrations

Isothermal titration calorimetry experiments were done on a MicroCal ITC 200 microcalorimeter at 298 K. Ubiquitin[TGWETWV] and PDZ samples were extensively dialyzed against 20 mM sodium phosphate buffer pH 6.5, 100 mM NaCl. The sample cell contained 0.05 mM of ubiquitin[TGWETWV] and the injection syringe was filled with 0.8 mM of PDZ. Experimental data was analyzed using the Microcal Origin software.

3. Results

3.1 Chemical shift perturbation analysis and titration of ubiquitin^{TGWETVW} with PDZ

The success of the method develop in this thesis depends on the recognition and binding of the TGWETWV-fused targets by the PDZ domain. This is why some of the first experiments performed were titrations in order to determine if PDZ binds to ubiquitin^{TGWETWV}. The chemical shift of a certain nucleus depends on its chemical environment; therefore chemical shifts in the spectrum of ubiquitin^{TGWETWV} were expected to change upon PDZ binding, especially those signals corresponding to residues recognized by PDZ. This titration (figure 3.1) was performed by adding increasing amounts of unlabeled wild type PDZ (not observed in the spectra) to a known amount of ^{15}N label ubiquitin^{TGWETWV}, the protein whose signals are detected.

It can be observed in figure 3.1 that there is a big difference in the spectrum of ubiquitin^{TGWETWV} before (red) and after addition of PDZ (green). The most probable explanation is that when the TGWETWV peptide is free, it interacts (folds-back) un-specifically/transiently with residues in the surface of ubiquitin, producing the observed perturbations. However, the addition of PDZ apparently "sequesters" this peptide and brings back chemical shifts comparable to those of the wild type protein. It is very important that the addition of the TGWETWV peptide as well as the binding to PDZ does not alter the structure of the target. In order to prove that there was no distortion of the structure of ubiquitin, the amide chemical shifts of ubiquitin^{TGWETWV} when it is fully bound to

PDZ were determined and compared to reported chemical shifts of wild type ubiquitin (figure 3.2b). The only differences are observed in the C-terminal, where the TGWETWV peptide is fused to ubiquitin.
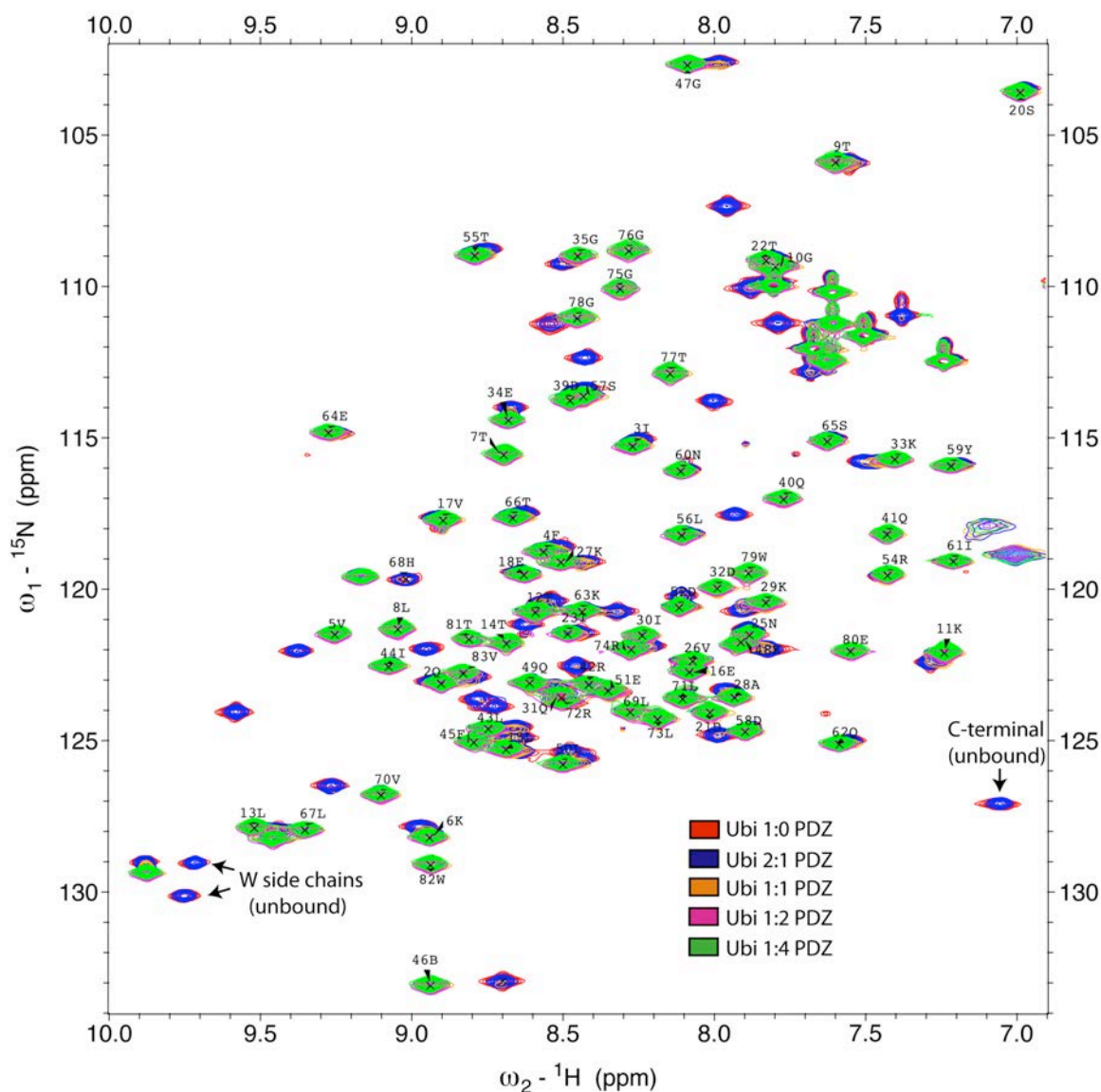
Figure 3.1 NMR titration of ubiquitin[TGWETWV] with wild type PDZ. Superposition of ^{1}H-^{15}N HSQC spectra of ^{15}N-ubiquitin[TGWETWV] after the addition of increasing amounts of PDZ. The assignment corresponds to ubiquitin[TGWETWV] saturated with PDZ. The signals corresponding to the C-terminal residue and tryptophan side chains of the TGWETWV peptide in the unbound state are marked with an arrow.

The titration experiments also showed that ubiquitin[TGWETWV] is completely in the bound conformation already with an equimolar amount of PDZ. This is clear if we observed the signals that disappear upon PDZ binding, for example

the C-terminal residue (V83) of ubiquitin[TGWETWV]. Before the addition of PDZ, this

signal appears in the right/lower region of the HSQC spectra. However, it starts to

disappear after the addition of a small amount of PDZ (ubiquitin[TGWETWV] 2:1 PDZ)

and cannot be observed anymore upon addition of an equimolar amount of PDZ.

There weren't observed further chemical shifts after the addition of an excess of

PDZ (ubiquitin[TGWETWV] 1:2 PDZ).
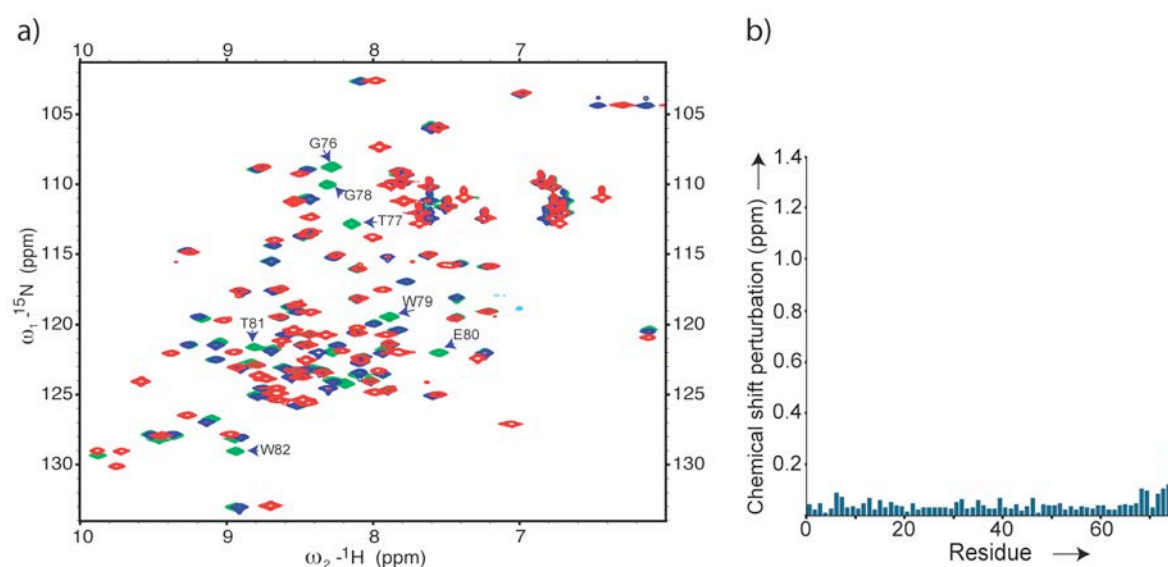
Figure 3.2 PDZ-binding to the C-terminal TGWETWV extension does not perturb the structure of ubiquitin. a) Superposition of ^{1}H-^{15}N HSQC spectra of wild-type ubiquitin (blue), unbound ubiquitin[TGWETWV] (red) and ubiquitin[TGWETWV] bound to wild-type PDZ (green). When PDZ is absent, the presence of the TGWETWV sequence at the C-terminus of ubiquitin produces a change in the chemical shift of several residues, probably because of a transient interaction of the peptide with the ubiquitin surface. Cross-peaks that belong to the C-terminal residues of ubiquitin[TGWETWV] when bound to PDZ (green) are labelled. b) Averaged, normalized ^{1}H/^{15}N chemical shift changes between wild-type ubiquitin (BMRB entry: 17769) and ubiquitin[TGWETWV] bound to PDZ-1 (Camacho-Zarco AR et al. 2014).

3.2 Chemical shift perturbation analysis and titration of MBP^{TGWETVW} with PDZ

An NMR titration was also performed in order to determine if PDZ was binding the TGWETWV peptide fused to the C-terminal of MBP. In this titration increasing amounts of unlabel PDZ to ^{15}N-MBP^{TGWETWV} were added (figure 3.3). It can be observed that there are no big differences in the different spectra. However, a rigorous observation shows that in analogy to the case of ubiquitin^{TGWETWV}, upon addition of PDZ the signals that correspond to C-terminal residues change their position, along with those signals that correspond to the tryptophan side chains that are present in the TGWETWV peptide (figure 3.3). After the addition of an equimolar amount of PDZ, the signal that corresponds to the C-terminal residue in the unbound state is still present in the spectrum. However, this signal disappears after the addition of an excess of PDZ (MBP 1:2 PDZ) because all the MBP^{TGWETWV} is completely bound to PDZ. This chemical shift was expected, because the chemical environment changes for C-terminal residues upon binding to PDZ.
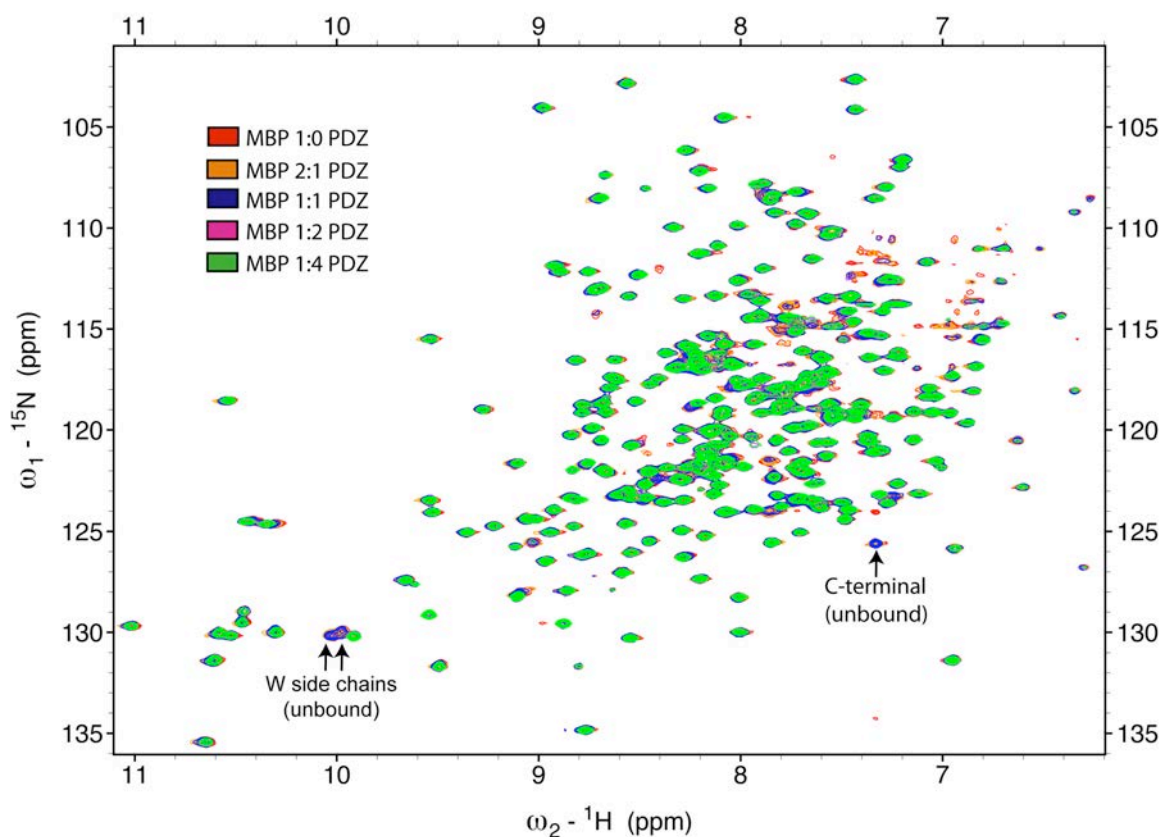
Figure 3.3 NMR titration of MBP^{TGWETWV} with wild type PDZ. Superposition of ^{1}H-^{15}N HSQC spectra of ^{15}N-MBP^{TGWETWV} upon the addition of different amounts of PDZ. The signals corresponding to the unbound state of the C-terminal residue and tryptophan side chains of the TGWETWV peptide are marked with an arrow.

In order to determine quantitatively if the structure of MBP changed due to the fusion of the recognition peptide or binding to PDZ, the chemical shifts of MBP^{TGWETWV} bound to PDZ were compared with those of wild type MBP (figure 3.4). The spectrum of wild type MBP (figure 3.4a, green) is almost identical to the spectrum of MBP^{TGWETWV} unbound (red) or bound to PDZ (blue).
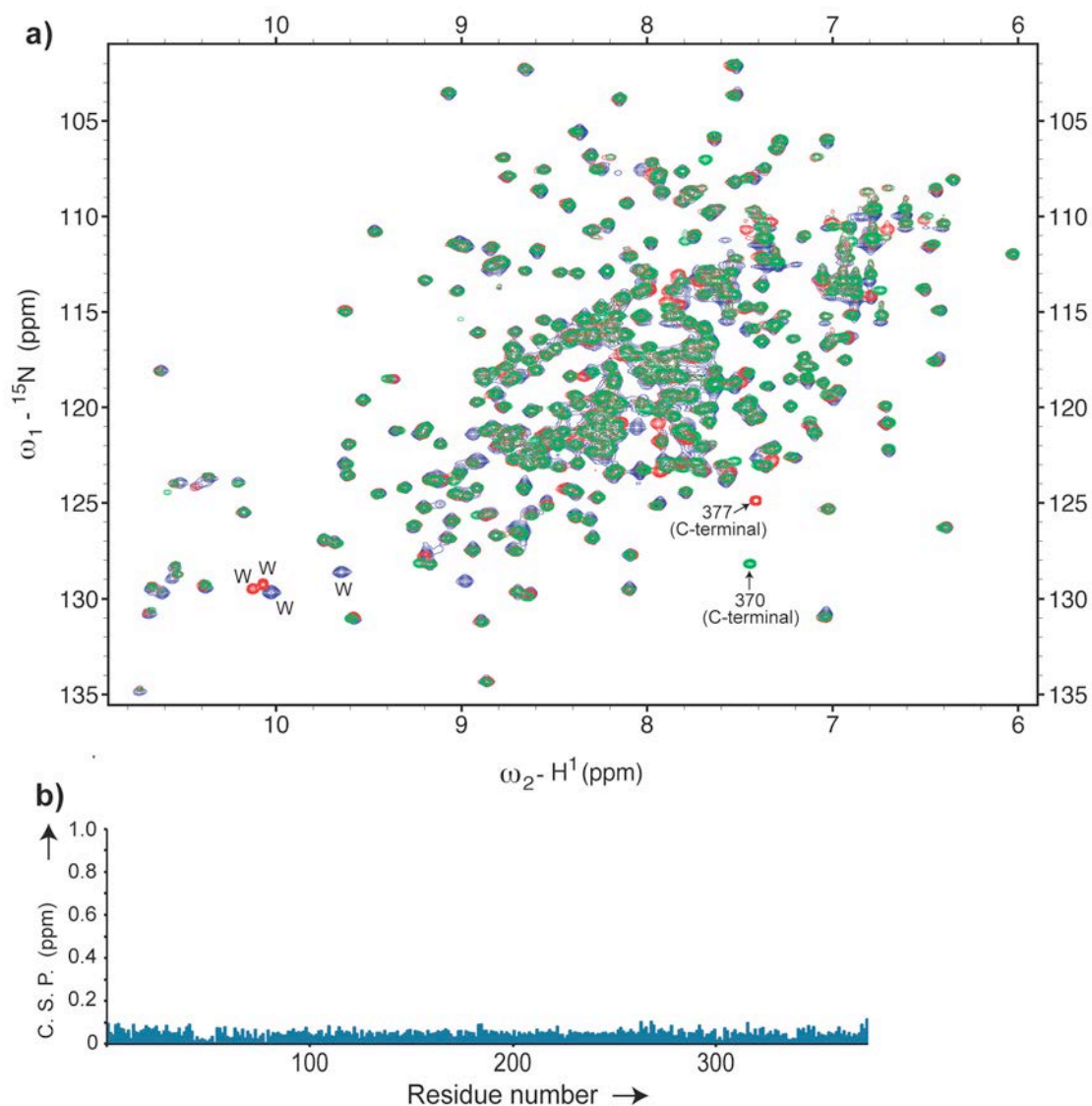
Figure 3.4 Chemical shifts in MBP^{TGWETWV} bound to wild-type PDZ. a) Superposition of ^{1}H-^{15}N HSQC spectra of wild-type MBP (green, 370 residues), unbound MBP^{TGWETWV} (red, 377 residues) and MBP^{TGWETWV} bound (blue) to PDZ-1, which had been tagged with CLaNP-5 and loaded with Lu^{3+} (added at a 2:1 molar excess). b) Averaged, normalized ^{1}H/^{15}N chemical shift changes between wild-type MBP and MBP^{TGWETWV} bound to wild-type PDZ (Camacho-Zarco AR et al. 2014).

A quantitative analysis in the form of a chemical shift perturbation plot shows that there is no change in the structure (figure 3.4b), therefore PDZ fulfills two important requirements to be used as a reporter: it binds and do not disturb the wild type structure of the two targets studied up to now.

3.3 Design and tagging yield of the double cysteine PDZ mutants

Synthetic tags that are attached to two cysteine residues have shown to be more rigid than those attach to a single one (Keizers PH et al. 2007), consequently a tag of this type called "caged lanthanide NMR probe 5" (CLaNP-5) was chosen to attach the paramagnetic Tm^{3+} or the diamagnetic Lu^{3+} to the designed PDZ mutants. The different double cysteine mutants to attach CLaNP-5 were designed in a way that all the tagging sites could be as separated as possible on the surface of PDZ. Since the rigidity of the lanthanide is essential, most of the residues selected to attach the lanthanide tag are forming secondary elements of the PDZ domain. The only exception was PDZ-5 (table 3.2, figure 3.5), which is located in a long loop ($\beta 3$- $\beta 4$) that is not so well defined when compared to residues in secondary structural elements (Skelton NJ et al. 2003).

	Mutation 1 and position	Mutation 2 and position	Tagging (%) efficiency	Distance (Å) between Cα
PDZ-1	Y72C ($\beta 5$)	L85C ($\alpha 2$)	95	8.4
PDZ-2	G80C ($\alpha 2$)	S84C ($\alpha 2$)	42	6.1
PDZ-3	R14C ($\beta 1$)	E94C ($\beta 6$)	67	6.9
PDZ-4	Q90C (loop)	T92C ($\beta 6$)	---	6.2
PDZ-5	K58C (dis.)	Q61C (dis.)	95	7.5
PDZ-6	S84C ($\alpha 2$)	T88C ($\alpha 2$)	80	6.3
PDZ-7	Q81C ($\alpha 2$)	S84C ($\alpha 2$)	85	4.5

Table 3.1 Residues selected to produce the double cysteine mutants. The numbering refers to that used in PDB 1N7T.

According to the literature, from 6 to 10 Å is the optimal distance between the Cα atoms of the residues selected to attach CLaNP-5 (Keizers PH et al. 2008). All the mutants accomplish this guideline with the exception of PDZ-7, which has its Cα carbons below this range. Regarding mutant PDZ-4, it proved to be too unstable to be used (strong precipitation); therefore it wasn't employed

furthermore. The tagging efficiency was quite variable between the different PDZ mutants (table 3.1). For example, mutants PDZ-1 and PDZ-5 were tagged almost completely, but other mutants had a relatively poor yield like PDZ-2 and PDZ-3 (table 3.1).
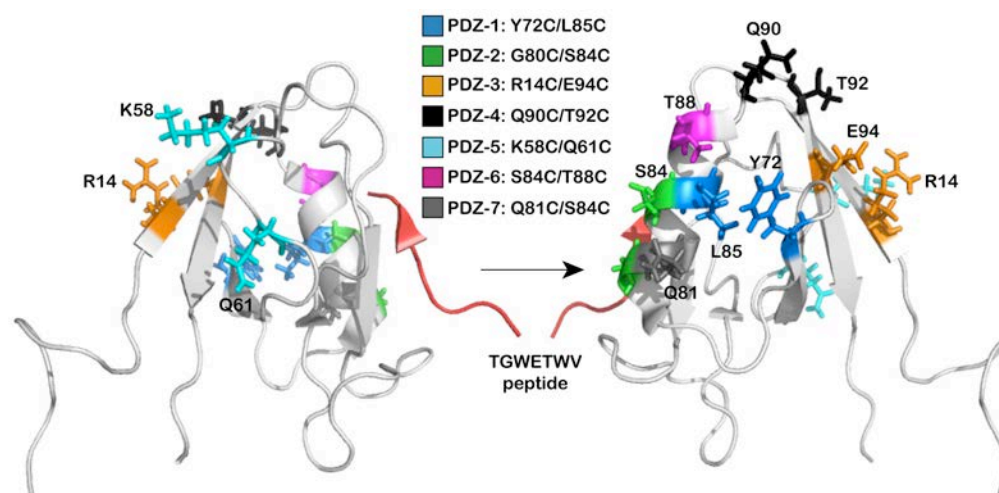
Figure 3.5 Location of the residues selected to produce the double cysteine mutants. These residues are shown in an NMR structure of Erbin PDZ (light gray) bound to the TGWETWV peptide (red) that has been fused to the C-terminal of the targets (ubiquitin and MBP) used in this work. The numbering of the mutated residues corresponds to that of the NMR structure1N7T.

The tagging efficiency was determined by HPLC-MS. For example, reduced PDZ-5 (before the tagging reaction) has a molecular weight of 10720.1, but after the tagging reaction with pre-loaded CLaNP-5 (Tm^{3+}), this mutant had a molecular weight of 11502.9, which is in accordance with the theoretical value of 11502.1. In figure 3.6a, the elution profile of the tagging mixture of PDZ-1 by reverse phase HPLC can be seen. In this case one single main peak corresponding to the tagged protein can be observed. However, two other small peaks were also detected; one corresponds to the untagged protein and another one corresponds to the formation of PDZ dimers. These dimers are not produced quantitatively during the tagging reaction (<5%), but they can be observed in SDS-PAGE electrophoresis (figure 3.6b) as a very weak band above the

successfully tagged PDZ mutant.
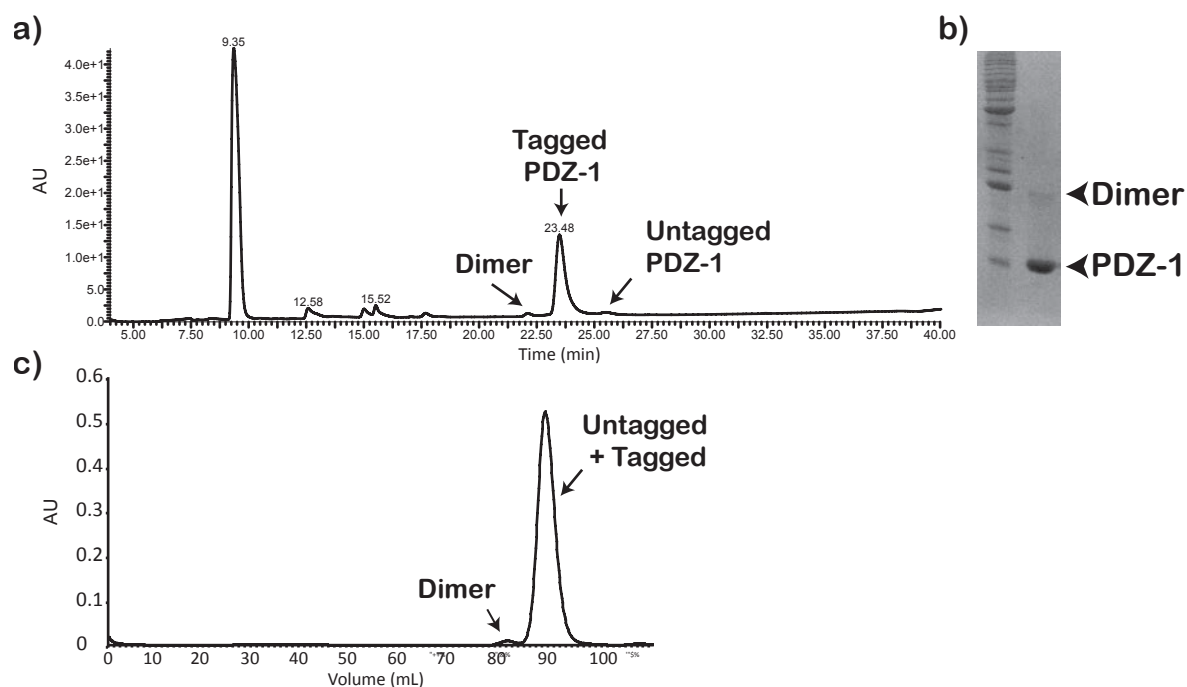
Figure 3.6 Analysis of the tagging reaction of PDZ-1. a) HPLC analysis with UV detection. The peak at 23.48 minutes corresponds to the expected molecular weight of PDZ-1 tagged with CLaNP-5 loaded with Tm^{3+}. b) SDS-PAGE after the tagging reaction. c) Gel filtration chromatography using a Superdex 75 column to separate a mixture of tagged and untagged PDZ.

In the case of mutants with low tagging yields, different purification methods were carried out in order to separate tagged from the untagged protein. Gel filtration chromatography using a Superdex 75 column was one of these methods. This column is designed to separate molecules in the range from 3 to 70 KDa; nevertheless it was impossible to separate these species by gel filtration (figure 3.6c).

Another attempt to separate untagged protein was done by using activated thiol sepharose 4B. This is a resin that binds covalently the thiol group of reduced cysteine residues. The purification procedure was done according to the recommendations of the manufacturer, however NMR spectra of the paramagnetic samples still show the presence of a diamagnetic untagged

population.

3.4 Isothermal titration calorimetric studies of the double cysteine PDZ mutants

In sections 3.1 and 3.2, it was shown that wild type PDZ could bind MBP^{TGWETWV} as well as ubiquitin^{TGWETWV}. However, the different double cysteine PDZ mutants are the real material of this project because these are the proteins that will be tagged with CLaNP-5 to bind and transfer the paramagnetic effects to the targets. Therefore, the affinity of these mutants for the targets was measured using isothermal titration calorimetry (table 3.2).

PDZ construct	Protein	K_d (µM)
PDZ wild type	MBP	0.8 ± 0.03
PDZ wild type	Ubiquitin	4.1 ± 0.6
PDZ-1	Ubiquitin	5.0 ± 1.5
PDZ-2	Ubiquitin	6.1 ± 0.6
PDZ-3	Ubiquitin	14.8 ± 1.3
PDZ-5	Ubiquitin	6.2 ± 1.2
PDZ-6	Ubiquitin	4.8 ± 0.5

Table 3.2 Dissociation constants of the different PDZ constructs for TGWETWV-fused targets (Camacho-Zarco AR et al. 2014).

The affinity of PDZ for the free TGWETWV peptide (K_d = 0.15 um) is higher than when it is fused to any of the two targets. Another interesting point is that the affinity of wild type PDZ for MBP^{TGWETWV} is higher than for ubiquitin^{TGWETWV}. A possible reason for the lower affinity of PDZ for ubiquitin^{TGWETWV} could be the possible transient interaction between the TGWETWV peptide and the surface of ubiquitin, the same interaction that is proposed to produce the chemical shift changes observed when ubiquitin^{TGWETWV} is not bound to PDZ (figure 3.1). In this hypothesis, the transient interaction

would "compete" with PDZ for binding the TGWETWV peptide. In addition, PDZ-3 binds with lower affinity to ubiquitin^{TGWETWV} than the other mutants. The reason for this lower affinity is unknown. However, the important fact of these ITC measurements is that all the PDZ mutants bind in the low micromolar range both targets. Actually, even the PDZ mutant with the lowest affinity has a dissociation constant sufficient for the purposes of this method because most NMR experiments require protein concentrations above 100 μM.

3.5 Analysis of residual dipolar couplings obtained from ubiquitin^{TGWETWV}.

By NMR titrations and ITC, we already knew that all the PDZ mutants were able to bind both targets. However, the CLaNP-5 tagged reporters were added to ^{15}N labeled ubiquitin^{TGWETWV} in order to test if they can transfer the paramagnetic effects to the targets.
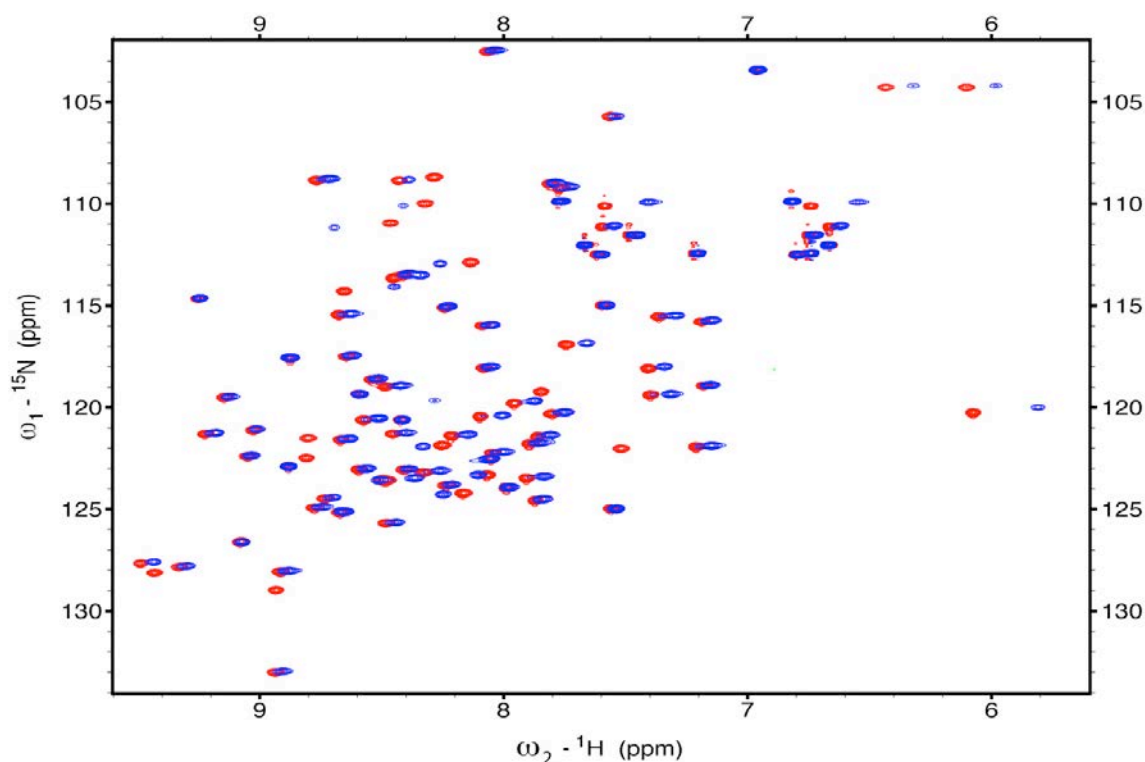
Figure 3.7 PDZ-1 tagged with CLaNP-5 preloaded with Lu^{3+} (red) or Tm^{3+} (blue) were added in excess (2:1 ratio) in order to saturate 15N-ubiquitin^{TGWETWV}. ^{1}H-^{15}N HSQC spectra were recorded at a ^{1}H Larmor frequency of 900 MHz and 310 K (Camacho-Zarco AR et al. 2014).

In figure 3.7 are overlapped two NMR spectra, a reference spectrum after addition of PDZ-1 loaded with the diamagnetic Lu^{3} (red) and another spectrum after adding PDZ-1 loaded paramagnetic (Tm^{3+}) to ^{15}N labeled ubiquitin^{TGWETWV}. A quick look at these spectra reveals changes in the chemical shift of several NMR signals produced by pseudocontact shifts (PCS). Moreover, it is also clear that the intensity of most of the signals in the paramagnetic spectrum is weaker

than the diamagnetic ones, a clear indication of the presence of paramagnetic

relaxation enhancement (PRE).
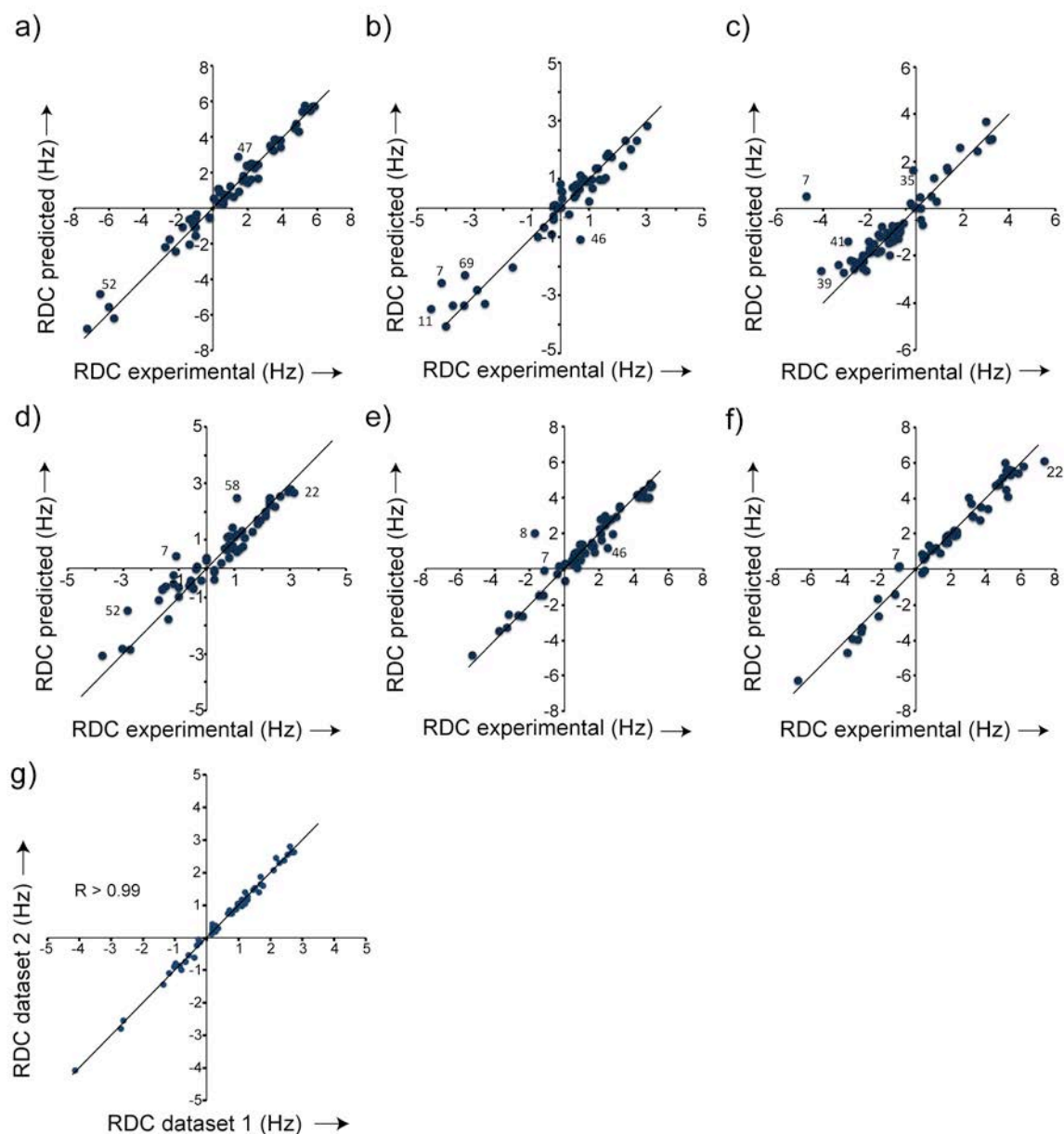
Figure 3.8 (**a-f**) Experimental versus back-calculated theoretical values of RDCs induced in ubiquitin[TGWETWV] upon binding of PDZ reporters 1, 2, 3, 5, 6 and 7 respectively. All datasets were acquired at a [1]H Larmor frequency of 900 MHz and the same temperature (310K) and buffer conditions. The black line on each plot represents y = x. **g**) Correlation of two experimental RDC datasets acquired from ^{15}N-labelled ubiquitin[TGWETWV] bound to PDZ-1 (Camacho-Zarco AR et al. 2014) at a [1]H Larmor frequency of 600 MHz using the BSD-IPAP HSQC pulse sequence (Yao LS et al. 2009) in the same experimental conditions.

All of these observations strongly suggest that paramagnetic effects were transmitted from the reporter PDZ-1 to the target that is ^{15}N-labelled ubiquitin^{TGWETWV}. Subsequently, orientational restraints in the form of residual dipolar couplings were measured after the addition of each PDZ mutant. The measured RDCs, which were induced in ubiquitin^{TGWETWV} due to binding of the paramagnetic PDZ variants, were used (along with the reported structure 1D3Z of wild type ubiquitin) to determine each of the alignment tensors and back-calculate theoretical RDC values. In figure 3.8 plots of experimental versus back-calculated RDCs for all the datasets produced by the PDZ reporters are presented.

It can be observed from these plots that all of the PDZ reporters were able to produce RDCs. Moreover, all the datasets correlate highly with the theoretical values. For example, PDZ-1 produced RDCs in the range from -7.3 to 5.8 Hz at 900 MHz with a Pearson's correlation of 0.99. Other PDZ mutants produced significantly smaller RDCs. PDZ-5 produced RDCs in the range from about -3 to 3 Hz and PDZ-3 from about -4 to 4Hz. Nonetheless, the Pearson's correlation coefficient was higher than 0.96 for all the datasets (table 3.3). A different quality parameter, the Q-factor, was below 0.2 in all cases, consistent with the high quality of the data.

The reproducibility of the data is an important factor that was tested. Two independent data sets of RDCs were acquired at a ^{1}H Larmor frequency of 600 MHz in the same experimental conditions. According to the theory, the RDCs were expected to decrease by a factor of 2.25 due to the change in the strength of the magnetic field. The magnitude of the RDCs decreased as expected, nonetheless the Pearson's coefficient was 0.98 when compared to theoretical values. The reproducibility was high, with an RMS between both datasets of just

0.14 (figure 3.8g).

	PDZ-1	PDZ-2	PDZ-3	PDZ-5	PDZ-6	PDZ-7
# RDCs	60	51	61	59	57	53
G. magnitude	4.7e-4	2.7e-4	2.3e-4	2.2e-4	3.8e-4	4.7e-4
Ax. component	-2.7e-4	-1.6e-4	1.4e-4	-1.2e-4	-2.2e-4	-2.7e-4
Rh. component	-1.3e-4	-0.6e-4	0.5e-4	-0.6e-4	-1.1e-4	-1.3e-4
Q-factor	0.1	0.18	0.16	0.14	0.1	0.11
RMS	0.4	0.51	0.37	0.32	0.38	0.51
R	0.99	0.96	0.97	0.98	0.99	0.99

Table 3.3 Characteristics of the RDC datasets and alignment tensors produced by the PDZ reporters in ubiquitin^{TGWETWV}. The alignment tensors were determined using the ubiquitin structure 1D3Z and the software PALES. The axial (A_a) and rhombic (A_r) component of the alignment tensor are defined as $A_a = S_{zz}$ and $A_r = 2/3\ (S_{xx} - S_{yy})$ respectively (Zweckstetter M. 2008). All of the RDCs were acquired at a ^{1}H Larmor frequency of 900 MHz and the same temperature (310K) and buffer conditions.

A further important goal of the present thesis was to develop a method capable of producing orientationally independent paramagnetic alignments. The difference in the orientation of the tensors listed in table 3.3 was therefore determined by obtaining the 5D angle between the alignment tensors induced in ubiquitin^{TGWETWV} (figure 3.9g). The analysis showed that the orientation of the alignments induced in ubiquitin were different by at least by 9° between the different mutants, but it reached for example up to 154° in the case of PDZ-3 and PDZ-7.
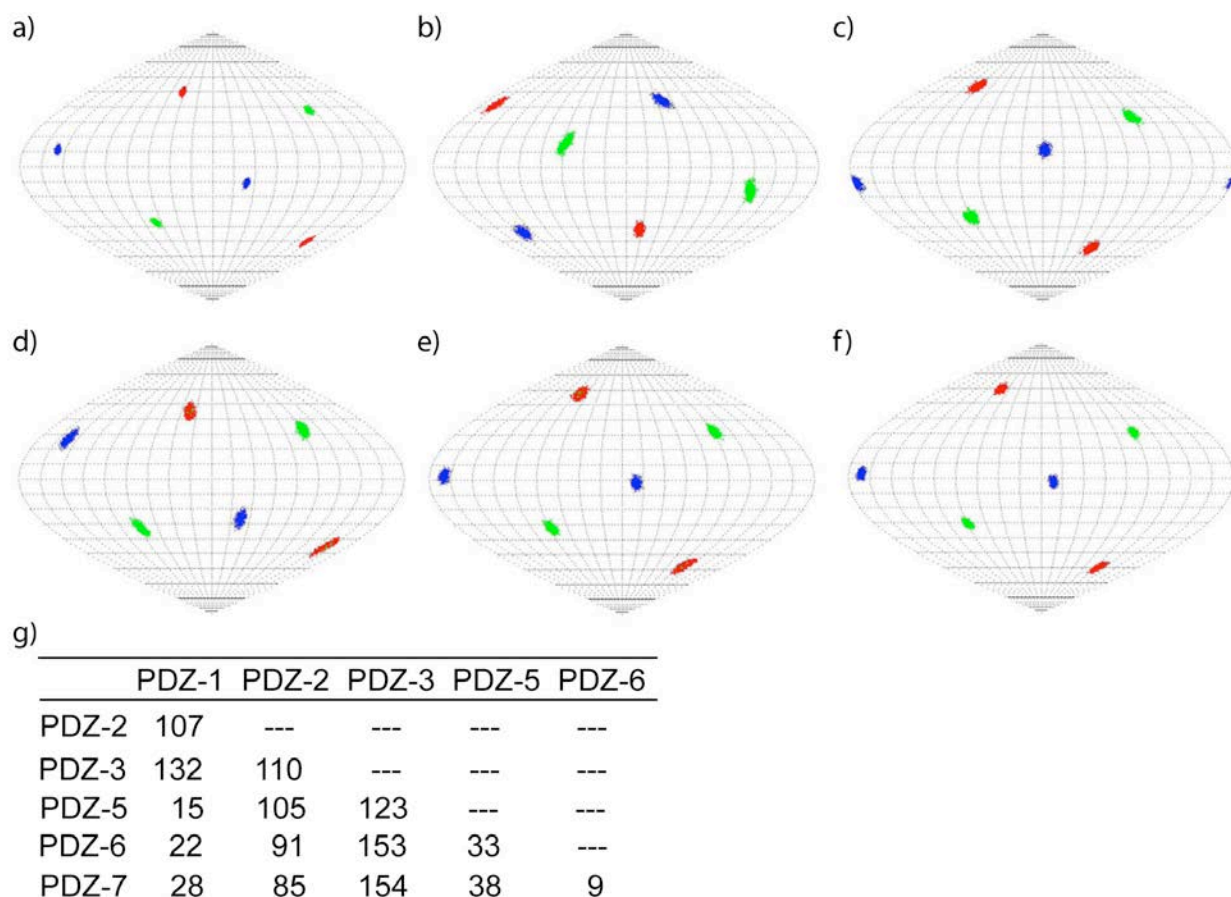
Figure 3.9 (**a**–**f**) Orientations of the alignment tensors transferred to ubiquitin^TGWETVW by the reporter PDZ mutants 1, 2, 3, 5, 6 and 7, respectively. The z, y and x axis are shown in red, blue and green in Sanson-Flamsteed projections. The uncertainties were evaluated by 1000 cycles of the structural noise Monte-Carlo method. **g**) 5D angles between the alignment tensors (Sass J et al. 1999) transferred to ubiquitin^TGWETVW.

The results from the measurement of RDCs in ubiquitin^TGWETWV were encouraging. Nevertheless it is important to prove the applicability of this method to more than one protein. The maltose binding protein, a bigger protein than ubiquitin, was used as a second target for the designed set of PDZ reporters.

3.6 Analysis of residual dipolar couplings obtained from MBP^{TGWETWV}.

The different PDZ reporters were added to a second protein to test the method, the 370 residues maltose binding protein (MBP^{TGWETWV}). The reporters, tagged with ClaNP-5 and loaded with Lu^{3+} or Tm^{3+} were added in excess (2:1) regarding the concentration of MBP^{TGWETWV} in order to saturate it in the samples. The spectra acquired after the addition of PDZ-1 can be observed in figure 3.10. There are shifts in the position of the signals after the addition of the paramagnetic PDZ-1, a clear indication of PCSs, just like in the case of ubiquitin^{TGWETWV}.
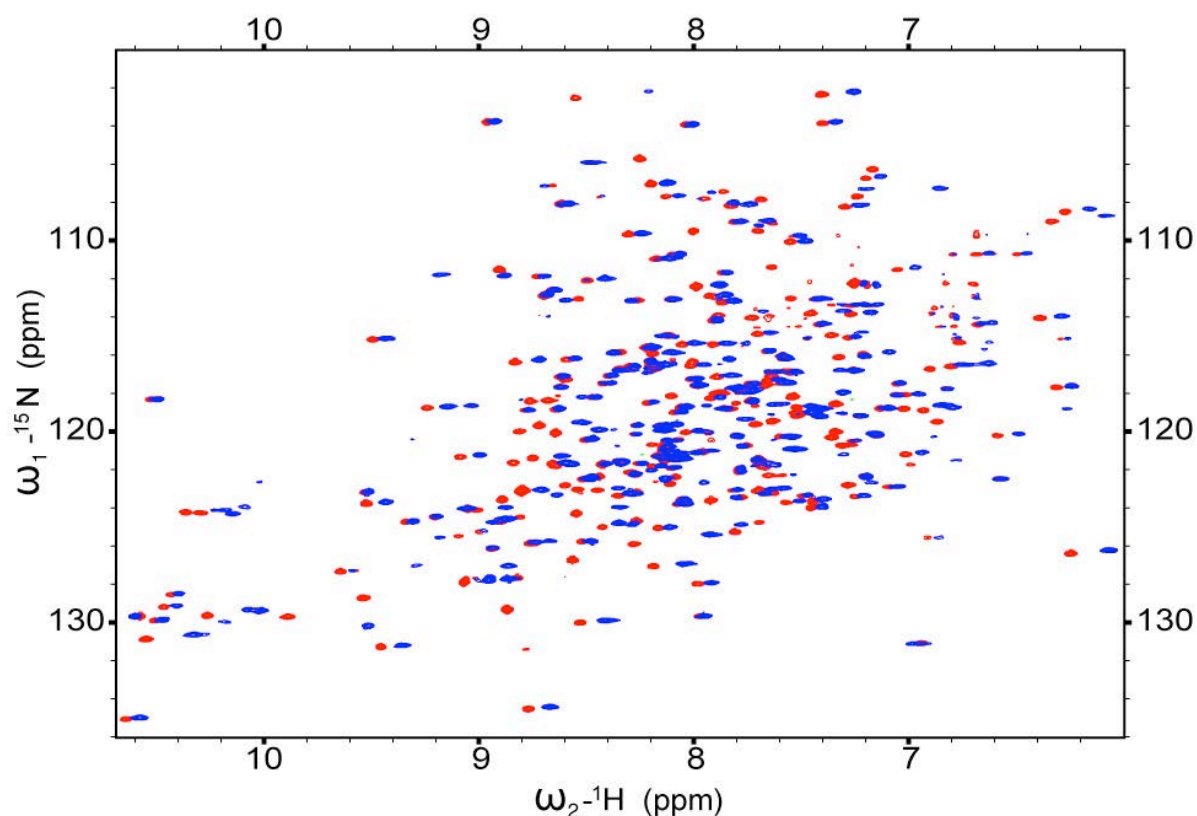
Figure 3.10 Superposition of 1H- 15N HSQC spectra of MBP^{TGWETWV} bound to PDZ-1, which had been tagged with CLaNP-5 preloaded with Lu^{3+} (red) or Tm^{3+} (blue). The spectra were recorded at a ^{1}H Larmor frequency of 900 MHz and 310 K (Camacho-Zarco AR et al. 2014).

Experimental RDCs were measured after the addition of each one of the PDZ mutants and these were fitted to the MBP structure 1DMB to determine the respective alignment tensors and back-calculate the theoretical RDC values (figure 3.11). PDZ-2 produced RDCs in the range from -11.2 to 7.9 Hz (figure 3.11b), the biggest of all the mutants. However, some PDZ mutants produced smaller RDCs. For example, RDCs produced by PDZ-3 were in the range from -3.5 to 3.5 Hz and those from PDZ-5 were from -4 to 5 Hz. The experimental RDCs were fitted to a reported 3D structure of MBP to determine the alignment tensors and back-calculate theoretical RDCs (figure 3.11).
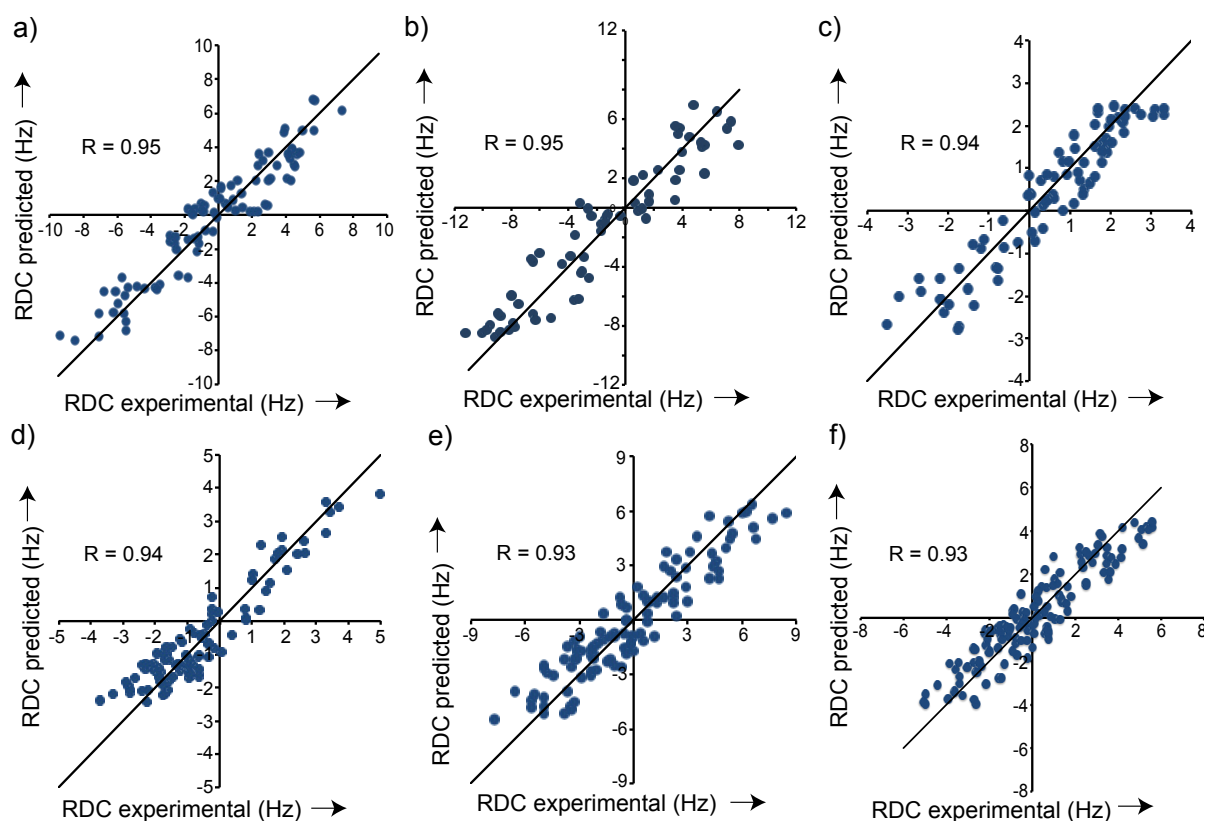
Figure 3.11 Comparison of experimental RDCs with values back-calculated from MBP's 3D structure (Camacho-Zarco AR et al. 2014). **a**) - **e**) Experimental N-H RDCs measured from 2D experiments in ^{2}H, ^{15}N-MBP^{TGWETWV} bound to PDZ-1, PDZ-2, PDZ-3, PDZ-5 and PDZ-6 respectively, were fit to the structure 1DMB using the software PALES. **f**) N-H RDCs were also measured by a 3D HNCO-based experiment at a 1H Larmor frequency of 700 MHz in MBPTGWWTWV bound to PDZ-1. All data were recorded at 310 K. The black lines in the plots mark y=x. Pearson's correlation factor, R, between experimental and back-calculated values are indicated.

The fit to the wild type MBP structure resulted in Pearson's correlation coefficients above 0.93 in all the cases and the Q-factor remained below 0.3 (table 3.4). The general magnitude and the axial component of the paramagnetic alignments produced by PDZ-3 and PDZ-5 are the smallest among the mutants, which is in accordance to the smaller magnitude of the RDCs produced by these mutants (table 3.4).

Table 3.4 Parameters of the alignment tensors transferred by the PDZ reporters to MBP[TGWETWV]. RDC data from PDZ-1 and PDZ-3 was acquired at [1]H-Larmor frequency of 800 MHz; the other datasets were acquired at 900 MHz. All data was acquired at 310 K.

	PDZ-1	PDZ-2	PDZ-3	PDZ-5	PDZ-6
G. magnitude	5.4e-4	6.6e-4	1.9e-4	2.5e-4	4.6e-4
Ax. component	-3.0e-4	-3.8e-4	-1.2e-4	1.6e-4	2.8e-4
Rh. component	-1.7e-4	-1.8e-4	-0.5e-4	0.3e-4	1.2e-4
Q-factor	0.23	0.26	0.29	0.24	0.28
RMS	1.2	1.6	0.68	0.6	1.4
R	0.95	0.95	0.94	0.94	0.93

The high quality of the data allowed an accurate determination of the orientation of the three axes of the tensors, which can be observed in figure 3.12 in Samson-Flamsteed projections. The orientation of the axes was quite different between the different PDZ reporters. The 5D angle revealed that the alignment tensors were separated by at least 30° for any pair of alignments, but this difference reached 90° and even 130° for other pairs, like in the case of PDZ-2 and PDZ-3.
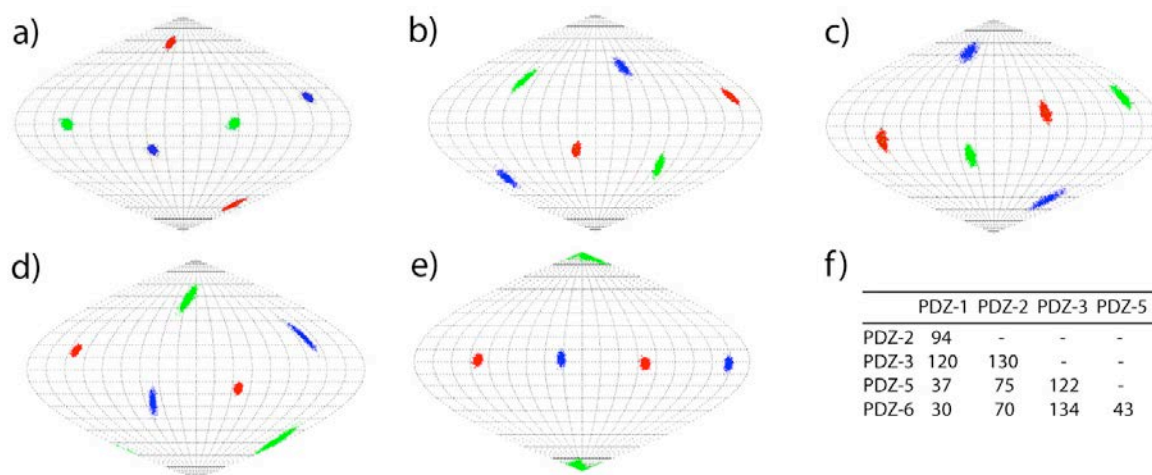
Figure 3.12 Orientations of the alignment tensors transferred to MBP^{TGWETVW} by the reporter PDZ mutants 1, 2, 3, 5 and 6 (**a–e**), respectively (Camacho-Zarco AR et al. 2014). The z, y and x axis are shown in red, blue and green in Samson-Flamsteed projections, respectively. The uncertainties were evaluated by 1000 cycles of the structural noise Monte-Carlo method (Zweckstetter M et al. 2002). **f**) 5D angles between the alignment tensors (Sass J et al. 1999) transferred to MBP^{TGWETVW}.

3.7 Analysis of pseudocontact shifts (PCS) observed in ubiquitin^{TGWETWV}.

Pseudocontact shifts are observed as changes in the chemical shift of a signal in NMR spectra due to the addition of a paramagnetic lanthanide (John M et al. 2007). PCSs of ^{1}H and ^{15}N are quite similar regarding their magnitude, producing signals displacements along nearly parallel lines in ^{1}H, ^{15}N-HSQC spectra. An example comes from the PCSs produced by PDZ-2, which produced large displacements (around -0.5 ppm in the ^{1}H dimension) in the case of residues 36, 39 and 41 (figure 3.13a). In accordance to RDC data, the magnitude of the measured PCSs was different depending on the PDZ variant that produced them. For example, PCSs produced by PDZ-3 (figure 3.13b) and PDZ-5 were too small (below 0.2 ppm) to be analyzed.
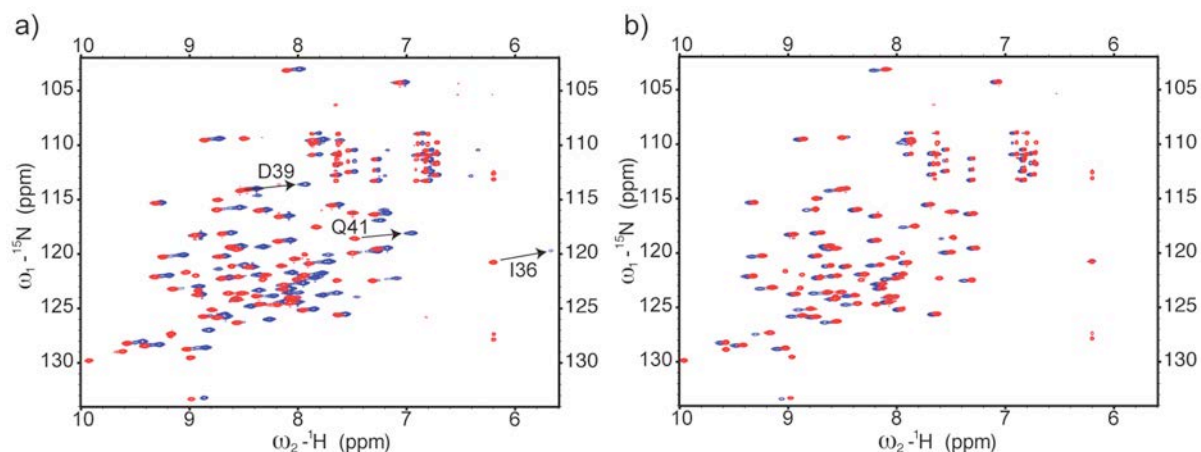
Figure 4.13 Overlapped ^1H, ^{15}N-HSQC spectra of ^2H, ^{15}N-ubiquitin^{TGWETWV} bound to **a)** PDZ-2 and **b)** PDZ-3 tagged with CLaNP-5 loaded with Lu^{3+} (red) or the paramagnetic Tm^{3+} (blue).

The PCSs produced by all the mutants were negative; the only exception was PDZ-3 (figure 3.13b), which produced shifts in the opposite direction compare to the other PDZ reporters (compare with figure 3.13a). The experimental PCSs from PDZ-1, PDZ-2, PDZ-6 and PDZ-7 were used together with the ubiquitin structure 1D3Z to calculate the tensors and then back-calculate the theoretical PCS values (figure 3.14). Most of the experimental PCS values were below -0.3 ppm. Nevertheless, the correlation between experimental and back-calculated values was above 0.97 for all the analyzed data.
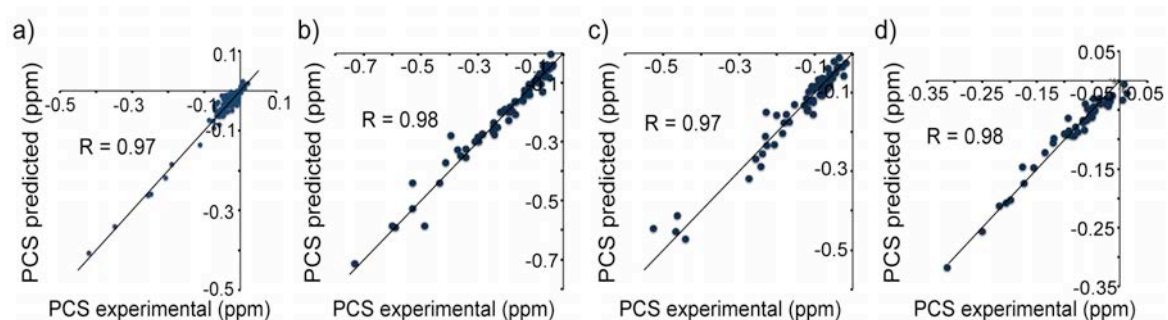
Figure 3.14 Comparison of experimental and back-calculated (^HN) PCSs in ubiquitin. (a-d) Experimental PCSs produced by PDZ-1, PDZ-2, PDZ-6 and PDZ-7 on ubiquitin^{TGWETWB} were fitted to the structure 1D3Z using the software Numbat (Schmitz C et al. 2008). The determined alignment tensors were used to back-calculate PCSs that were compared to experimental PCSs.

3.8 Analysis of pseudocontact shifts (PCS) observed in MBP^{TGWETWV}

PCSs were also produced after the addition of the PDZ reporters to MBP^{TGWETWV}. Diamagnetic as well as paramagnetic spectra were recorded for each one of the PDZ mutants and then compared to determine PCSs. PCS are clearly present after the addition of paramagnetic PDZ-1 (figure 3.10). Moreover, PCSs were observed after the addition of PDZ-2 and PDZ-6. The reporters PDZ-3 and PDZ-5 produced significantly smaller PCSs on MBP^{TGWETWV} (figure 3.15b,c).
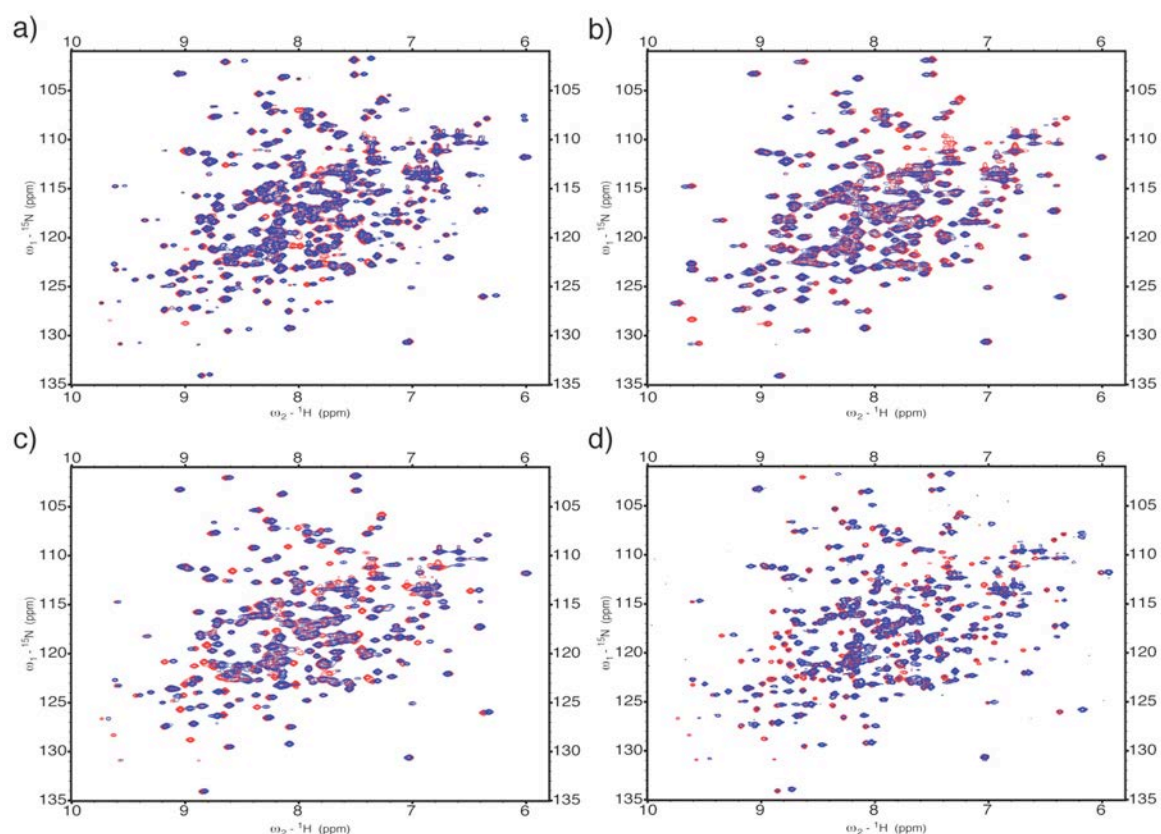
Figure 3.15 Superposition of ^{1}H, ^{15}N-HSQC spectra of ^{2}H, ^{15}N-MBP^{TGWETWV} bound to the PDZ reporters tagged CLaNP-5 loaded with Lu^{3+} (red) or the paramagnetic Tm^{3+} (blue). (**a-d**) Spectra recorded after addition of PDZ-2, PDZ-3, PDZ-5 and PDZ-6 respectively at 310K.

Experimental PCSs produced by PDZ-1, PDZ-2 and PDZ-6 had a similar range, from -0.6 to 0.1 ppm (figure 3.15). Experimental PCSs produced by these reporters were fitted to the reported 3D structure of wild type MBP (PDB code:

1DMB). The alignment tensors were determined and used to back-calculate theoretical PCSs, which were compared to the experimental ones (figure 3.16). The correlation coefficients obtained for PDZ-1, PDZ-2 and PDZ-6 were above 0.97 for these datasets. In the case of PDZ-3 and PDZ-5, the alignment tensors could not be determined due to the small magnitude of these PCSs.
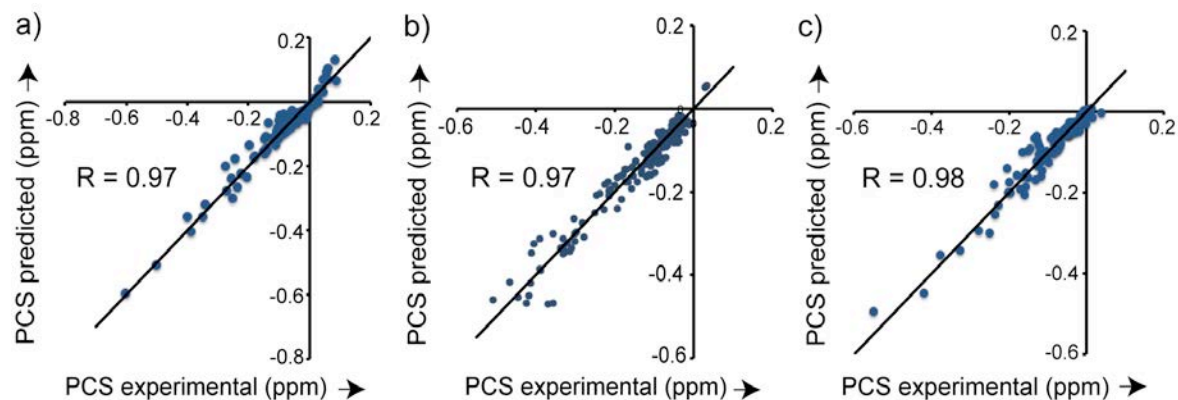
Figure 3.16 Comparison of experimental and back-calculated (^{H}N) PCSs. (a-c) Experimental PCSs produced by PDZ-1, PDZ-2 and PDZ-6 on MBP^{TGWETWB} were fitted to the structure 1DMB using the software Numbat (Schmitz C et al. 2008). The determined alignment tensors were used to back-calculate PCSs.

3.9 Analysis of paramagnetic relaxation enhancement observed in ubiquitin^{TGWETWV}

Paramagnetic relaxation enhancement is observed in NMR spectra as a distance-dependent decrease in the intensity of NMR signals, in the present method, the distance between a certain atomic nucleus from the target and the paramagnetic center in the lanthanide attached to the PDZ reporter. However, the addition of high concentrations of a paramagnetic PDZ (CLaNP-5/Tm^{3+}) could produce in addition "solvent-PRE-effect". This is unspecific PRE due to the presence of unbound paramagnetic reporter in the solvent that could interfere with the accurate measurement of PRE produced by PDZ bound to

ubiquitin[TGWETWV]. According to the literature (Clore GM et al. 2009), solvent-PRE is not observed when using concentrations of lanthanide below 0.5 mM, the concentration of the paramagnetic PDZ reporters used in this work. The presence of solvent-PRE in our studies was verified experimentally by comparing the signal intensity of the NMR spectra of two samples with the same concentration of wild type ubiquitin (I.e. without the PDZ binding motif), but one containing in addition paramagnetic PDZ-6 at the concentration used in the present experiments (figure 3.17).
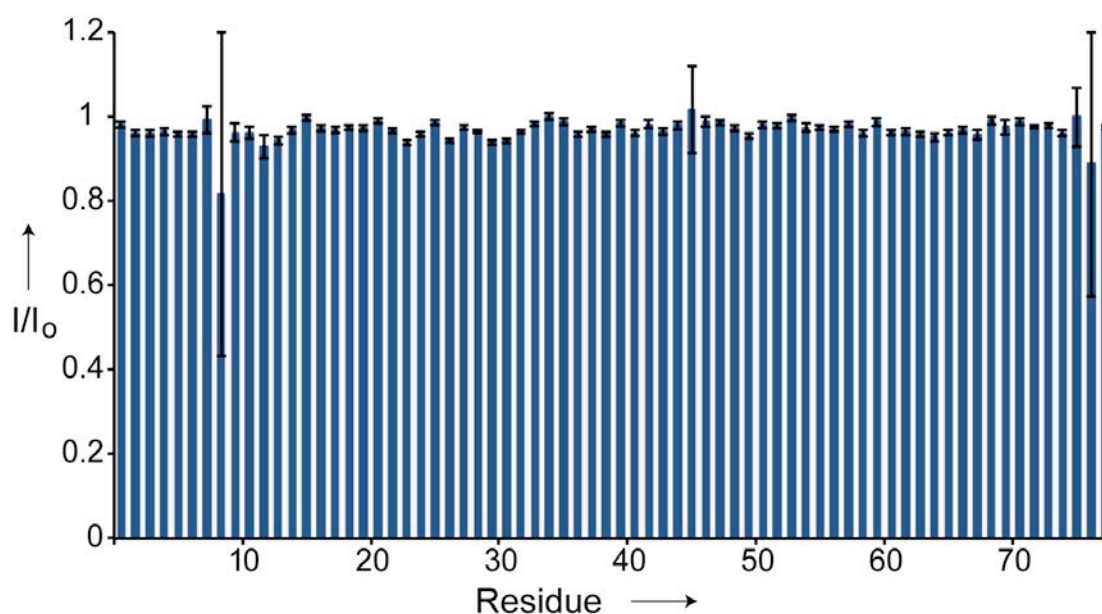
Figure 3.17 Ratio of signal intensities in ^{1}H,^{15}N HSQC spectra of ^{15}N-labeled wild type ubiquitin in the absence (I_0) or presence of 0.5 mM (two-fold excess) of CLaNP-5/Tm^{3+} tagged PDZ-6.

The data showed that signal intensities were very similar, demonstrating that the solvent-PRE-effect does not contribute significantly in the current conditions. PRE was measured as the intensity ratio of the signals recorded in the diamagnetic (I_0) and paramagnetic samples (figure 3.18).
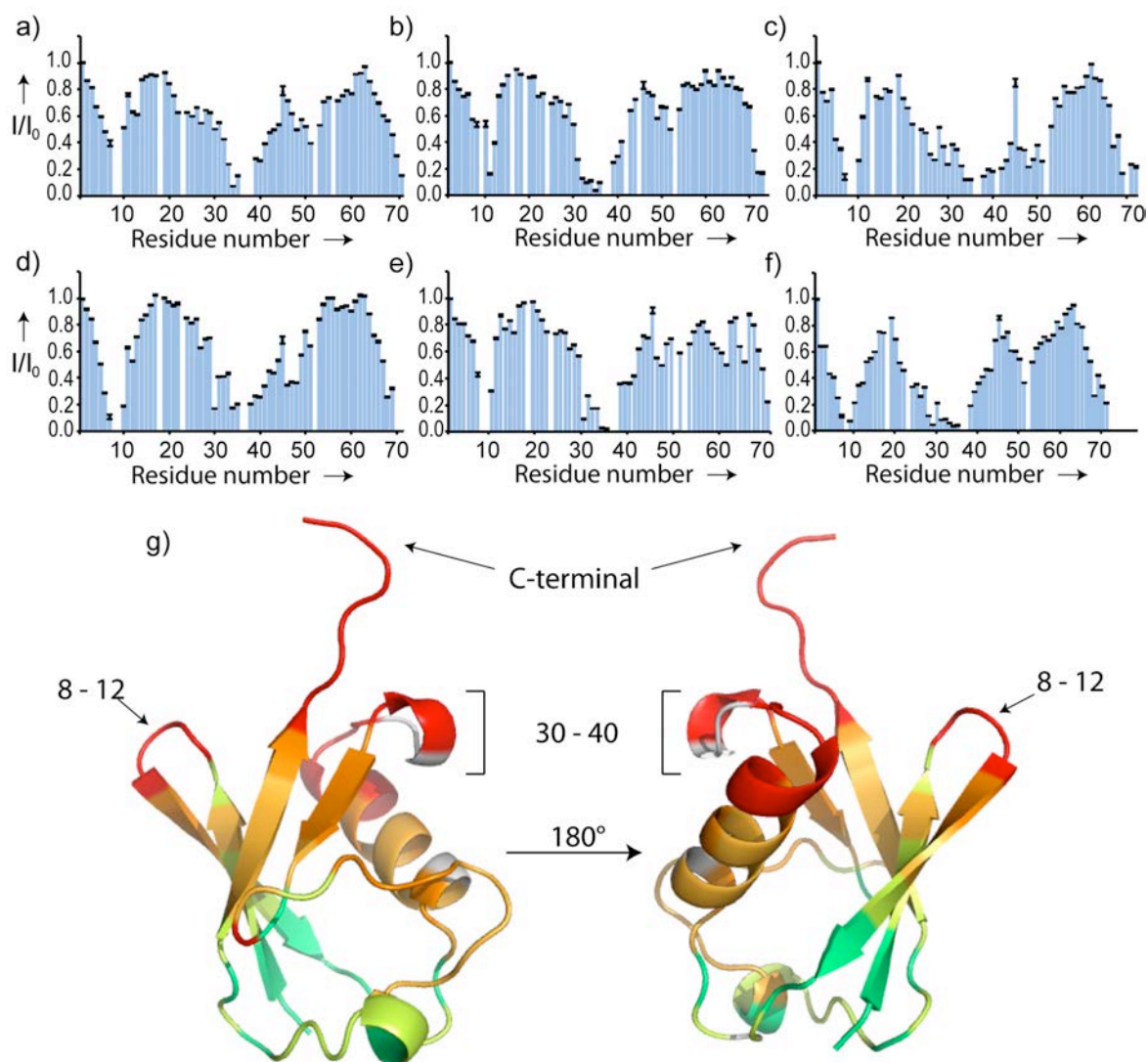
Figure 3.18 PRE profiles in ubiquitin[TGWETWV] upon addition of PDZ tagged with CLaNP-5 preloaded with Tm^{3+}. (**a**-**f**) Intensity ratios (paramagnetic/diamagnetic sample) produced due to the addition of PDZ-1, PDZ-2, PDZ-3, PDZ-5, PDZ-6 and PDZ-7 respectively. Error bars were calculated based on signal to noise ration in the NMR spectra. Only cross-peaks not strongly affected by signal overlap were included into the analysis. **g**) PRE broadening induced by PDZ-1 was mapped onto ubiquitin's 3D structure (PDB code: 1D3Z). From red (most affected) to green (unaffected), distance-dependent changes in signal intensity are shown.

Residue-specific analysis showed that the regions spanned by residues 8-12, 30-40 and the C-terminal region are most affected by PRE after the addition of the different paramagnetic PDZ reporters. The intensity profile produced by PDZ-7 was plotted onto the 3D structure of ubiquitin to highlight the most broadened regions (figure 3.18g); regions 8-12 and 30-40 are close to the C-

terminal region, where PDZ is binding. Conversely, residues that didn't experience PRE (green) are far from the C-terminus.

3.10 Analysis of Paramagnetic Relaxation Enhancement observed in MBP^{TGWETWV}.

The transferred PRE from the paramagnetic PDZ reporters to MBP^{TGWETWV} was measured in addition to restraints obtained from RDCs and PCSs. Signals corresponding to residues close to the C-terminal region were most affected (figure 3.19a-d). For example, the addition of paramagnetic PDZ-1 strongly broadened signals from residues 46 to 55 and 69-80, resulting in the disappearance in the paramagnetic spectra (Figure 3.19a).
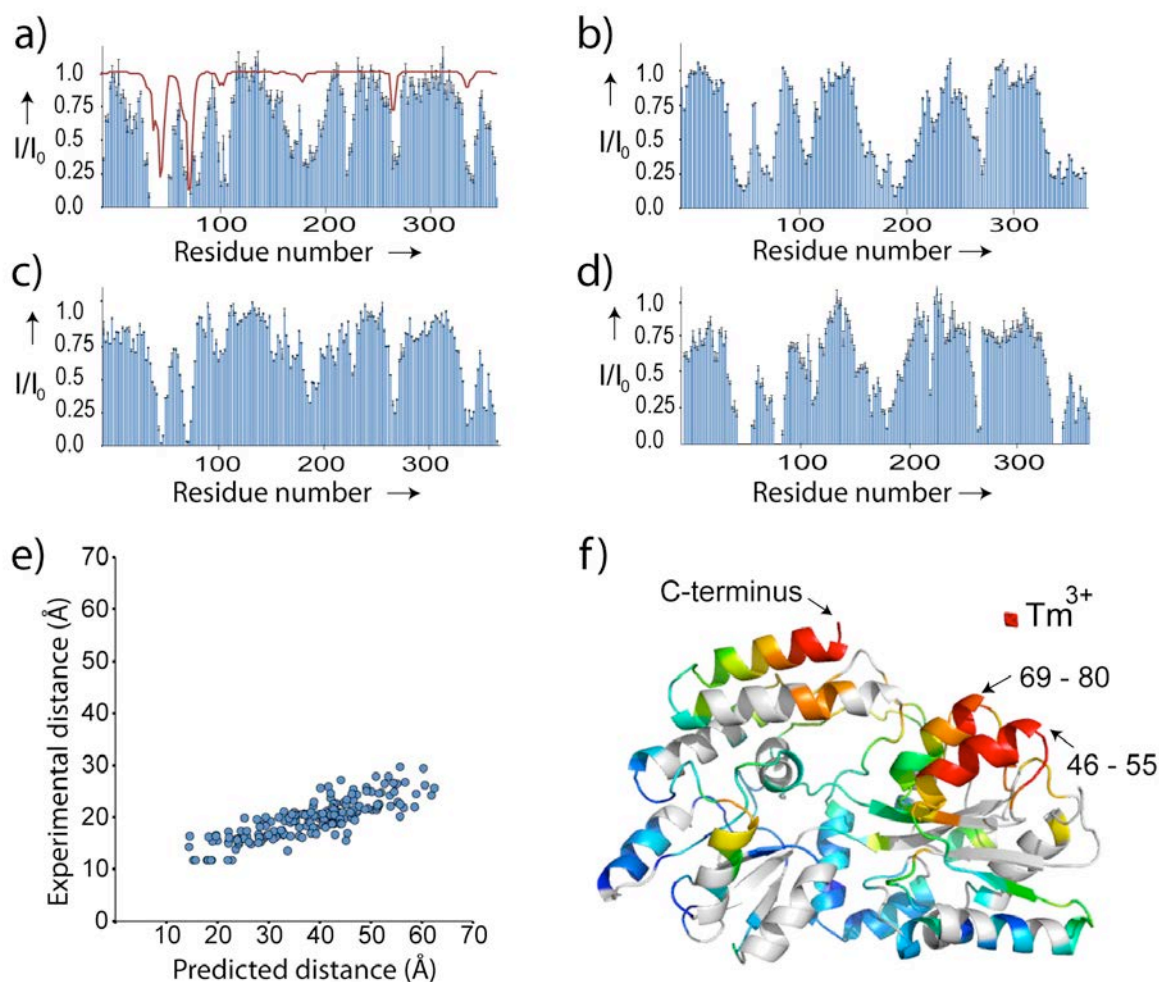
Figure 3.19 PRE profiles observed in MBP^{TGWETWV} upon addition of the PDZ reporters. (**a-d**) PRE profiles (intensity ratios) due to the addition of PDZ-1, PDZ-3, PDZ-5 and PDZ-6, respectively. Error bars were calculated based on signal-to-noise ratios in the NMR spectra (Camacho-Zarco AR et al. 2014). Only cross-peaks not strongly affected by signal overlap were included into the analysis. The line in the plot which shows the PDZ-1 data, indicates the back-calculated intensity ratios obtained from the distance between the amide proton and the paramagnetic center. **e**) Experimental intensity ratios measured after the addition of PDZ-1 were converted into distances between the amide proton and the paramagnetic center and compared to predicted distances derived from MBP's 3D structure (PDB code: 1DMB). **f**) PRE broadening induced by PDZ-1 was mapped onto MBP's 3D structure. From red (most affected) to blue (unaffected), distance-dependent changes in signal intensity are shown. The red sphere marks the position of the lanthanide derived from experimental PCSs.

The decrease in the signal intensities produced by paramagnetic PDZ-1 (Tm^{3+}) was back calculated by taking into account that it is mainly due to Curie relaxation (Koehler J et al. 2011). However, it is necessary to determine the position of the lanthanide with respect to MBP in order to back-calculate the PRE effects. PCSs can be used to determine the position of the lanthanide because they depend on both, the distance between the lanthanide and the observed spin but also the orientation of the alignment tensor. Therefore, the experimental PCSs analyzed before (figure 3.16a) were used to determine the location of the lanthanide (when adding PDZ-1) in the 3D structure of MBP (figure 3.19f).

Back-calculation of the PRE-induced intensity profile shows less broadening than it is observed experimentally (figure 3.19a). An explanation for this difference may come from dynamic processes of the lanthanide with respect to the position of the target, a possibility that was explored experimentally in this work.

3.11 ^{15}N R$_2$ spin-relaxation rates of ubiquitin, MBP and their complexes with PDZ

One of the main challenges regarding the study of large biomolecules by NMR is that signal intensity decreases if the molecular weight increases. Larger molecules produce weaker NMR signals and vice versa. This is because dipole-dipole relaxation, the main mechanism of magnetization decay, is modulated by rotational motion (Solomon I, 1955). This is especially relevant when acquiring 3D NMR experiments because they provide more signal resolution but are less sensitive than 2D NMR experiments. In order to study the effect of PDZ binding on the relaxation properties of the target protein, a time constant that describes the signal decay and determines the linewidth of NMR signals (R$_2$) was measured for ubiquitin, MBP and their complexes with PDZ.
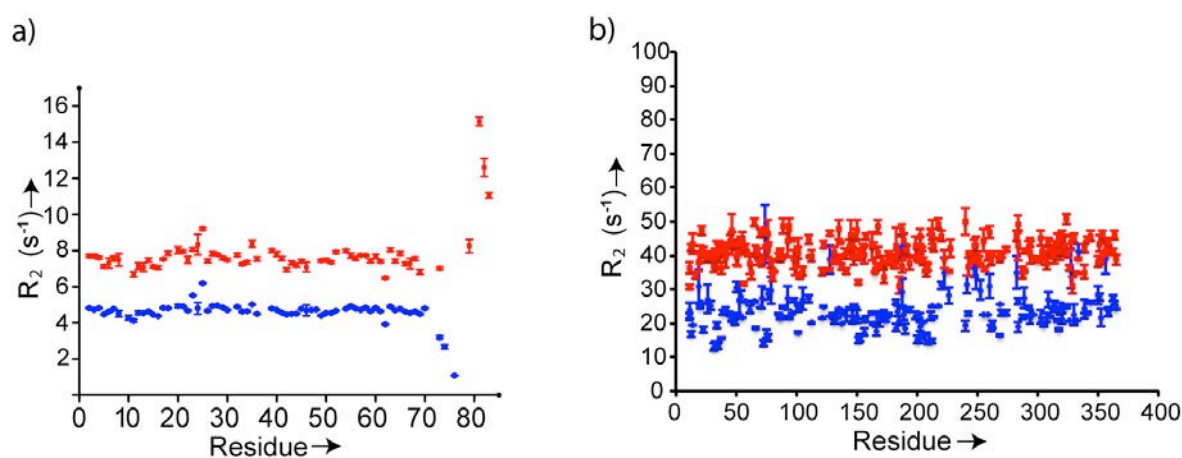
Figure 3.20 ^{15}N R$_2$ spin-relaxation rates of **a**) wild type ubiquitin (blue) and ubiquitin^{TGWETWV} bound to wild type PDZ (red). **b**) Unbound MBP^{TGWETWV} (blue) or bound to wild type PDZ (red). The experiments were recorded at 310 K, 600 MHz (Camacho-Zarco AR et al 2014).

Upon binding to PDZ, the average R$_2$ values in the case of ubiquitin (figure 3.20a) increased from 4.7 to 7.5 Hz and from ~24 to ~44 Hz in MBP (figure 3.20b). In order to test the impact of the increased molecular weight, a 3D experiment was recorded to measure RDCs in MBP^{TGWETWV} bound to PDZ-1

(figure 3.11f). In this experiment, a larger amount of RDCs could be measured due to its higher resolution. Nonetheless the correlation with theoretical data was comparable to RDCs measured with 2D experiments (figure 3.11a-e).

3.12 Paramagnetic effects measured directly on tagged PDZ-1

In the method develop in this thesis the paramagnetic effects are transferred from the CLaNP-5 tagged PDZ reporters to targets that are fused to the TGWETWV recognition peptide. However, the usual way to employ a lanthanide tag is to attach it directly to the target protein and measure the paramagnetic effects that are produced by the paramagnetic center. In order to learn more about the characteristics of the paramagnetic alignment in PDZ (before its transmission to the TGWETWV-fused targets), the paramagnetic effects were measured directly on ^{15}N-labelled PDZ-1.
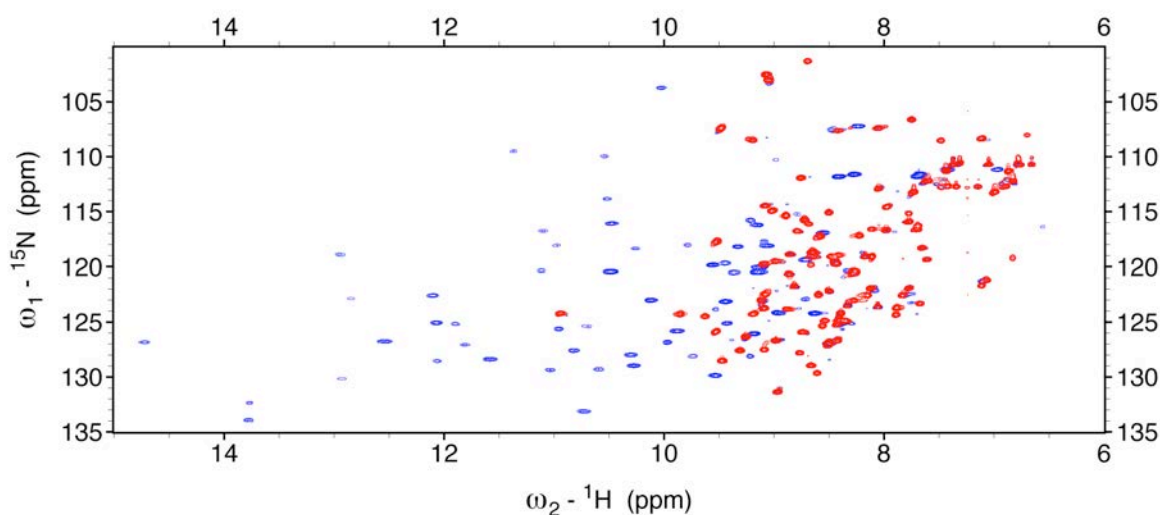
Figure 3.21 Superposition of ^{1}H, ^{15}N HSQC spectra of ^{15}N label PDZ-1 tagged with CLaNP-5 loaded with diamagnetic (red) Lu^{3+} or paramagnetic (blue) Tm^{3+} (Camacho-Zarco AR et al. 2014).

PCS induced directly in PDZ-1 were quite big. Some signals were observed even at 14 ppm in the ^{1}H dimension, meaning that PCS in some cases

were even bigger than 4 ppm. However, not all the signals that appear in the paramagnetic spectrum could be used in the analysis, because their intensity was too small and this complicated the necessary re-assignment. Besides PCS, RDCs were observed in PDZ-1 and ranged from -31.2 to 18 Hz (figure 3.22). Experimental paramagnetic effects were used along with the reported structure of PDZ to determine the alignment tensor and compare it to the transferred alignments transmitted from PDZ-1 to ubiquitin[TGWETWV] and MBP[TGWETWV]. The general magnitude of the alignment produced in PDZ-1 is 1.9e-3 and the axial component of the tensor is 1.14e-3, approximately four-fold bigger than the alignment transferred to the TGWETWV-fused targets tested up to now (table 3.3 and 3.4).
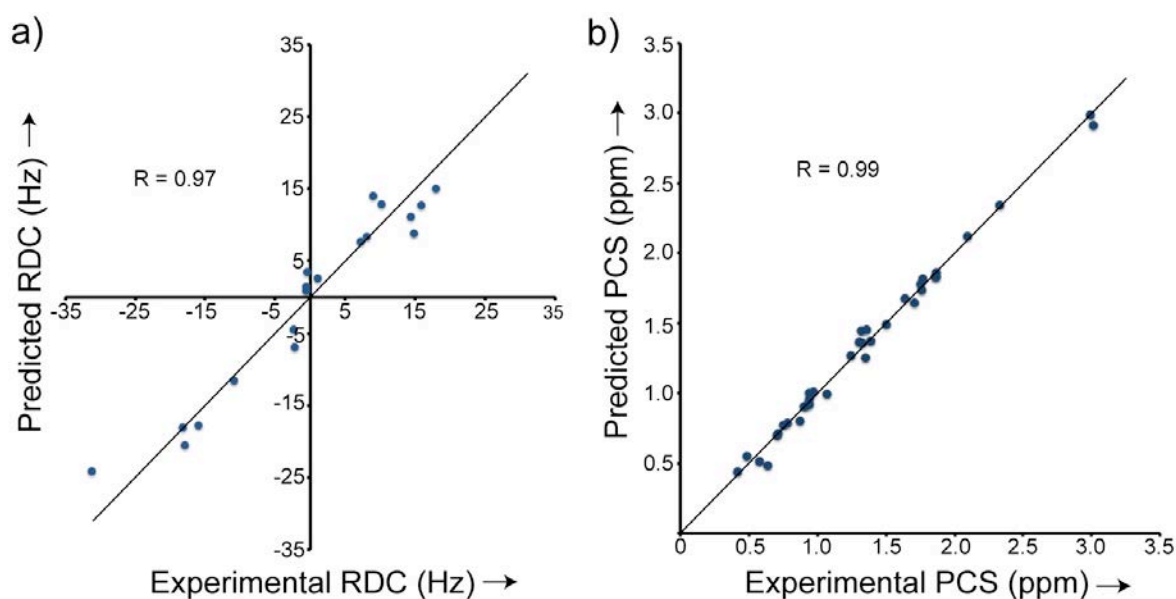
Figure 3.22 Comparison of experimental and back-calculated a) RDCs and b) PCSs observed in ^{15}N-labelled PDZ-1 (Camacho-Zarco AR et al. 2014). Experimental data were fit to the 3D structure 1N7T in order to determine the alignment tensor using the software PALES for RDC (Zweckstetter M et al. 2008) and NUMBAT for PCS (Schmitz C et al. 2008). Experiments were recorded at a [1]H Larmor frequency of 900 MHz, 310 K. The straight line indicates y=x.

3.13 ^{15}N R$_{1\rho}$ spin-relaxation rates of ubiquitin^{TGWETWV} bound to PDZ.

There are several reasons that could explain the decrease in the paramagnetic alignment transferred from PDZ-1 to the TGWETWV-fused targets. One of them is the presence of intermolecular motion between the PDZ reporter and the target protein. In order to explore this hypothesis, the backbone mobility of ubiquitin^{TGWETWV} in complex with wild type PDZ was studied through R$_{1\rho}$ spin-relaxation rates (Palmer AG et al. 2003). Time-dependent conformational fluctuations in the μs -ms timescale can be quantified by this kind of analysis (figure 3.23).
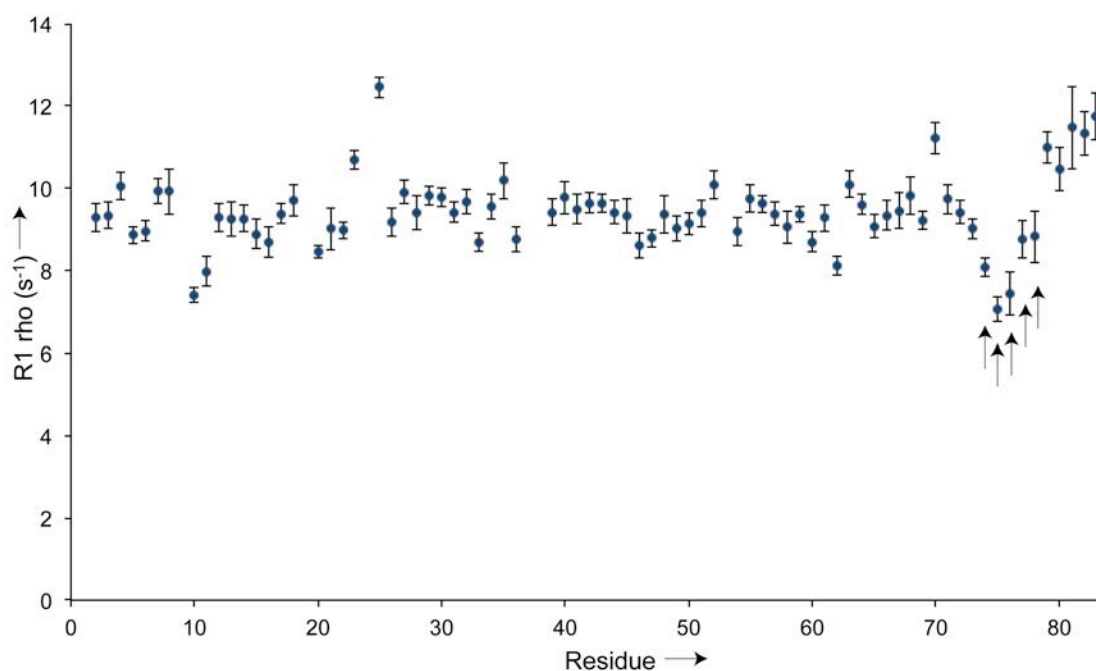
Figure 3.23 ^{15}N R$_{1\rho}$ spin-relaxation rates of ubiquitin^{TGWETWV} bound to wild type PDZ (Camacho-Zarco AR et al. 2014). The black arrows indicate the last three residues of ubiquitin and the first two residues of the PDZ recognition sequence. Experiments were recorded at a ^{1}H Larmor frequency of 600 MHz (298 K).

According to this analysis, the most mobile residues of ubiquitin^{TGWETWV} bound to PDZ are three last three residues of ubiquitin (residues 74 to 76) and the first two residues of the recognition peptide, i.e. TG of the peptide

TGWETWV. In contrast, the last five residues of the recognition peptide don't appear to be mobile, consistent with a strong binding to PDZ. Thus, the linker residues in between ubiquitin^{TGWETWV} and PDZ are flexible, potentially providing an explanation for the decrease in paramagnetic effects upon transmission to the target protein.

3.14 Paramagnetic effects transferred to ubiquitin^{WETWV}

The potential influence of the flexibility of the "linker residues" on the magnitude of the alignment transferred from the PDZ reporters to ubiquitin^{TGWETWV} was tested through a new ubiquitin mutant. It is reported in the literature that the first two residues of the recognition sequence (TG) do not have a central role on its binding to PDZ (Skelton NJ et al. 2003). On the other hand, the C-terminal residues of ubiquitin^{TGWETWV} in complex with PDZ are quite flexible according to our data (figure 3.23). Therefore, the new mutant with a "shorter linker" was designed by deleting the last residue of wild type ubiquitin (G76) and the two N-terminal residues of the recognition peptide (TG). This new mutant was called ubiquitin^{WETWV} and diamagnetic and paramagnetic PDZ-1 were added in order to study the paramagnetic effects transferred to this mutant (figure 3.24).
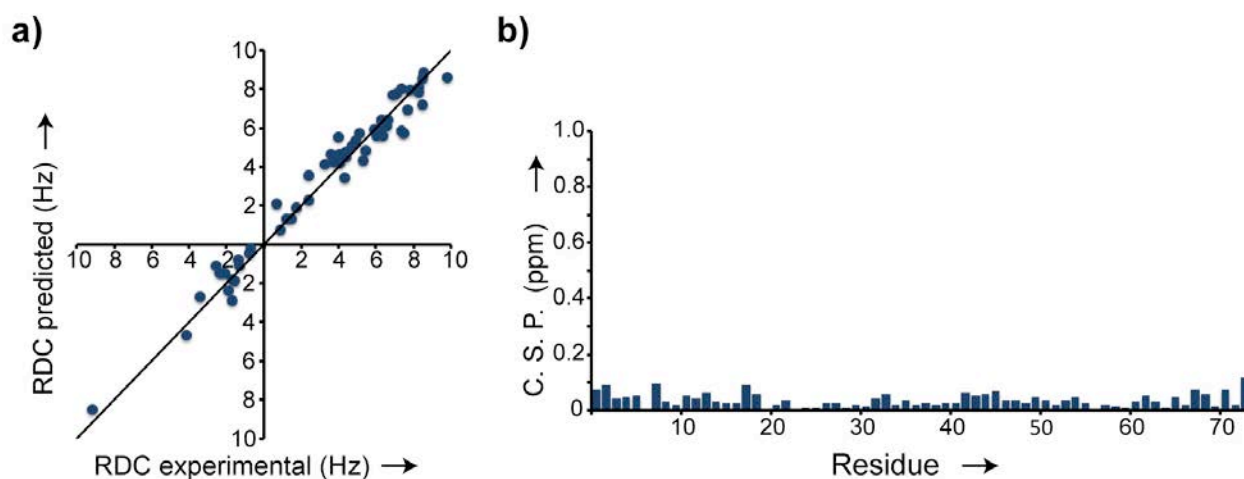
Figure 3.24 RDCs and chemical shift perturbation in ^{15}N-labelled ubiquitin^{WETWV} upon binding to PDZ-1 (Camacho-Zarco AR et al. 2014). **a**) Experimental RDCs were fitted to the ubiquitin 3D structure 1D3Z and compared to back-calculated RDCs. The RDCs were obtained at a 1H-Larmor frequency of 900 MHz and 310 K. **b**) Average, normalized 1H/15N chemical shift changes between ubiquitin^{WETWV} and ubiquitin^{TGWETWV}.

The correlation between experimental and back-calculated RDCs remained high as before. However, the RDCs measured in the same conditions in ubiquitin^{WETWV} increased in magnitude by ~40% when compared to those from ubiquitin^{TGWETWV} (figure 3.8a and figure 3.24a). The general magnitude of the alignment increased accordingly from 4.6e^{-4} in ubiquitin^{TGWETWV} (table 3.3) to 6.3e^{-4} in the new mutant. This evidence strongly suggests that the length of the "linker region" has an important role for transmission of paramagnetic effects from the PDZ reporters to the target protein. It is important to note that a chemical shift perturbation analysis shows that the wild type structure of ubiquitin was not affected in this new mutant (figure 3.24b).

4. Discussion

4.1 NMR titrations to study PDZ binding to TGWETWV-fused targets

The binding of PDZ to the targets (ubiquitin and MBP) fused to the recognition peptide TGWETWV was probed through NMR (figures 3.1 and 3.3). In these titrations the target proteins (the molecule under NMR observation) were ^{15}N labeled, so ^{15}N-HSQC experiments were recorded to determine changes in the chemical shift of the target's residues due to the addition of different amounts of PDZ.

The position of the signals is quite sensitive to the chemical environment. Therefore, changes upon addition of PDZ were expected to locate in the amide signals that belong to C-terminal residues recognized by PDZ. Both targets reported changes not only in the amide signals from their C-terminal residues (figure 3.1 and 3.3), but also in the signals from the side chains ($N\varepsilon$-$H\varepsilon_2$ groups) of the two tryptophan residues that form part of the TGWETWV sequence. These were clear evidences of PDZ binding.

The case of ubiquitin was peculiar due to the fact that not only the chemical shift of residues in the C-terminal changed upon PDZ binding, but the signals from several other residues too (figure 3.2a). The difference between the free and bound conformation can be produced by transient interactions between the recognition peptide and residues in the surface of ubiquitin. For example, the two tryptophan residues of the TGWETWV sequence could be interacting with the hydrophobic patch of ubiquitin (Leu8, Ile 44 and Val 70) that is known to be close to its C-terminal region (Winget JM et al. 2010). In other words, the addition of PDZ would sequester/bind the TGWETWV peptide.

A further conclusion is deduced from the co-existence of two distinctive sets of peaks (different chemical shifts), one for the free conformation and another one from the bound conformation after addition of a non-saturating amount of PDZ (ubiquitin^{TGWETWV} 2:1 PDZ). This is a sign that PDZ binding occurs on the slow NMR time scale, a sign of tight binding. Slow exchange means that the change in the chemical shift between the two conformations (free and bound) is larger than the rate constant of interconversion, pointing to a stable complex. In the case of MBP^{TGWETWV}, there were changes just in the chemical shift of residues in the C-terminal region before and after the addition of PDZ (figure 3.3). Hence, there aren't transient interactions between the recognition peptide and residues in the surface of MBP.

The chemical shift perturbation plots (figure 3.2b, 3.4b) show that there isn't distortion of the wild type structure of the targets, which was also confirmed through the high correlation between the experimental and back-calculated RDC data for both targets. This is a very important point, because if the fusion of the recognition peptide or PDZ binding perturbs the structure of the targets, the method developed in this thesis couldn't be applied.

4.2 The designed PDZ reporters and their tagging with CLaNP-5

The affinity of PDZ for their targets was determined by ITC (table 3.2). Interestingly, the affinity of wild type PDZ was five times higher for MBP than for ubiquitin. This is most probably related to the hypothetical transient interactions between some surface residues of ubiquitin and the recognition peptide. These transient interactions would compete with PDZ binding and therefore decrease its affinity constant. However, the affinity for both targets is smaller than the affinity for the peptide by itself, which is 0.15 μM (Skelton NJ et al. 2002). The observed lower affinity could be due to steric hindrance from the target proteins as they are comparatively much bigger than the peptide.

All the PDZ mutants designed to tag CLaNP-5 had affinity constants in the low micro molar range for ubiquitin[TGWETWV] (table 3.2 and figure 3.5). This shows that it was a good decision to choose a very well studied protein like PDZ and its ligand in this work. Thanks to the information reported in the literature, it was possible to avoid mutating one of the eighteen residues in and close to the PDZ binding site that are known to reduce the affinity by more than 10-fold (Skelton NJ et al. 2002). Even the PDZ mutant with the lowest affinity (PDZ-3, 14.8 μM) had sufficient affinity for standard NMR experiments because they usually employ protein concentrations higher than 100 μM.

The efficiency of CLaNP-5 tagging varied a lot between the different PDZ mutants, from 42 to almost 100%, even though the side chains of all residues were pointing to the solvent. Moreover, the distance between Cα carbons of the mutated residues was also in the recommended range, between 6 and 10 Å (Keizers PH et al. 2008). This heterogeneous behavior had already been observed in another protein called pseudoazurin (Keizers PH et al. 2008), where

three different mutants were designed to tag CLaNP-5 and the mutant with the lowest tagging yield (60%) was located in an α-helix. PDZ-2 had the lowest tagging yield and in this case the cysteine residues are located also in an α-helix. Therefore, it is possible that the distance between continuous rings in α-helixes is too short to allow a high yield of tagging. In the case of PDZ-2, the distance was 6.1 Å, the shortest among the designed PDZ mutants. In contrast to the scenario in PDZ-2, the mutant with the most optimal distance was PDZ-1, with 8.4 Å. This mutant could be tagged almost completely. This shows that it is better to design the double cysteine mutants with a distance between their Cα carbons as close as possible to the middle point of the recommended range (~8 Å).

The presence of untagged PDZ in the paramagnetic samples (ClaNP-5/Tm^{3+}) represents a problem because then two sets of signals appear on each spectrum. One of the sets are the expected paramagnetic signals due to the transmission of the paramagnetic effects, but in addition appear diamagnetic signals due to the presence of the untagged protein. This represents a problem because the diamagnetic and paramagnetic signals may overlap, interfering with the accurate determination of the signal intensity, chemical shift etc. It was attempted to separate tagged from untagged PDZ by two different methods. The first method was gel filtration chromatography (figure 3.6c); nevertheless it was impossible to separate the two populations most probably because the molecular weight difference is smaller than 1 KDa. The second employed method was chosen in order to trap PDZ domains with cysteine residues in a reduced state (thiol sepharose 4B). This method was chosen because untagged protein might still have cysteine residues in a reduced state. Apparently this is not the case, since the untagged protein couldn't be removed through this method as observed

from NMR spectra (figure 3.6). Judging from SDS polyacrylamide gels, the presence of a significant amount of PDZ dimers can be ruled out too (figure 3.6b). One remaining option is that the untagged population of protein is forming intramolecular disulfide bridges. This is an option because the Cα involved in this kind of bond can have a distance between 4 and 9 Å (Richardson JS 1981). In this case, the protein would have almost the same molecular weight as reduced PDZ, but it would be chemically unreactive to Sepharose 4B.

A further method to separate tagged from untagged protein could be reverse phase HPLC. It has been observed that tagged and untagged protein can be separated through this method (figure 3.6a); nevertheless it results in unfolding of the protein due to the hydrophobic solvents. Refolding tests of the tagged protein haven't been performed, but there are hints in the literature that suggests that it might be feasible (Zhang H et al. 2008).

4.3 RDC restraints observed in ubiquitin and MBP

All the tagged PDZ mutants were added to ubiquitin[TGWETWV] and MBP[TGWETWV] in order to test if the paramagnetic effects could be transmitted to these target proteins. PDZ-4 was the only exception, because it precipitates quantitatively in the same experimental conditions used to test the other mutants, so it couldn't be used anymore. This means that most of the PDZ mutants turn out to be stable, but this was just because there was a lot of information about the structure of PDZ. In the case of not so well characterized proteins it is clear that the probability of producing unstable proteins could be higher. In this way PDZ-4 highlights an advantage of the present method over direct attachment of the lanthanide on the target. It is an advantage because six PDZ mutants are already known to be stable and can be added to any target protein. In contrast, the traditional method requires designing cysteine mutants of each target that is being studied, a protein that most of the times will not be as well structurally characterized as PDZ.

Paramagnetic alignment was transmitted from all the different PDZ reporters to ubiquitin[TGWETWV] and MBP[TGWETWV]. This was proved due to the occurrence of RDCs in both targets. The magnitude of the RDCs in ubiquitin, which depends on the magnitude of the transmitted alignment, was different among the PDZ mutants. For example, PDZ-1 produced RDCs in the range of -8 to 7 Hz, while PDZ-3 and PDZ-5 produced significantly smaller RDCs (figure 3.8). Furthermore, in the test with MBP[TGWETWV] these two mutants also transferred the smallest paramagnetic alignments. All the PDZ mutants were tagged with the same lanthanide tag (ClaNP-5/Tm^{3+}) and the experiments were recorded in the same conditions. Therefore, this suggests that the difference in magnitude

between the different alignments arises from the rigidity of the lanthanide tag on each PDZ reporter.

The smaller magnitude of the alignment produced by PDZ-5 is apparently easy to explain, because this is the only PDZ mutant that doesn't have its tagging site on a secondary structural element. The cysteine residues of PDZ-5 are located in a long loop, a site that might be more mobile. In contrast, the residues (R14C and E94C) mutated in PDZ-3 are located in two adjacent beta strands that are far from the binding site of PDZ. There is no previous information in the literature about the impact of these residues on the stability or activity of PDZ, nevertheless the ITC experiments done in this work show that this mutant has the lowest affinity for ubiquitin^{TGWETWV} among the PDZ mutants (table 3.2). A possible scenario is that the two cysteine mutations destabilized the structure of the beta strands where they are located, decreasing the normal rigidity of these structural elements and decreasing at the same time the affinity of PDZ for the TGWETWV peptide.

The RDCs measured in ubiquitin and MBP are of high quality, as deduced from comparisons between experimental and back-calculated data (figures 3.8 and 3.11). Nonetheless, it is clear that quality indicators like the Q-factor and the Pearson's correlation (R) for ubiquitin are better than those obtained from MBP. The lower quality of MBP data is mainly due to the lower resolution of the MBP structure as well as the lower accuracy of the NMR experiment used to record the RDC data. The accuracy of the IPAP experiment used to record the ubiquitin experiments (Yao LS et al. 2009) is the highest among the experiments reported in the literature. However, it is not recommended for proteins with high molecular weight (like MBP) because of the rapid decay of the faster relaxing component of

the 1H-15N doublet in high-molecular weight proteins (Yao L et al. 2009).

Uncertainties of the calculated alignment tensors were evaluated by adding Gaussian noise to the structures of ubiquitin and MBP, which were used to determine the alignment tensors (Zweckstetter M et al. 2002). The orientation of the tensors was well defined, as judged from the small spread of the orientation of the tensors axes as represented in Sanson-Flamsteed projections (figure 3.9 and 3.12). Nevertheless, the most remarkable feature of the paramagnetic alignments is that they have different orientations, which was one of the major goals of this work.

In the case of ubiquitin[TGWETWV], the 5D angles between the alignment tensors reached up to 154 degrees, which is the case for mutants PDZ-3 and PDZ-7. However, the 5D angle between PDZ-6 and PDZ-7 was just 9 degrees, therefore some mutants produced paramagnetic alignments with an orientation more different than others. For the pair of PDZ-6 and PDZ-7, their similar orientation could be due to the close location of their tagging site on the surface of PDZ (figure 3.5). Actually, PDZ-6 and PDZ-7 share one tagging residue (S84C), so it is not difficult to imagine that the location of the lanthanide most probably is quite similar in these mutants.

The case of PDZ-2 is quite interesting. Even though the tagging site of this mutant is very close to that of PDZ-6 and PDZ-7, the orientation of the alignment tensor produced by PDZ-2 is quite different (figure 3.9g). The lanthanide tag already loaded with an ion and attached to a protein has a total charge of 3+, so interactions with close polar side chains of PDZ are possible (like T88 or Q81). PDZ-3 was another mutant that produced an alignment with a very different orientation too, but in this case it should be related to the position of the tagging

site, which is quite far from the location of the other tagging sites (figure 3.5).

In the case of MBP^{TGWETWV}, the relative orientation of the alignment tensors was conserved (figure 3.12). For example, mutants PDZ-2 and PDZ-3 produced alignments with very different orientations respect to the other PDZ reporters. This implies that the orientation of the alignments is largely independent of the target protein and its interaction with the PDZ reporter.

A possibility to increase the number of independent paramagnetic alignments regarding orientation could be to use a different lanthanide tag. There are reports in the literature about tags that also attach to double cysteine mutants but employ different chelating systems (Liu WM et al. 2012). The differences in the coordination sphere change the orientation of the alignment tensors even when the same double cysteine mutants are used.

A further possibility could be to use lanthanide tags that attach to just one cysteine residue. Indeed, most of the tags reported in the literature bind to just one cysteine residue, so there is a bigger diversity of chelating systems among this type of tags (Su XC et al. 2010). The only limitation is the usually smaller paramagnetic alignment produced by these tags. However, there are available some bulky lanthanide tags that attach the lanthanide almost as rigid as CLaNP-5, so these tags might be used together with PDZ in the present method (Häussinger D et al. 2009; Keizers PH et al. 2007).

4.4 PCS restraints observed in ubiquitin and MBP

The signals of the different amide groups in NMR spectra showed the characteristic shifts due to the effect of PCS in both, ubiquitin[TGWETWV] and MBP[TGWETWV]. The different PDZ reporters produced just one set of paramagnetic peaks (figure 3.13 and 3.15), which means that the lanthanide tag (CLaNP-5) doesn't sample multiple conformations; otherwise several paramagnetic signals could be observed for each amide group. The observed conformational homogeneity of CLaNP-5 is in agreement with data reported in the literature (Keizers PH et al. 2007).

In general, the magnitude of the PCS transmitted to ubiquitin and MBP was smaller than in previous reports that used the same lanthanide tag and paramagnetic center (CLaNP-5/Tm^{3+}). For example, when this lanthanide tag was attached to the protein pseudoazurin, it produced PCS up to 5.5 ppm (Keizers PH et al. 2007). The smaller magnitude of the PCS transmitted to the targets, implies that these could've been scaled down because of intermolecular dynamics between the reporter PDZ mutants and the targets.

The magnitude of the PCS decreased in our method, nevertheless the correlation to back-calculated data stayed over 0.97 in the four cases where meaningful PCS could be measured in ubiquitin[TGWETWV] (figure 3.14). The decrease in the magnitude of the PCS could be actually an advantageous feature. This is because bigger PCS force to re-assign the signals in NMR spectra in order to know which signals correspond to which particular residue. Signal assignment could be a very challenging process in NMR spectroscopy, especially for large proteins (John M et al. 2007). This process could become even more complicated if PRE decreases the signal intensity of many residues.

In the present method, the magnitude of the PCS was smaller than 0.7 ppm, so it was possible to manually assign the paramagnetic signals produced by the PDZ reporters in ubiquitin and MBP.

The magnitude of the PCS varied between the different mutants. The different magnitude of the alignment tensors, which had already been determined through experimental RDC data (table 3.3 and 3.4), explains the different magnitude of the PCS between the different mutants. Consistent with the RDC data, the PCS produced by PDZ mutants 1, 2, 6 and 7 had the biggest magnitude among the mutants. In contrast, PCSs produced by the PDZ reporters 3 and 5 were too small to be analyzed. PCSs depend also on the distance between the observed nucleus and the paramagnetic center, and these two PDZ mutants have the farthest tagging sites with respect to the binding site of TGWETWV, the point that connects the target protein and the PDZ reporter.

If bigger PCSs are required, then other lanthanides could be employed in order to generate them. For example, lanthanides like Dy^{3+} and Tb^{3+} are known to produce larger PCS due to their larger magnetic susceptibility anisotropy (Otting G et al. 2010).

4.5 PRE restraints are observed in ubiquitin and MBP

In addition to RDC and PCS, the effect of PRE in the signals from ubiquitin^{TGWETWV} and MBP^{TGWETWV} was observed after the addition of all the PDZ reporters. In the case of ubiquitin^{TGWETWV}, several regions were affected by PRE in all the mutants, in particular residues 8-12 and 30-40. The decrease in the signal intensity produced by PRE is distance dependent, so these residues are closer to the paramagnetic lanthanide attached to PDZ. Consistent with this interpretation, these residues are close in space to the C-terminal region, fused to the sequence TGWETWV (figure 3.18g).

There were several residues affected in ubiquitin, nonetheless the signals from most of the residues could still be detected and analyzed, i.e. these signals were able to provide structural information. This is a clear difference between the current method and the traditional method consisting on attaching the lanthanide directly to the target molecule. In the current method, the lanthanide is farther from the target. For example, a lanthanide tag called Cys-Ph-TAHA loaded with Tm^{3+} was directly tagged to ubiquitin (Peters F et al. 2011). In this case, only 57% of the signals could be analyzed to obtain RDCs due to signal broadening due to PRE. However, in the present method 70% (PDZ-2) or more of the signals could be analyzed in any dataset.

The mutants that produced on average the weakest PRE were PDZ-3 and PDZ-5 (figures 3.18 and 3.19). This has two different but complementary explanations that are similar to those explaining the smaller PCS produced by these mutants. The first one is related to the lower rigidity of the tag in these mutants, because this would produce an averaging of the PRE among the different conformations sampled by the lanthanide (Koehler J et al. 2011). The

second reason could be the bigger distance between the tagging site of these PDZ mutants and the binding site of the TGWETWV peptide in PDZ. The lanthanide is simply farther from the target protein (figure 3.5).

In the case of MBP^{TGWETWV}, the most affected residues by PRE were also close to the C-terminal region of MBP, as expected (figure 3.19f). The experimental intensity ratios produced by PDZ-1 were compared to back calculated ones. The data doesn't seem to correlate very well, but the reason has its origin in the anisotropic magnetic susceptibility of Tm^{3+}. In this type of paramagnetic centers, there is significant cross-correlation with other relaxation mechanisms and in addition exchange contributions from conformational dynamics could be different in the diamagnetic and paramagnetic sample (Pintacuda G et al. 2004; Clore GM et al. 2009). These are the main reasons that explain why paramagnetic centers with isotropic magnetic susceptibility (like Gd^{3+} or Cu^{2+}) are employed to obtained distance restraints from PRE.

A remarkable characteristic of the present method is that it is not necessary to have previous knowledge of the three-dimensional structure of the target protein. This makes a clear difference with the traditional method of lanthanide tagging, because it depends on choosing residues located on the surface of the target protein, with side chains pointing to the solvent. In the developed method, it is just necessary to fuse the TGWETWV peptide to the C-terminal region of the target. The present method is also more powerful than those methods where a lanthanide binding peptide is fused to the C or N terminal of the target protein (Wöhnert J et al. 2003; Martin JL et al. 2007). This is because several orientationally independent datasets of paramagnetic restraints can be produced from one mutant of the target protein, not just one. In addition,

the method is also flexible regarding the election of the paramagnetic center, in clear contrast to some lanthanide binding peptides like the ATCUN motif, that just bind with high affinity either Cu^{2+} or Ni^{2+} (Donaldson WL et al. 2001). This is could be an important feature of a certain method, because PRE produced by Cu^{2+} are observed up to 25 Å from the position of the metal, but the effects from Gd^{3+} are observed up to 35 Å (Iwahara J et al. 2003).

4.6 The effect of PDZ binding in the relaxation properties (R_2) of the targets

Upon binding to PDZ, the R_2 relaxation rates of both targets were shown to increase (figure 3.20). This suggests that ubiquitin^{TGWETWV} and MBP^{TGWETWV} do not behave dynamically as independent proteins after binding to PDZ. This is further supported by correlation time of the complex MBP^{TGWETWV}/PDZ, which was calculated by Dr. N. Rezaei-Ghaleh using the program HYCUD (Rezai-Ghaleh N et al. 2013). The correlation time of a protein or any molecule is the time it takes to rotate through one radian, which is in the order of nanoseconds in the case of proteins. The correlation time of wild type MBP is 16.2 ns according to the literature (Gardner KH et al.1998). However, the calculated correlation time for MBP^{TGWETWV} bound to PDZ is higher, amounting to 28.9 ns.

The increase in the R_2 relaxation rates and the correlation time of the complexes supports the view that the target proteins are hydrodynamically coupled and do not tumble as separate proteins (Halle B et al. 2009). This explains the transmission of the paramagnetic effects to the target proteins and suggests that the motion of PDZ relative to the targets affects the degree of transmission of the paramagnetic effects.

The increase in the correlation time of the targets didn't affect the acquisition of RDC data through 3D experiments (Permi P et al. 2000), since a bigger number of RDCs could be acquired and the correlation with back-calculated data stayed in 0.93 (figure 3.11f), which is in the range observed from data recorded through 2D experiments. This is a significant point, because it means that this method can be applied to other high molecular weight proteins and probably membrane proteins. It is challenging to study membrane proteins by liquid-state NMR because the molecular weight of the micelle or bicelle adds

to the system's size.

In the current thesis the PDZ domain was used as a reporter, binding the targets and transmitting the paramagnetic effects. However, the method is not limited to use PDZ as reporter. In fact, smaller proteins than PDZ could have a smaller impact on the relaxation properties of the targets and potentially improve the acquisition of the data. Actually, the only requirement for a certain protein to work as a reporter is the high affinity binding to a recognition sequence attached to the C-terminal of the target. Moreover, a different reporter could bind the target proteins in the N-terminal region, a possibility that leads to the opportunity of transferring even further different paramagnetic alignments through a different orientation.

4.7 Impact of the linker residues in the alignment transferred to the targets

As mentioned before, the paramagnetic alignment transferred to the target proteins is smaller than the alignments reported in the literature due to the direct attachment of CLaNP-5 loaded with Tm^{3+} on the target. This suggests an additional source of flexibility that scales down the paramagnetic alignment transferred to the targets in the present method.

The $R_{1\rho}$ relaxation rates (^{15}N) of this complex showed that the last three wild type residues of ubiquitin^{TGWETWV} and the first two residues of the recognition peptide (TG) are the most flexible in the μs-ms timescale. The data is in agreement to what is known in the literature, because the C-terminal residues don't have a rigid structure (Winget JM et al. 2010) and the N-terminal residues of the TGWETWV do not have a critical role on its recognition by PDZ. Actually, the removal of the two N-terminal residues of the peptide produces a 7-fold improvement on its affinity to PDZ (Skelton NJ et al. 2002).

These evidences indicate that probably the flexible C-terminal region of ubiquitin, together with the N-terminal residues of the peptide TGWETWV, were scaling down the paramagnetic alignment produced on PDZ. In order to gather more information to support this hypothesis, the paramagnetic alignment produced directly on PDZ-1 was determined. It was found to be to be 4-fold bigger than the alignment transmitted to ubiqutin^{TGWETWV} or MBP^{TGWETWV}, producing larger RDC and PCS (figure 3.22). This data supported the hypothesis that due to flexibility of the linker residues, the paramagnetic alignment was not transmitted completely to the targets. The impact of the length of the linker residues on the transmission of paramagnetic alignments has already observed before. For example, when calmodulin (loaded with Tb^{3+}) was used to transmit

paramagnetic effects to dihydrofolate reductase, a four-residue linker allowed measuring RDCs from +4.0 to -7.4 Hz. However, a much longer linker (14 residues) didn't allow recording significant RDCs (Feeney J et al. 2001).

The new and shorter target mutant ubiquitin[WETWV] had as an aim to test if a bigger alignment is transmitted due to its smaller linker. An increase of 40% in the magnitude of the alignment was found as a result of the removal of these residues (figure 3.24). This confirms the hypothesis that intermolecular dynamics between PDZ and the target proteins are an important factor decreasing the transferred alignments.

5. References

\#   Allegrozzi M, Bertini I, Janik MBL, Lee YM, Liu G, Luchinat C. Lanthanide-induced pseudocontact shifts for solution structure refinements of macromolecules in shells up to 40 Å from the metal ion. J Am Chem Soc 122 (2000) 4154–4161.

\#   Allen KN & Imperiali B. Lanthanide-tagged proteins - an illuminating partnership. Curr Opin Chem Biol 14 (2010) 247-254.

\#   Barry CD, North ACT, Glasel JA, Williams RJP & Xavier AV. Quantitative determination of mononucleotide conformations in solution using lanthanide ion shift and broadening NMR probes. Nature 232 (1971) 236–245.

\#   Barthelmes K, Reynolds AM, Peisach E, Jonker HRA, DeNunzio NJ, Allen NK, Imperiali B & Schwalbe H. Engineering encodable lanthanide-binding tags into loop regions of proteins. J Am Chem Soc 133 (2011) 808-819.

\#   Battiste JL & Wagner J. Utilization of site-directed spin labeling and high resolution heteronuclear magnetic resonance for global fold determination of large proteins with limited nuclear overhauser effect data. Biochemistry 39 (2000) 5355-5365.

\#   Bertini I, Janik MBL, Lee YM, Luchinat C & Rosato A. Magnetic susceptibility tensor anisotropies for a lanthanide ion series in a fixed protein Matrix. J Am Chem Soc 123 (2001) 4181-4188.

\#   Bertini I, Gelis I, Katsaros N, Luchinat C & Provenzani A. Tuning the affinity for lanthanides of calcium binding proteins. Biochemistry 42 (2003) 8011-8021.
\#   Bertini I, Luchinat C, Parigi G & Pierattelli R. NMR spectroscopy of paramagnetic metalloproteins. Chembiochem 6 (2005) 1536-1549.

\#   Biekofsky RR, Muskett FW, Schmidt JM, Martin SR, Browne JP, Bayley PM & Feeney J. NMR approaches for monitoring domain orientations in calcium-binding proteins in solution using partial replacement of Ca^{2+} by Tb^{3+}. FEBS Letters 460 (1999) 519–526.

\#   Billeter M, Wagner G & Wüthrich K. Solution NMR structure determination of proteins revisited. J. Biomol. NMR 42 (2008) 155-158.

\#   Boehr DD, Dyson HJ & Wright PE. An NMR perspective on enzyme dynamics. Chem Rev 106 (2006) 3055-3079.

\#   Bouvignies G, Meier S, Grzesiek S & Blackledge M. Ultrahigh-resolution backbone structure of perdeuterated protein GB1 using residual dipolar couplings from two alignment media. Angew Chem Int Ed 48 (2006) 8166-8169.

\#	Camacho-Zarco AR, Munari F, Wegstroth M, Liu MW, Ubbink M, Becker S, Zweckstetter M. Multiple Paramagnetic Effects Through a Tagged Reporter Protein. Angew Chem Int Ed Engl. 2014 Oct 7. doi: 10.1002/anie.201408615

\#	Cornilescu G, Marquardt JL, Ottiger M & Bax A. Validation of protein structure from anisotropic carbonyl chemical shifts in a dilute liquid. J Am Chem Soc 120 (1998) 6836-6837.

\#	Clore GM & Iwahara J. Theory, practice, and applications of paramagnetic relaxation enhancement for the characterization of transient low-population states of biological macromolecules and their complexes. Chem Rev 109 (2009) 4108-4139.

\#	Delaglio F, Grzesiek S, Vuister GW, Zhu G, Pfeifer J & Bax A. NMRPipe: a multidimensional spectral processing system based on UNIX pipes. J Biomol NMR 3 (1995) 277-293.

\#	Donaldson LW, Skrynnikov, Choy WY, Muhandiram DR, Sarkar B, Forman-Kay JD & Kay LE. Structural characterization of proteins with an attached ATCUN motif by paramagnetic relaxation enhancement spectroscopy. J Am Chem Soc 123 (2001) 9843-9847.

\#	Egorov TA, Svenson A, Rydén L & Carlsson J. A rapid and specific method for isolation of thiol-contaning peptides from large proteins by thiol-disulfide exchange on a solid support. Proc Natl Acad Sci USA 72 (1975) 3029-3033.

\#	Feeney J, Birdsall B, Bradbury AF, Biefkofsky RR & Bayley PM. Calmodulin tagging provides a general method of using lanthanide induced magnetic field orientation to observe residual dipolar couplings in proteins in solution. J Biomol NMR 21 (2001) 41-48.

\#	Gaponenko D, Dvoretsky A, Walsby C, Hoffman BM, Rosevear PR. Calculation of z-coordinates and orientational restraints using a metal binding tag. Biochemistry 39 (2000) 15217-15224.

\#	Gaponenko V, Howarth JW, Columbus L, Gasmi-Seabrook G, Yuan J, Hubbell WL & Rosevear PR. Protein global fold determination using site-directed spin and isotope labeling. Protein Sci 9 (2000) 302-309.

\#	Gaponenko V, Sarma SP, Altieri AS, Horita DA, Li J & Byrd R. Improving the accuracy of NMR structures of large proteins using pseudocontact shifts as long-range restraints. J Biomol NMR 28 (2004) 205-212.

\#	Gardner KH, Zhang X, Gehring K & Kay LE. Solution NMR studies of a 42 Kda Escherichia coli maltose binding protein/beta-cyclodextrin complex: chemical shift assignments and analysis. J Am Chem Soc 120 (1998) 11738-11748.

\#	Goddard TD & Kneller DG. Sparky 3. University of California, San

Francisco.

\#   Green H & Freeman R. Band-selective radiofrequency pulses. J Magn Reson 93 (1991) 93 -141.

\#   Halle B. The physical basis of model-free analysis of NMR relaxation data from proteins and complex fluids. J Chem Phys 131 (2009) 224507-224520.\#   Hass M & Ubbink M. Structure determination of protein-protein complexes with long-range anisotropic paramagnetic NMR restraints. Curr Op Struc Bio 24 (2014) 45-53.

\#   Häussinger D, Huang JR & Grzesiek S. DOTA-M8: An extremely rigid, high-affinity lanthanide chelating tag for PCS NMR spectroscopy. J Am Chem Soc 131 (2009) 14761-14767.

\#   Henzler-Wildman K & Kern D. Dynamic personalities of proteins. Nature 450 (2007) 964-972.

\#   Hershko A & Ciechanover A. The ubiquitin system. Annu Rev Biochem 67 (1998) 425-479.

\#   Iwahara J, Anderson DE, Murphy EC & Clore GM. EDTA-derivatized deoxythymidine as a tool for rapid determination of protein binding polarity to DNA by intermolecular paramagnetic relaxation enhancement. J Am Chem Soc 125 (2003) 6634-6635.

\#   John M & Otting G. Strategies for measurements of pseudocontact shifts in protein NMR spectroscopy. Chem Phys Chem 8 (2007) 2309-2313.

\#   Kay LE & Gardner KH. Solution NMR spectroscopy beyond 25 kDa. Curr Opin Struct Biol. 7 (1997) 722-731.

\#   Keisers PH, Desreux JF, Overhand F & Ubbink M. Increased paramagnetic effect of a lanthanide protein probe by two-point attachment. J Am Chem Soc 129 (2007) 9292-9293.

\#   Keizers PH, Saragliadis A, Hiruma Y, Overhand M & Ubbink M. Design, synthesis, and evaluation of a lanthanide chelating protein probe: CLaNP-5 yields predictable paramagnetic effects independent of environment. J Am Chem Soc 130 (2008) 14802-14812.

\#   Keizers PH & Ubbink M. Paramagnetic tagging for protein structure and dynamics analysis. Prog Nucl Magn Reson Spectrosc 58 (2011) 88-96.

\#   Koehler J & Meiler J. Expanding the utility or NMR restraints with paramagnetic compounds: background and practical aspects. Prog Nucl Magn Reson Spectrosc 59 (2011) 360-389.

\#   Lakomek NA, Lange OF, Walter KFA, Fàres C, Egger D, Lunkenhiemer P,

Meiler J, Grubmüller H, Becker S, de Groot B & Griesinger C. Residual dipolar couplings as a tool to study molecular recognition of ubiquitin. Biochem Soc Trans 36 (2008) 1433-1437.

\# Lange OF, Lakomek NA, Fares C, Schröder GF, Walter KFA, Becker S, Meiler J, Grubmüller H, Griesinger C & de Groot BL. Recognition Dynamics up to microseconds revealed from and RDC-derived ubiquitin ensemble in solution. Science 320 (2008) 1471-1475.

\# Leonov A, Voigt B, Rodriguez-Castañeda F, Sakhaii P & Griesinger C. Convenient synthesis of multifunctional EDTA-based chiral metal chelates substituted with an S-mesylcysteine. Chemistry 11 (2005) 3342-3348.

\# Losonczi JA, Andrec M, Fischer MWF & Prestegard JH. Order matrix analysis of residual dipolar couplings using singular value decomposition. J Magn Reson 138 (1999) 334-342.

\# Ma C & Opella SJ. Lanthanide ions bind specifically to an added "EF-hand" and orient a membrane protein in micelles for solution NMR spectroscopy. J Magn Reson 146 (2000) 381-384.

\# Martin LJ, Hähnke MJ, Nitz M, Wöhnert J, Silvaggi NR, Allen KN, Schwalbe H & Imperialli B. Double-lanthanide-binding tags: design, photophysical properties, and NMR applications. J Am Chem Soc 129 (2007) 7106-7113.

\# Massi F, Grey MJ & Palmer AG. Microsecond timescale backbone conformational dynamics in ubiquitin studied with NMR R1p relaxation experiments. Protein Science 14 (2005) 735-742.

\# O'Connell MR, Gamsjaeger R & Mackay JP. The structural analysis of protein-protein interactions by NMR spectroscopy. Proteomics 9 (2009) 5224-5232.

\# Ottiger M, Delaglio F & Bax A. Measurement of J and dipolar couplings from simplified two-dimensional NMR spectra. J Magn Reson 131 (1998) 373-378.

\# Otting G. Prospects for lanthanides in structural biology by NMR. J Biomol NMR 42 (2008) 1-9.

\# Otting G. Protein NMR using paramagnetic ions. Annu Rev Biophys 39 (2010) 387-405.

\# Palmer AG & Massi F. Characterization of the dynamics of biomacromolecules using rotating-frame spin relaxation NMR spectroscopy. Chem Rev 106 (2006) 1700-1719.

\# Peters F, Maestre-Martinez M, Leonov A, Kovačič L, Boelens R & Griesinger C. Cys-Ph-TAHA: a lanthanide binding tag for RDC and PCS enhanced protein NMR. J Biomol NMR 51 (2011) 329-337.

\# Pintacuda G, Moshref A, Leonchiks A, Sharipo A, Otting G. Site-specific labelling with a metal chelator for protein-structure refinement. J Biomol NMR 28 (2004) 351-361.

\# Pintacuda G, Park AY, Keniry MA, Dixon NE & Otting G. Lanthanide labeling offers fast NMR approach to 3D structure determinations of protein-protein complexes. J Am Chem Soc 128 (2006) 3696-3702.

\# Prestegard JH, Bougault CM & Kishore AI. Residual dipolar couplings in structure determination of biomolecules. Chem Rev 104 (2004) 3519-3540.

\# Raman S, Lange OF, Rossi P, Tyka M, Wang X, Aramini J, Liu G, Ramelot TA, Eletsky A, Szyperski T, Kennedy MA, Prestegard J, Montelione GT, Baker D. Science 327 (2010) 1014-1018.

\# Rezaei-Ghalei N, Klama F, Munari F & Zweckstetter M. Predicting the rotational tumbling of dynamic multidomain proteins and supramolecular complexes. Angew Chem Int Ed Engl 52 (2013) 11410-11414.

\# Richardson JS. The anatomy and taxonomy of protein structure. Adv Protein Chem 34 (1981) 167-339.

\# Saio T, Ogura K, Yokochi M, Kobashigawa Y & Inagaki F. Two-point anchoring of a lanthanide-binding peptide to a target protein enhances the paramagnetic anisotropic effect. J Biomol NMR 44 (2009) 157-166.

\# Sass J, Cordier F, Hoffmann A, Rogowski M, Cousin A, Omichinski JG, Löwen H & Grzesiek S. Purple membrane induced alignment of biological macromolecules in the magnetic field. J Am Chem Soc 121 (1999) 2047-2055.

\# Schmitz C, Stanton-Cook MJ, Su XC, Otting G & Huber T. Numbat: an interactive software tool for fitting dh-tensors to molecule coordinates using pseudocontact shifts. J Biomol NMR 41 (2008) 179-189.

\# Sharff AJ, Rodseth LE & Quiocho FA. Refined 1.8-Å structure reveals the mode of binding of beta-cyclodextrin to the maltodextrin binding protein. Biochemistry 32 (1993) 10553-10559.

\# Solomon I. Relaxation processes in a system of two spins. Phys Rev Lett 9 (1955) 559–565.

\# Spurlino JC, Lu GY, Quiocho FA. The 2.3-Å resolution structure of the maltose- or maltodextrin- binding protein, a primary receptor of bacterial active transport and chemotaxis. J Biol Chem 266 (1991) 5202-5219.

\# Su XC, Huber T, Dixon NE, Otting G. Site-specific labelling of proteins with a rigid lanthanide-binding tag. Chembiochem 10 (2006) 1599-1604.

\# Su XC, McAndrew K, Huber T & Otting G. Lanthanide-binding peptides for

NMR measurements of residual dipolar couplings and paramagnetic effects from multiple angles. J Am Chem Soc 130 (2008) 249-273.

\#   Su XC & Otting G. Paramagnetic labelling of proteins and oligonucleotides for NMR. J Biomol NMR 46 (2010) 101-112.

\#   Tang C, Ghirlando R, Clore GM. Visualization of transient encounter complexes in protein-protein association. J Am Chem Soc 444 (2006) 383-386.

\#   Tolman JR, Flanagan JM, Kennedy MA & Prestegard JH. Nuclear magnetic dipole interactions in field-oriented proteins: information for structure determination in solution, Proc Natl Acad Sci USA 92 (1995) 9279–9283.

\#   Vijay-Kumar S, Bugg CE & Cook WJ. Structure of ubiquitin refined at 1.8 Å resolution. J Mol Biol 194 (1987) 531-544.

\#   Wallace AC, Laskowski RA, Thorton JM. LIGPLOT: a program to generate schematic diagrams of protein-ligand interactions. Protein Eng. 8 (1995) 127-134.

\#   Winget JM & Mayor T. The diversity of ubiquitin recognition: hot spots and varied specificity. Molecular Cell 38 (2010) 627-635.

\#   Wöhnert J, Franz KJ, Nitz M, Imperiali B, Schwalbe H. Protein alignment by a coexpressed lanthanide-binding tag for the measurement of residual dipolar couplings. J Am Chem Soc 125 (2003) 13338-13339.

\#   Wüthrich K. NMR studies of structure and function of biological macromolecules (Nobel lecture). J Biomol NMR 27 (2003) 13-39.

\#   Yagi H, Pilla KB, Maleckis A, Graham B, Huber T & Otting G. Three-dimensional protein fold determination from backbone amide pseudocontact shifts generated by lanthanide tags at multiple sites. Structure 21 (2013) 883-890.

\#   Yang D & Kay LE. Improved 1HN-detected triple resonance TROSY-based experiments. J Biomol NMR 13 (1999) 181-185.

\#   Yao L, Ying J & Bax A. Improved accuracy of 15N-1H scalar and residual dipolar couplings from gradient-enhanced IPAP-HSQC experiments on protonated proteins. J Biomol NMR 43 (2009) 161-170.

\#   Ye F & Zhang M. Structures and target recognition modes of PDZ domains: recurring themes and emerging pictures. Biochem J 455 (2013) 1-14.

\#   Zhang H, Yu M, Hu M, Qian L, Chen L, Shi M, Shen B & Guo N. Overexpression, refolding, purification of Erbin PDZ domain from Escherichia coli and preparation of its polyclonal antibody. Prep Biochem Biotechnol 38 (2008) 282-293.

\#   Zweckstetter M & Bax A. Evaluation of uncertainty in the alignment tensors obtained from dipolar couplings. J Biomol NMR 23 (2002) 127-137.

\#   Zweckstetter M. NMR: prediction of molecular alignment from structure using the PALES software. Nat Protoc 3 (2008) 679-690.

Appendix

A)

Experimental ^{1}H-^{15}N RDC data recorded from ubiquitin^{TGWETWV} bound to the different PDZ reporters (figure 4.8).

Residue	PDZ-1	Residue	PDZ-2	Residue	PDZ-3	Residue	PDZ-5
2	0.62	2	-0.43	2	1.39	2	0.81
3	5.14	3	6.04	3	-2.54	3	2.28
4	4.96	4	6.63	4	-3.34	4	2.46
5	3.51	5	5.82	5	-1.81	5	2.1
6	2.19	6	4.98	6	-1.91	6	1.1
7	0.35	7	1.95	7	-4.71	7	-1.09
8	3.92	11	3.76	11	1.89	11	-0.37
11	-0.99	13	-2.07	12	0.3	12	1.29
12	2.59	14	2.26	13	-0.77	13	1.82
13	2.59	16	5.71	14	-2.26	14	1.92
14	3.9	17	7.32	15	-2.66	15	2.91
15	5.76	18	3.79	16	-1.17	16	1.82
16	3.62	20	3.56	17	0.02	17	1.64
17	3.3	21	-2.07	18	2.66	18	0.27
18	-0.2	23	-1.98	20	1.33	20	-0.01
20	-1.15	25	2.99	21	0.68	21	0.65
21	2.27	26	7.18	22	-2.14	22	3.15
22	5.34	27	4.71	23	-0.98	23	1.18
23	2.23	28	1.13	25	-2.04	25	-0.35
25	0.29	29	4.45	26	-1.49	26	1.36
26	2.39	30	2.85	27	-0.75	27	0.27
27	0.59	32	3.9	28	-0.69	28	-1.73
28	-2.5	33	4.22	29	-2.3	29	0.82
29	1.95	34	-1.65	30	-1.16	30	0.73
30	1.7	39	3.38	31	-1.63	32	-1.46
31	-1.01	40	8.39	32	-1.23	33	1
32	-1.76	41	-0.13	33	-1.14	34	-1.18
33	2.01	43	1.47	34	-1.52	35	-3.75
34	-0.94	44	0.12	35	-0.1	36	-0.64
35	-7.26	46	2.73	36	3.16	40	0.73

40	0.43	47	3.1	39	-4.07	41	-0.55
41	1.2	48	2.79	40	0.22	42	-1
42	-1.19	49	4.42	41	-2.92	43	-0.55
43	0.06	50	4.18	42	-0.93	44	0
44	0.29	55	-4	43	-1.45	45	0.99
45	1.01	56	2.19	44	-0.77	46	1.1
46	2	57	1.36	45	0.9	47	0.92
47	1.47	58	-2.03	46	-0.52	48	0.27
48	-2.13	59	-10.45	47	-1.66	49	1.28
49	1.7	60	-7.18	48	3.27	50	-1.01
50	-0.21	61	3.52	49	-0.05	51	-0.18
51	-0.98	62	5.96	50	-1.17	52	-2.83
52	-6.47	63	5.85	51	-0.22	54	-3.01
54	-6	64	5.77	52	3.03	55	0.92
55	1.75	65	6.16	54	0.19	56	2.28
56	4.71	66	1.46	55	-2.03	57	2.1
58	5.6	67	3.83	56	-2.8	58	1.09
59	4.79	68	-1.42	57	-2.57	59	2.65
60	0.62	69	-7.45	58	-2.71	60	-0.46
61	3.35	70	6.75	59	-2.39	61	0.82
62	-1.03			60	-1.22	62	-0.55
63	-5.67			61	-0.67	63	-2.74
64	5.33			62	-1.01	64	2.27
65	-1.32			63	0.79	65	-1.6
66	5.85			64	-2.3	66	3.02
67	3.54			65	-0.96	67	2.28
68	1.51			66	-3.1	68	0.54
69	0.9			67	-1.97	69	-1.19
70	-2.76			68	-0.94	70	-1.37
				69	0.23		
				70	-0.91		

Residue	PDZ-6	Residue	PDZ-7
2	-1.18	2	-2.13
3	4.19	3	4.8
4	4.28	4	4.99
5	2.97	5	5.26
6	2.54	6	3.17
7	-1.13	7	-0.94
8	-1.72	11	-3.14
11	-2.38	13	3.31
12	1	14	5.2
13	2.08	15	5.51
14	3.19	16	2.19
15	4.95	17	0.47
16	2.02	18	-3.61
17	1.19	20	-1.19
18	-2.66	21	0.34
20	-1.45	22	7.36
21	0.76	23	3.67
23	2.8	25	1.72
25	0.9	26	3.72
26	2.42	27	2.2
27	1.69	28	-0.98
28	-0.31	29	4.14
29	2.71	39	6.19
30	2.07	40	1.73
32	0.42	41	2.33
33	2.08	42	0.57
34	0.57	43	1.39
39	5.03	44	2.13
40	0.71	45	0.53
41	1.52	46	1.82
42	0.43	47	3.05
43	0.95	48	-3.3
44	1.06	49	1.73
45	0.03	50	1.14
46	2.49	51	-2.18

47	2.34	52	-6.73
48	-3.28	54	-3.09
49	1.05	55	3.26
50	0.67	56	5.87
51	0.06	57	5.43
52	-5.28	58	4.6
54	-3.22	59	5.37
55	2.32	60	1.84
56	4.78	61	1.92
57	4.88	62	0.92
58	4.6	63	-3.89
59	4.23	64	5.19
60	1.73	65	0.76
61	2.13	66	5.12
62	0.45	67	4.76
63	-3.74	68	2.34
64	4.53	69	0.36
65	0.53	70	0.52
66	4.93		
67	3.2		
68	1.61		
69	0.72		
70	-0.39		

B)

Experimental PCS data (^{N}H) recorded from ubiquitin^{TGWETWV} bound to PDZ (figure 4.14).

Residue	PDZ-1	Residue	PDZ-2	Residue	PDZ-6	Residue	PDZ-7
2	0.002	2	-0.036	2	-0.028	2	-0.014
3	-0.008	3	-0.068	3	-0.061	3	-0.046
4	-0.02	4	-0.092	4	-0.074	4	-0.05
5	-0.036	5	-0.131	5	-0.105	5	-0.096
6	-0.031	6	-0.17	6	-0.086	6	-0.092

7	-0.048	7	-0.212	7	-0.105	12	-0.119
8	-0.008	8	-0.296	8	-0.066	13	-0.121
11	-0.061	11	-0.221	11	-0.115	14	-0.083
12	-0.06	12	-0.118	12	-0.117	15	-0.066
13	-0.052	13	-0.142	13	-0.119	16	-0.059
14	-0.031	14	-0.073	14	-0.104	17	-0.037
15	-0.014	15	-0.078	15	-0.081	18	-0.047
16	0.008	16	-0.049	16	-0.061	20	-0.023
17	0.004	17	-0.051	17	-0.041	21	-0.047
18	0.002	18	-0.057	18	-0.049	22	-0.088
20	0	20	-0.044	20	-0.036	23	-0.136
21	-0.005	21	-0.069	21	-0.064	25	-0.173
23	-0.049	23	-0.191	22	-0.116	26	-0.156
25	-0.042	25	-0.167	23	-0.181	27	-0.206
26	-0.038	26	-0.178	25	-0.185	29	-0.219
27	-0.056	27	-0.248	26	-0.167	30	-0.249
28	-0.06	28	-0.242	27	-0.206	39	-0.313
29	-0.039	29	-0.191	28	-0.243	40	-0.198
30	-0.06	30	-0.245	29	-0.226	41	-0.176
31	-0.099	31	-0.341	30	-0.255	42	-0.076
32	-0.069	32	-0.31	32	-0.466	43	-0.094
33	-0.058	33	-0.283	33	-0.463	44	-0.054
34	-0.193	34	-0.371	34	-0.527	45	-0.018
35	-0.351	36	-0.53	36	-0.441	46	0.005
36	-0.254	39	-0.601	39	-0.274	48	0.014
40	-0.077	40	-0.589	40	-0.228	49	0.008
41	-0.061	41	-0.529	41	-0.201	50	-0.063
42	-0.017	43	-0.36	43	-0.128	55	-0.08
43	-0.031	44	-0.244	44	-0.075	56	-0.067
44	-0.017	45	-0.204	45	-0.08	57	-0.045
45	-0.032	46	-0.12	46	-0.053	58	-0.051
46	-0.035	47	-0.12	47	-0.023	59	-0.05
47	-0.031	48	-0.164	48	-0.07	60	-0.037
48	-0.044	49	-0.284	49	-0.091	61	-0.035
49	-0.036	50	-0.3	50	-0.121	62	-0.022
50	-0.037	51	-0.396	51	-0.176	63	-0.014
51	-0.063	52	-0.412	52	-0.238	64	-0.018
52	-0.082	54	-0.23	54	-0.231	65	-0.026
54	-0.073	55	-0.135	55	-0.154	66	-0.021

55	-0.043	56	-0.113	56	-0.104	67	-0.06
56	-0.022	57	-0.084	57	-0.081	68	-0.05
58	-0.028	58	-0.102	58	-0.104	69	-0.1
59	-0.035	59	-0.117	59	-0.108	70	-0.064
60	-0.029	60	-0.092	60	-0.09		
61	-0.024	61	-0.09	61	-0.081		
62	-0.017	62	-0.064	62	-0.061		
63	-0.005	63	-0.039	63	-0.037		
64	-0.005	64	-0.049	64	-0.044		
65	-0.014	65	-0.062	65	-0.057		
66	-0.019	66	-0.082	66	-0.067		
67	-0.026	67	-0.135	67	-0.082		
68	-0.02	68	-0.187	68	-0.066		
69	-0.023	69	-0.244	69	-0.076		
70	-0.004	70	-0.342	70	-0.073		
72	0.015	71	-0.434	71	-0.017		
		72	-0.487				
		73	-0.732				

C)

1H and 15N chemical shifts from an HSQC spectrum of ubiquitin[TGWETWV] bound to wild type PDZ. The data was recorded at 298 K and a ^{1}H Larmor frequency of 700 MHz.

Residue	^{15}N	^{1}H
2	122.932	8.887
3	115.083	8.24
4	118.606	8.539
5	121.319	9.23
6	128.039	8.911
7	115.446	8.675
8	121.185	9.037
9	105.755	7.579
10	109.206	7.776
11	121.96	7.214
12	120.656	8.579
13	127.775	9.497
14	121.675	8.675
15	125.124	8.665

16	122.575	8.061
17	117.565	8.875
18	119.322	8.598
20	129.271	6.964
21	123.938	7.992
22	109.015	7.808
23	121.327	8.463
25	121.369	7.862
26	122.239	8.049
27	118.978	8.485
28	123.449	7.906
29	120.301	7.805
30	121.401	8.217
31	123.475	8.481
32	119.818	7.975
33	115.586	7.376
34	114.24	8.656
35	108.836	8.428
36	120.26	6.08
39	113.639	8.458
40	116.866	7.745
41	118.041	7.406
42	123.027	8.391
43	124.446	8.728
44	122.384	9.051
45	124.893	8.767
46	107.109	8.918
47	128.394	8.081
48	121.66	7.888
49	122.961	8.595
50	125.654	8.482
51	123.198	8.338
52	120.473	8.103
54	119.408	7.404
55	108.811	8.765
56	118.06	8.083
57	113.476	8.414
58	124.574	7.875
59	115.785	7.19

60	115.953	8.087
61	118.941	7.19
62	124.973	7.57
63	120.586	8.422
64	114.664	9.254
65	114.985	7.603
66	117.503	8.65
67	127.788	9.328
68	119.396	9.139
69	123.888	8.252
70	126.671	9.081
71	123.486	8.099
72	123.475	8.481
73	124.194	8.187
74	121.859	8.266
75	109.97	8.313
76	108.692	8.276
77	112.725	8.135
78	110.911	8.441
79	119.321	7.869
80	121.905	7.53
81	121.542	8.782
82	128.964	8.927
83	122.608	8.808

D)

Experimental ^{1}H-^{15}N RDC data recorded from MBP^{TGWETWV} bound to PDZ (figure 4.11).

Residue	PDZ-1	Residue	PDZ-2	Residue	PDZ-3
12	4.22	12	-1.74	12	-2.22
13	-1.22	31	-7.76	16	-1.74
14	-4.82	34	0.66	22	1.78
16	4.58	51	-6.44	23	1.26
19	-5.6	53	-8.16	24	2.34
23	-6.0	55	5.36	32	0.74
25	-0.76	56	-3.2	33	-3.5
29	-2.82	63	-3.82	37	0.82
32	-0.36	67	1.22	38	-0.68
33	5.7	69	-7.5	63	0.02
36	-2.84	70	1.46	70	0.06

37	-1.84	73	-3.62	73	-0.6
45	-0.34	77	-6.0	74	-2.22
49	2.92	90	-7.98	76	0.34
63	4.5	94	7.96	86	3.08
66	-3.44	98	-2.36	89	2.3
69	-1.48	99	-0.34	92	-1.18
94	5.6	102	3.46	94	-1.74
99	-5.56	103	-3.14	96	0.84
101	-1.48	111	-1.42	99	0
103	-0.9	112	-3.0	101	2.2
112	-2.6	113	-1.24	103	1.88
121	4.36	156	3.68	111	0.98
127	1.12	157	5.32	112	1.1
128	0.38	163	-3.32	127	-0.82
131	-4.38	165	0.88	128	2.6
135	0.5	166	-5.2	135	2.1
136	-2.86	169	3.82	136	1.62
137	3.08	170	7.14	137	0.62
140	-0.08	171	-1.28	138	2.76
146	-7.1	172	4.52	139	1.96
147	-5.48	176	3.78	140	1.34
149	-8.5	181	3.52	144	-1.76
151	3.46	182	1.66	146	0.6
152	-2.36	183	-2.66	149	0.62
156	3.96	184	-9.5	150	1.48
165	-1.24	187	-9.12	153	-0.78
166	-1.04	188	-8.66	156	-1.52
171	4.22	189	-8.94	164	-1.12
175	2.38	190	-8.78	165	0.14
176	3.86	191	-10.04	166	2.0
182	-5.34	247	-6.44	171	0.36
183	-0.82	249	0.58	172	-2.74
185	-5.46	251	-11.2	174	1.1
187	-1.38	252	-9.76	175	-1.36
188	-0.26	255	1.2	185	0.14
190	0.86	256	7.4	187	2.38
194	1.4	258	-6.64	188	3.06
200	4.06	260	-2.92	194	1.6
207	-1.84	262	5.52	200	1.12
209	0.12	301	6.44	201	1.92
212	-2.48	302	4.78	202	1.54
217	4.28	304	-4.46	204	-0.06
220	2.8	305	-7.86	207	2.28
222	1.0	327	3.98	208	-2.66
226	4.66	329	-1.74	209	1.88
228	7.32	330	1.68	211	-0.62
243	-9.4	332	-2.54	213	1.78
246	5.0	333	3.54	228	-3.2
251	0.6	341	-3.54	242	-0.78
252	0.14	349	-6.28	246	-2.18
255	-1.82	351	-1.46	249	-0.3
256	-6.76	356	2.28	252	2.02

258	0.74			255	1.78
260	1.86			258	0.92
288	-0.94			262	-0.64
289	2.94			289	0.92
292	-0.04			291	1.34
293	4.78			294	1.18
296	0.06			296	1.7
300	-3.8			301	0.48
301	-7.1			303	-2.1
302	4.36			304	0.08
305	2.12			305	3.32
306	1.34			307	1.32
307	2.22			308	1.7
310	2.96			309	3.32
312	2.36			310	0.4
316	-5.74			316	1.62
318	-2.52			317	1.78
320	-6.1			320	0.28
324	-6.24			326	1.08
326	2.34			333	-1.96
329	5.66			352	2.38
332	2.64			355	-0.76
333	4.1			356	0.44
351	-1.56			361	-1.4
356	-3.62				
358	-1.16				
365	-1.42				

Residue	PDZ-5	Residue	PDZ-6
16	1.58	12	4.74
25	-2.06	13	2.22
28	-0.92	14	-0.02
29	-0.9	16	2.92
31	-0.24	18	-3.12
32	-2.06	19	-7.66
33	3.42	20	-6.56
36	-1.94	22	-3.66
42	-0.36	24	-4.38
58	-2.8	25	-4.76
63	1.94	33	8.4
66	-1.8	34	1.82
68	-0.96	35	-0.02
69	-1.24	36	-3.28
70	-0.34	37	-2.36
73	-1.82	42	2.94
77	-0.64	56	2.9
79	-2.42	63	0.74
85	-1.08	66	-1.64
89	-0.66	68	-1.28
96	0.40	85	0.92

98	-1.64	86	-3.28
99	-1.86	88	5.3
101	-1.58	89	0.54
111	-1.88	93	2.36
112	-1.56	94	6.56
113	-1.7	99	-4.92
115	3.3	111	0.72
128	-1.48	112	-2.94
136	-2.44	113	-0.38
139	-0.62	127	2.18
140	-0.54	128	-0.54
141	3.3	131	-3.82
144	1.94	135	-2.18
146	-2.2	136	-1.98
148	-0.22	138	-0.38
165	-1.68	140	-0.54
166	-1.10	141	1.28
169	-2.0	147	-3.48
171	-0.8	149	-4.94
172	1.04	150	-5.66
174	-0.48	151	-0.36
181	-2.62	153	5.28
185	-2.26	155	4.2
187	-1.24	156	5.48
188	-2.3	164	0.2
190	-0.22	166	0.36
191	-0.62	169	-3.1
194	-0.22	171	4.56
200	1.0	172	6
204	-2.84	175	4.38
205	-2.78	178	-0.18
207	-0.98	181	-4.92
208	1.22	182	-2.36
212	-2.92	184	-2.36
213	-0.82	185	-5.48
217	0.04	187	-1.1
220	-1.38	188	-1.84
222	-1.78	189	0.72
226	3.7	190	-2.18
228	4.96	191	-1.46
247	-1.24	200	1.1
249	-0.06	201	-3.46
251	-0.94	202	2.02
252	0.8	203	-2.2
253	2.1	204	-3.28
256	0.82	207	-2.92
258	2.66	208	0.56
260	-0.64	209	-1.1
274	-0.58	210	4.36

288	1.44	211	6.74
289	1.74	213	1.66
292	0.82	217	4.2
294	1.8	222	-0.36
299	2.64	223	-4.92
300	-1.6	228	6.58
301	-0.2	243	-5.66
304	2.42	244	2.36
305	-1.28	246	6.2
307	-1.16	247	-3.1
309	-0.36	249	3.46
310	-1.04	252	-1.1
313	-0.4	258	-0.18
314	-2.16	260	2.2
317	-0.94	262	5.1
318	-1.46	287	-0.36
324	-3.3	288	-4.92
327	-3.74	289	-0.74
330	-1.76	296	-2.36
332	1.28	299	2.38
341	-1.88	300	-0.36
349	-1.64	302	7.64
351	-2.32	303	3.1
356	-1.78	305	-1.28
358	-0.96	307	1.64
365	-0.9	310	1.28
		312	-2.02
		314	-1.64
		316	-3.84
		320	-0.72
		324	-3.46
		326	-0.7
		329	4.74
		349	-2.92
		356	-0.18
		359	-3.64

E)

Experimental (^{N}H) PCS data recorded from MBP^{TGWETWV} bound to the PDZ reporters (figure 4.16).

Residue	PDZ-1	Residue	PDZ-2	Residue	PDZ-6
12	-0.089	12	-0.053	12	-0.125
13	-0.082	16	-0.036	13	-0.092
14	-0.071	26	-0.03	14	-0.079
16	-0.033	31	-0.056	16	-0.078

19	-0.002	32	-0.068	18	-0.044
20	-0.001	33	-0.066	19	-0.044
22	0.017	34	-0.051	20	-0.052
23	0.023	36	-0.017	21	-0.047
24	0.035	37	-0.015	22	-0.034
25	0.028	38	-0.039	23	-0.034
26	0.039	43	-0.06	24	-0.032
28	0.06	44	0	25	-0.025
29	0.043	51	-0.214	26	-0.019
31	0.054	52	-0.114	31	-0.007
32	0.058	53	-0.281	32	0.009
33	0.081	54	-0.229	33	0.012
36	0.088	55	-0.172	34	0.013
37	0.042	56	-0.101	35	-0.014
38	0.012	60	-0.04	36	-0.042
42	-0.196	62	-0.095	37	-0.056
44	-0.277	63	-0.111	42	-0.12
45	-0.427	66	-0.21	43	-0.16
63	-0.183	67	-0.214	56	-0.327
66	-0.271	68	-0.3	63	-0.202
68	-0.387	69	-0.388	66	-0.278
69	-0.503	70	-0.319	68	-0.379
70	-0.604	71	-0.304	69	-0.42
74	-0.308	73	-0.128	70	-0.551
80	-0.014	77	-0.053	79	-0.206
86	-0.03	79	-0.043	85	-0.019
87	-0.031	88	-0.032	86	-0.046
92	-0.077	90	-0.051	87	-0.042
93	-0.084	92	-0.054	88	-0.049
94	-0.101	93	-0.077	93	-0.103
96	-0.14	94	-0.084	94	-0.122
98	-0.225	95	-0.099	96	-0.064
99	-0.35	96	-0.108	98	-0.238
101	-0.341	98	-0.154	99	-0.344
102	-0.402	99	-0.154	103	-0.241
103	-0.257	101	-0.169	111	-0.107
111	-0.093	102	-0.126	112	-0.083
112	-0.071	103	-0.061	113	-0.091
122	-0.012	111	-0.079	127	-0.022
127	-0.025	112	-0.061	128	-0.025
128	-0.027	113	-0.072	130	-0.042
130	-0.034	120	-0.094	131	-0.023
131	-0.027	153	-0.039	134	-0.012
135	-0.013	156	-0.083	135	-0.012
136	-0.018	157	-0.099	136	-0.012

137	-0.012	163	-0.097	137	-0.005
140	-0.011	164	-0.085	138	-0.004
144	-0.009	165	-0.09	139	-0.009
145	-0.007	166	-0.12	140	-0.006
146	-0.013	168	-0.183	141	-0.003
147	-0.019	169	-0.33	143	0.001
149	-0.027	170	-0.336	144	-0.004
150	-0.041	171	-0.182	146	-0.011
151	-0.041	172	-0.215	147	-0.015
152	-0.056	174	-0.152	148	-0.019
153	-0.103	175	-0.261	149	-0.028
155	-0.145	176	-0.355	150	-0.046
156	-0.11	177	-0.404	151	-0.054
164	-0.062	180	-0.368	152	-0.085
165	-0.064	181	-0.592	153	-0.124
166	-0.071	182	-0.33	156	-0.117
168	-0.106	183	-0.41	164	-0.07
169	-0.112	184	-0.389	165	-0.076
171	-0.119	185	-0.227	166	-0.086
172	-0.147	187	-0.109	169	-0.156
174	-0.153	188	-0.149	170	-0.038
175	-0.178	189	-0.193	171	-0.156
176	-0.205	190	-0.122	172	-0.181
182	-0.076	191	-0.116	174	-0.164
183	-0.063	192	-0.084	175	-0.199
185	-0.056	194	-0.072	176	-0.227
187	-0.062	209	0.034	177	-0.198
188	-0.063	246	-0.033	178	-0.075
190	-0.056	247	-0.045	181	-0.17
191	-0.06	249	-0.037	182	-0.131
194	-0.057	251	-0.043	183	-0.116
200	-0.036	252	-0.038	184	-0.115
201	-0.022	253	-0.027	185	-0.098
202	-0.023	255	-0.052	187	-0.077
204	-0.019	256	-0.089	188	-0.086
205	-0.015	258	-0.109	189	-0.088
206	-0.023	260	-0.098	190	-0.075
207	-0.013	262	-0.082	191	-0.074
209	0.025	263	-0.108	200	-0.036
211	0.018	268	-0.07	201	-0.016
213	-0.01	299	-0.035	202	-0.013
217	-0.01	300	-0.036	203	-0.025
220	-0.008	301	-0.05	204	-0.016
226	-0.043	302	-0.044	205	-0.011
240	-0.056	303	-0.055	207	-0.011

241	-0.058	304	-0.038	208	-0.014
242	-0.013	305	-0.033	209	0.015
243	-0.017	324	-0.063	210	-0.002
246	-0.034	326	-0.066	211	0.041
247	-0.046	327	-0.078	212	0.037
249	-0.036	329	-0.131	213	0.005
251	-0.038	330	-0.165	217	-0.006
252	-0.036	332	-0.3	220	0.001
255	-0.049	333	-0.417	222	-0.005
256	-0.064	340	-0.508	223	-0.012
258	-0.099	341	-0.329	228	-0.065
260	-0.112	342	-0.445	240	-0.065
262	-0.103	344	-0.237	241	-0.056
288	0.027	347	-0.132	242	-0.016
289	0.028	349	-0.196	243	-0.019
292	0.008	350	-0.165	244	-0.028
294	-0.008	351	-0.089	246	-0.036
296	-0.008	355	-0.045	247	-0.047
300	-0.033	356	-0.076	249	-0.035
301	-0.049			252	-0.03
302	-0.039			256	-0.071
304	-0.035			258	-0.104
305	-0.025			260	-0.118
306	-0.014			262	-0.13
307	-0.008			288	-0.019
309	-0.015			289	-0.026
310	-0.009			292	-0.032
312	-0.019			296	-0.034
313	-0.016			299	-0.059
314	-0.018			300	-0.061
316	-0.02			301	-0.067
317	-0.028			302	-0.064
318	-0.026			303	-0.082
319	-0.033			304	-0.068
324	-0.059			305	-0.048
326	-0.067			306	-0.04
327	-0.07			307	-0.035
329	-0.115			309	-0.033
330	-0.143			310	-0.026
332	-0.237			312	-0.038
333	-0.251			313	-0.024
338	-0.115			314	-0.032
340	-0.244			316	-0.028
341	-0.147			317	-0.035
349	-0.135			318	-0.035

350	-0.099			319	-0.038
351	-0.09			320	-0.049
355	-0.096			324	-0.07
356	-0.085			326	-0.067
358	-0.06			327	-0.075
365	-0.03			329	-0.125
				330	-0.152
				332	-0.236
				333	-0.25
				349	-0.166
				350	-0.145
				351	-0.125
				352	-0.134
				353	-0.128
				355	-0.184
				356	-0.185
				358	-0.119
				359	-0.151

F)

^{1}H and ^{15}N chemical shifts from a TROSY spectrum of MBP^{TGWETWV} bound to wild type PDZ. The data was recorded at 310 K and a ^{1}H Larmor frequency of 700 MHz.

Residue	^{15}N	^{1}H	Residue	^{15}N	^{1}H
8	125.757	10.114	187	109.666	8.357
10	127.109	9.021	188	127.997	8.027
11	122.285	8.691	189	115.525	7.953
12	123.13	8.865	190	124.999	8.203
13	107.084	8.24	191	107.78	8.182
14	117.213	7.935	192	121.514	8.624
15	119.082	7.56	193	116.703	8.518
16	108.094	8.671	194	122.375	7.628
17	120.905	8.179	195	119.817	7.697
19	111.783	8.907	196	117.746	8.565
20	122.32	8.317	197	123.289	8.568
21	121.406	8.109	198	120.392	7.858
22	120.779	7.794	199	120.314	7.429
23	123.408	7.83	200	124.756	9.379
24	107.143	8.712	201	114.219	7.973
25	123.205	8.307	202	111.713	7.916
26	123.158	7.67	203	116.557	8.331

27	120.399	8.122	204	114.38	7.464
28	124.561	8.857	205	118.84	8.682
29	122.339	8.131	206	125.377	9.052
30	116.693	7.597	207	113.121	8.152
31	107.504	7.911	208	116.833	7.314
32	113.08	8.589	209	131.081	6.974
33	124.741	7.727	210	117.715	7.842
36	125.479	9.142	211	115.048	8.182
37	127.701	8.867	212	124.787	8.955
38	127.304	9.618	213	120.988	7.597
39	115.577	8.268	214	117.828	7.853
41	121.612	8.196	217	119.688	8.314
42	119.587	8.746	219	117.007	7.709
43	120.351	7.386	220	108.865	7.693
44	124.174	10.454	222	110.781	6.843
46	120.749	8.229	223	127.676	8.662
47	117.337	8.636	224	114.588	8.065
49	115.131	6.886	225	113.622	9.137
50	111.145	7.747	226	122.899	7.141
51	125.639	8.387	227	122.076	8.418
52	118.286	7.456	228	110.965	8.23
53	106.076	7.277	242	122.034	7.855
54	109.225	7.806	243	107.769	8.493
56	105.551	8.363	244	121.006	8.195
58	118.167	8.697	245	119.878	9.468
59	114.425	7.638	246	123.642	8.095
60	124.873	8.91	247	125.737	8.559
61	126.596	8.641	249	111.913	8.779
62	121.638	9.161	250	122.19	9.549
63	126.536	6.322	251	129.96	10.552
64	116.386	8.06	252	103.815	9.005
65	119.443	7.692	253	122.633	8.224
66	116.961	6.967	255	118.252	7.971
67	116.992	7.662	256	123.594	7.628
68	107.72	7.301	258	118.768	9.297
69	107.885	7.743	259	122.299	8.749
70	119.486	6.906	260	116.344	8.853
71	122.997	8.587	261	129.395	11.058
72	122.895	8.637	262	134.574	8.808
73	112.299	7.292	263	126.983	8.756
74	109.543	8.042	264	123.997	9.11
75	114.133	7.783	265	110.993	9.406
76	116.176	7.396	266	123.979	10.298
77	126.203	8.992	267	126.129	8.242
78	121.238	8.191	268	131.405	8.831

80	112.837	8.733	269	118.426	8.243
82	124.026	9.067	270	113.881	7.501
84	119.674	8.182	272	119.958	8.857
85	118.882	7.926	273	119.673	7.763
86	117.476	8.476	274	118.529	8.819
87	117.224	8.041	275	120.841	7.367
88	117.487	7.787	276	120.588	8.379
89	120.321	7.642	277	118.542	7.854
90	117.296	7.704	278	119.123	7.578
92	113.001	7.961	279	118.663	8.35
93	111.423	7.102	280	120.288	8.418
94	120.256	6.647	281	113.16	8.402
95	115.866	7.255	282	109.086	7.693
96	118.967	6.984	283	116.694	7.153
97	106.41	6.965	284	121.732	8.084
98	121.658	7.034	285	119.578	7.824
99	127.236	9.685	286	108.901	8.509
101	102.549	8.586	287	122.363	8.5
102	121.49	7.755	288	115.939	8.403
103	123.637	8.941	289	113.208	8.31
104	113.005	8.79	290	119.856	8.188
105	117.601	7.656	291	121.438	7.719
106	114.129	8.958	292	120.212	7.166
108	115.661	8.491	293	116.054	7.257
109	118.622	7.855	294	117.612	8.649
110	121.452	8.767	295	116.277	8.226
111	123.776	9.558	296	119.162	7.284
112	117.71	6.367	297	116.284	7.623
113	123.345	8.407	299	122.561	8.573
114	108.472	7.465	300	103.989	8.074
115	122.488	7.283	301	123.993	7.509
116	129.894	8.636	302	110.773	8.147
117	122.115	9.053	303	117.486	7.632
118	121.503	9.298	304	115.176	6.355
119	125.759	8.774	305	129.728	8.031
120	116.087	8.146	306	112.684	8.719
121	118.105	7.106	307	122.518	6.636
122	120.054	8.312	308	121.685	8.475
124	124.026	9.067	309	115.807	7.709
127	118.715	8.11	310	117.792	6.873
128	109.009	7.856	311	121.356	8.135
129	124.199	10.142	312	118.269	8.526
130	118.323	10.562	313	117.625	7.087
131	116.886	7.585	314	121.633	8.28
132	121.912	8.186	316	117.143	8.433

134	118.426	7.791	317	123.343	7.531
135	120.322	7.596	318	123.031	7.853
136	118.935	8.81	319	118.955	8.121
137	117.54	8.013	320	115.078	7.329
138	118.897	7.459	321	119.685	8.158
139	121.547	8.388	322	121.668	8.22
140	124.438	9.24	323	115.645	8.276
141	122.382	7.251	324	120.052	8.084
142	116.035	7.634	325	116.47	8.228
143	108.036	7.87	326	118.035	7.059
144	120.218	7.843	327	106.681	7.233
145	109.87	7.568	328	121.767	8.478
146	123.235	9.573	329	127.944	9.123
147	117.097	8.659	330	125.162	8.476
148	121.964	8.159	332	118.348	7.576
149	120.458	8.56	333	108.944	6.377
150	116.216	8.638	335	116.842	8.369
151	123.369	7.297	336	118.805	7.855
152	113.289	7.923	339	119.034	7.458
153	114.116	6.445	340	118.48	8.723
155	118.026	7.922	341	115.01	7.4
156	112.39	8.041	342	122.179	8.347
157	106.253	7.572	343	118.556	8.618
158	124.505	8.36	344	121.136	8.103
160	111.841	6.416	345	113.881	7.501
161	119.775	6.933	346	123.042	7.742
162	115.556	7.972	347	116.17	8.128
163	121.11	6.649	348	118.675	7.743
164	115.23	9.557	349	121.351	8.778
165	103.845	7.453	350	122.998	8.489
166	108.252	7.361	351	121.364	9.129
169	108.382	6.294	352	108.368	7.879
170	125.899	8.816	353	110.073	7.6
171	129.992	8.562	354	121.411	8.207
172	127.112	8.228	355	113.851	7.315
174	102.358	7.449	356	112.04	8.528
175	118.874	7.07	357	121.544	8.699
176	120.22	8.708	358	115.444	8.102
177	124.035	9.031	359	118.866	7.563
182	121.226	7.057	361	116.49	8.051
183	114.497	6.726	362	122.001	7.716
184	114.881	7.752	363	120.468	8.143
185	116.61	6.859	364	121.9	7.739

G)

^{1}H and ^{15}N chemical shifts from an HSQC spectrum of PDZ-1 tagged with CLaNP-5 loaded with Lu^{3+} (diamagnetic). The data was recorded at 310 K and a ^{1}H Larmor frequency of 600 MHz.

Residue	^{15}N	^{1}H	Residue	^{15}N	^{1}H
6	118.755	8.245	57	115.921	7.771
7	122.574	8.593	58	118.733	8.653
8	123.504	8.332	59	118.325	7.656
9	125.247	8.424	60	116.636	7.697
10	119.088	8.171	61	118.887	8.854
11	121.764	8.817	63	116.779	8.789
12	124.214	8.394	64	123.323	7.672
13	126.307	9.252	65	124.9	8.348
14	126.713	8.42	66	125.916	8.74
15	122.492	9.079	67	120.635	8.865
16	124.835	8.407	68	124.355	7.891
17	123.825	8.881	69	124.882	8.537
18	127.097	8.51	70	124.501	9.627
19	121.938	8.121	71	101.285	8.694
20	120.398	8.26	72	119.072	8.486
22	122.566	7.833	73	117.709	8.909
23	124.217	15.944	74	129.669	8.61
24	102.517	9.069	75	123.044	8.275
25	116.688	7.978	76	123.768	9.091
26	114.466	9.08	77	116.294	7.692
27	111.928	8.754	78	125.36	8.559
28	114.972	9.019	79	124.3	9.854
29	108.485	9.195	80	103.042	9.051
30	108.337	7.112	81	121.203	7.07
31	122.57	8.149	82	123.693	7.885
32	117.769	9.523	83	116.608	8.111
33	107.386	8.051	84	112.906	8.053
34	117.251	8.582	85	121.659	7.875
35	107.627	8.415	86	115.177	7.773
36	114.579	7.973	87	116.133	8.683
38	119.131	8.109	88	108.533	7.48
39	119.159	8.646	89	121.691	7.113
41	115.088	8.5	90	119.824	8.662
42	121.908	7.771	91	115.358	8.889

43	126.956	8.494	92	117.192	8.221
44	107.394	9.48	93	127.536	9.088
45	119.512	8.985	94	127.814	8.766
46	124.285	9.19	95	128.536	9.475
47	125.89	9.53	96	120.611	8.281
48	127.606	9.307	97	123.012	9.113
49	119.374	7.611	98	119.793	9.087
50	118.733	8.653	99	131.38	8.967
51	128.977	8.662	100	126.717	8.98
53	115.742	8.723	101	122.194	8.498
54	106.627	7.748	102	119.731	8.432
56	119.52	8.447	103	123.621	8.056

H)

Experimental (^{N}H) PCS data recorded directly from PDZ-1 tagged with diamagnetic (Lu^{3+}) or paramagnetic (Tm^{3+}) CLaNP-5 (figure 4.22) at 310 K.

Residue	PCS	Residue	PCS
8	0.641	49	1.246
9	0.753	50	0.902
10	0.94	51	0.873
11	1.308	53	0.419
13	2.328	54	0.489
14	1.859	56	0.917
15	2.987	57	0.785
24	0.973	59	1.067
25	1.352	60	1.362
26	1.388	61	1.639
27	1.753	63	1.505
28	2.095	64	1.771
29	1.326	98	3.014
30	1.865	99	1.759
41	0.703	100	1.318
42	0.939	101	0.945
44	1.869	102	0.716
48	1.704	103	0.574

I)

Experimental ^{1}H-^{15}N RDC data recorded directly from PDZ-1 tagged with diamagnetic (Lu^{3+}) or paramagnetic (Tm^{3+}) CLaNP-5 (figure 4.22) at 310 K. (figure 4.22).

Residue	RDC
9	-0.5
10	14.82
12	8.14
18	-16.02
30	-10.82
41	-18.24
42	-2.34
44	-31.2
47	1
53	8.96
54	-0.58
56	14.38
57	-0.56
58	-2.18
59	7.16
61	10.18
76	-17.96
98	17.98
102	15.9

J)

Experimental ^{1}H-^{15}N RDC data recorded from ubiquitin^{WETWV} bound to PDZ-1 (figure 4.24).

Residue	RDC	Residue	RDC
2	-0.79	42	0.7
3	8.28	43	4.32
4	8.31	44	4.73
6	6.32	45	3.6
7	5.33	46	4
8	7.36	48	-4.15
9	-1.55	49	2.43
11	-1.29	50	2.43
12	7.49	51	-3.44
14	8.5	54	-9.13

15	8.47	55	4.06
16	4.39	56	6.6
17	4.39	57	6.27
18	-1.89	58	7.06
20	-2.36	59	6.9
21	4.04	60	1.47
22	7.8	61	5.12
23	6.06	62	-1.69
25	1.72	64	7.37
26	6.57	65	-2.06
27	3.24	66	8.52
28	-1.35	67	7.66
29	4.89	68	5.41
30	6.37	69	3.75
32	-0.72	70	-1.72
33	6.25	71	0.87
39	9.79	72	-2.52
41	1.18	73	5.93

K)

^{1}H and ^{15}N chemical shifts from an HSQC spectrum of ubiquitin$^{\text{WETWV}}$ bound to wild type PDZ.

Residue	^{15}N	^{1}H	Residue	^{15}N	^{1}H
2	122.884	8.879	41	118.074	7.404
3	115.087	8.237	42	123.032	8.403
4	118.622	8.538	43	124.466	8.729
5	121.295	9.219	44	122.399	9.048
6	128.064	8.912	45	124.925	8.774
7	115.438	8.671	46	132.991	8.933
8	121.1	9.023	47	102.516	8.064
9	105.705	7.564	48	121.769	7.891
10	109.217	7.765	49	123.038	8.592
11	121.915	7.207	50	125.67	8.479
12	120.597	8.572	51	123.183	8.325
13	127.658	9.486	52	120.437	8.093
14	121.571	8.665	54	119.37	7.394
15	125.158	8.666	55	108.834	8.764
16	122.524	8.05	56	118.049	8.079

17	117.564	8.871	57	113.497	8.41
18	119.33	8.591	58	124.566	7.869
20	103.425	6.958	59	115.781	7.186
21	123.932	7.984	60	115.984	8.084
22	109.008	7.808	61	118.931	7.178
23	121.292	8.453	62	124.961	7.557
25	121.427	7.858	63	120.596	8.42
26	122.214	8.043	64	114.65	9.25
27	118.97	8.483	65	114.965	7.593
28	123.466	7.903	66	117.489	8.643
29	120.295	7.798	67	127.82	9.326
30	121.386	8.212	68	119.495	9.141
31	123.555	8.483	69	123.816	8.232
32	119.786	7.955	70	126.591	9.075
33	115.521	7.361	71	123.315	8.066
34	114.286	8.653	72	123.555	8.483
35	108.854	8.427	73	124.209	8.163
36	120.245	6.074	74	121.849	8.251
39	113.64	8.451	75	109.996	8.322
40	116.903	7.742	76	108.694	8.284

L)

Pulse sequence to obtain ^{15}N R_2 relaxation rates of ubiquitin, MBP and their complexes with PDZ. Dr. Saskia Villinger wrote this pulse sequence.

```
; 15N-T2 relaxation experiment with TROSY read-out
; for 15N, 15N13C, 2H15N and 2H15N13C labelled proteins
; written according to NL by savi 15/08/2012
; see footnotes

#include <Avance.incl>
#include <Grad.incl>
#include <Delay.incl>

define list<loopcounter> cpmglist=<$VCLIST>

define loopcounter vc_max

define loopcounter COUNTER1
define loopcounter COUNTER2
define loopcounter COUNTER3

#define LABEL_CN  ; switch on for 13C labelled samples
#define TEMP_COMPENSATION
```

```
"in0=inf2*0.5"

# ifdef LABEL_CN
"d0=97u-p4*2+p7*0.66-p1*0.5"
#else
"d0=100u+p7*0.66-p1*0.5"
#endif /*LABEL_CN*/

"d11=30m"
"d21=500u-p30*0.5"
"DELTA=2.65m"
"DELTA1=2.65m"
"DELTA2=2.65m-p22-p11-300u"
"DELTA3=2.65m-p23-p10-300u"
"DELTA4=260u-p24-p1*0.66"
"DELTA5=d21-p1*2.15-3u"
"DELTA6=d21-p1*2.15-13u"
"DELTA7=d21-10u"
"DELTA8=d21-13u-p4*2"

"d27=p24+35u"

"l1=1"
"l2=1"
"l3=td1"


"cnst21=176"
"cnst22=56"
"cnst18=-1"



"spoff4=bf2*((cnst22-cnst21)/1000000)"

aqseq 312



1    ze
     1m
     "vc_max=0"

; ----- Count maximum number of cpmg points from cpmglist ---------------------

9    20u
     if "cpmglist > vc_max"
       {
       20u
       "vc_max=cpmglist"
       }

     3m cpmglist.inc
     lo to 9 times l3

     3m cpmglist.res

; ----- start -----------------------------------------------------
```

```
2     d11 do:f2
      1m LOCKH_OFF
      3m
3      1m
      1m
4      3m
5      2m BLKGRAD
      10u pl1:f1
      10u pl4:f2
      10u pl7:f3


; ------ set counters for cpmg loop and temperature correction ----------------

      20u
      "COUNTER1=cpmglist-1"
      20u
      "COUNTER2=(vc_max-cpmglist+1)*4"
      20u
      "COUNTER3=cpmglist-2"
      20u

      (p7 ph0):f3     ; purge pulse for 15N magnetization before d1
      5u



;---------temperature compensation and d1 recovery delay---------
# ifdef TEMP_COMPENSATION

 "d17=d1-40u-((d21*2+p30)*COUNTER2)"

      10u fq=cnst18(bf ppm):f3
      10u pl30:f3

      if "COUNTER2>=1"
      {
10     d21
      (p30 ph16):f3
      d21
      lo to 10 times COUNTER2
      }
              ; 15N pulses are applied far off-resonance
      10u
      10u fq=0:f3
      d17
# else
      d1
# endif
      1m UNBLKGRAD
      10u pl7:f3

;------- kill steady state 15N ------------
      (p7 ph0):f3
      5u
      p20:gp6
      200u


;------- first INEPT Hz-> 2HxNz -----------
      (p1 ph0):f1
      5u
      DELTA gron0 ; soft gradient to prevent radiation damping
```

```
      5u  groff
      (center(p1*2 ph0):f1 (p7*2 ph0):f3)
      5u
      DELTA gron0
      5u groff


;------- rephase  2HxNz to Nz------ --------
      (p1 ph5):f1  (p7 ph0):f3
      5u
      DELTA1 gron1 ; soft gradient to prevent radiation damping
      5u groff
      (center (p1*2 ph0):f1 (p7*2 ph0):f3)
      5u
      DELTA1 gron1
      5u groff
      (p7 ph6):f3 ; phase-cycle Nz, -Nz for Freeman-Hill decay
      5u
;-----------------------------------------
      (p1 ph2):f1 ; purge pulse to kill any residual HzNz
      5u
      p21:gp7  ; cleaning gradient
      100u
      100u


;------15N T1 relaxation period--------------
;------ excitation pulse --------------------------------------------------

      (p7 ph18):f3                                  ; rotate -Nz to Ny


;---- N-1 loop --------------
      if "COUNTER1==0" goto 20
      if "COUNTER1>=1"
      {
14    5u
      DELTA7 pl30:f3
      5u
      (p30 ph16):f3
      d21
      lo to 14 times COUNTER1
      }

;---- 1 times with 1H decoupling composite pulse ----------------------------
      d21
      (p30 ph16):f3
      DELTA5
      (p1 ph0 3u p1*2.3 ph1 3u p1 ph0):f1
      5u
      DELTA6 gron9
      5u groff
      (p30 ph16):f3
      5u
      DELTA7 gron9
      5u groff


;---- N-2 loop -------------------------------------------------------
      if "COUNTER3>=1"
      {
15    5u
      DELTA7 gron9
      5u groff
```

```
(p30 ph16):f3
5u
DELTA7 gron9
5u groff
lo to 15 times COUNTER3
}
```

;----1x with 13C decoupling in the middle ---------------------------------------

```
5u
DELTA7 gron9
5u groff
(p30 ph16):f3
5u
DELTA8 gron9
5u groff
(p4*2 ph0 3u 3u pl2 p4*2:sp4 ph0):f2
5u
DELTA8 gron9*-1
5u groff
(p30 ph16):f3
5u
DELTA7 gron9*-1
5u groff
```

;----N-2 loop --

```
      if "COUNTER3>=1"
      {
16    5u
      DELTA7 gron9*-1
      5u groff
      (p30 ph16):f3
      5u
      DELTA7 gron9*-1
      5u groff
      lo to 16 times COUNTER3
      }
```

;---- 1x with 1H decoupling composite pulse -------------------------------------

```
5u
DELTA7 gron9*-1
5u groff
(p30 ph16):f3
5u
DELTA6 gron9*-1
5u groff
(p1 ph0 3u p1*2.3 ph1 3u p1 ph0):f1
DELTA5
(p30 ph16):f3
d21
```

;---- N-1 loop --

```
      if "COUNTER1>=1"
      {
17    5u
      DELTA7 pl30:f3
      5u
      (p30 ph16):f3
      5u
      DELTA7 pl7:f3
      5u
```

```
      lo to 17 times COUNTER1
      }
      goto 21


;--- if counter1 is 0 --------------------------------------------------
20    5u
      DELTA7 pl30:f3
      5u
      (p30 ph16):f3
      DELTA5
      (p1 ph0 3u p1*2.3 ph1 3u p1 ph0):f1

;----1x with 13C decoupling in the middle --------------------------------------
      5u
      DELTA6 gron9
      5u groff
      (p30 ph16):f3
      5u
      DELTA8 gron9
      5u groff
      (p4*2 ph0 3u 3u pl2 p4*2:sp4 ph0):f2
      5u
      DELTA8 gron9*-1
      5u groff
      (p30 ph16):f3
      5u
      DELTA6 gron9*-1
      5u groff
      (p1 ph0 3u p1*2.3 ph1 3u p1 ph0):f1
      DELTA5
      (p30 ph16):f3
      5u
      DELTA7 pl7:f3
      5u
;---------------------------------------------------------------------------------


;----- flip back to Nz/-Nz-----------------------------------------------------
21
      (p7 ph8):f3                              ; rotate back to -Nz

      5u
      p21:gp8  ; cleaning gradient
      100u
      100u

;------Echo/ Anti-echo encoding for TROSY read-out-----------
77    3u
      3u pl4:f2
      3u pl1:f1
      if "l1==1"
      {
      (p7 ph7):f3
      10u
      p25:gp5
      200u
      (p7*2 ph7):f3
      10u
      p25:gp5*-1
      }
```

```
        else
        {
        (p7 ph17):f3
            10u
        p25:gp5*-1
        200u
        (p7*2 ph17):f3
        10u
        p25:gp5
        }
;------ t1 (15N) evolution period ----------------------------
        d0
# ifdef LABEL_CN
        (p4*2 ph0 3u 3u pl2 p4*2:sp4 ph0):f2
# endif
        d0
;------ start TROSY read-out---------------------------------
        if "l1==1"
        {
        (p1 ph1):f1    ; Echo
        3u
        3u pl0:f1
        (p11:sp11 ph11:r):f1
        6u
        }
        else
        {
        (p1 ph3):f1    ; Anti-Echo
        3u
        3u pl0:f1
        (p11:sp11 ph13:r):f1
        6u
        }
        5u pl1:f1
;goto 999 ; optimization of  water supression
        DELTA2
        p22:gp2
        300u
        (center (p1*2 ph0):f1 (p7*2 ph0):f3)
        7u
        p22:gp2
        DELTA2
        300u pl0:f1
;---------------------------------------------
        (p11:sp12 ph12:r):f1
        5u
        3u pl1:f1
        if "l1==1"
        {
        (p1 ph0):f1 (p7 ph1):f3  ; Echo
        }
        else
        {
        (p1 ph0):f1 (p7 ph3):f3     ; Anti-Echo
        }
        ;goto 999 ; for optimization of  water supression
        DELTA3
        p23:gp3
        200u
        100u pl10:f1
```

```
    (center(p10 ph10:r 5u pl1 p1*2 ph0 5u pl10 p10 ph10:r):f1 (p7*2 ph0 d27):f3)
    5u
;goto 999 ; for optimization of  water supression
    p23:gp3
    DELTA3
    DELTA4
    (p7 ph0):f3
    5u
    p24:gp4 ; Echo/Anti-echo decoding gradient
999    5u
    5u pl31:f2
    20u BLKGRAMP
    go=2 ph31 cpds2:f2
    1m do:f2
    1m LOCKH_OFF

    d11 do:f2 mc #0 to 2
    F1QF(cpmglist.inc & iu2)
    F2EA(cpmglist.res & iu1 & ru2, id0 & ru1)

1m
1m BLKGRAD
exit

ph0=0
ph1=1
ph2=2
ph3=3
ph5=1
ph6=1 1 1 1  3 3 3 3
ph8=0
ph10=2
ph11=3
ph12=0
ph13=1
ph16=3
ph7=1 0 3 2
ph17=1 2 3 0
ph18=2
ph31=1 2 3 0  3 0 1 2


;-------------NOTES---------------------

;o1p = 4.7 ppm
;o2p=176 ppm (CO)
;o3p=119 ppm

;NS=8*n
;in0=inf/2
;SW=1/(2*in0)
;echo-antiecho in N15 (process as Complex in NmrDraw before splitting the spectra)


; 1H pulses

;p1:  90 deg hard 1H pulse @pl1
;pl1: 1H 90 deg
;pl0: 120 dB
;p10: 1200u (@ 600 MHz) 90 deg soft rectangular water flip-back pulse
```

;p11: 1900u (@ 600 MHz) 90 deg Sinc1.1000 water flip-back pulse (sp11,sp12)
;p15: 2000u (@ 600 MHz) 180 deg IBurp2 pulse on 1H (sp15)
;sp5: 180 deg IBurp2 pulse on 1H (sp15)
;sp11: 90 deg Sinc1.1000 water flip-back pulse
;sp12: 90 deg Sinc1.1000 water flip-back pulse
;spnam5: IBurp2
;spnam11: Sinc1.1000
;spnam12: Sinc1.1000
;spoffs5: 2340Hz @ 600 MHz (8.6 ppm) , should be centered in amide region but not touch the water

; 13C pulses

;p4: 13CO selective 180 deg (23.7*2us @ 600 MHz) @pl4
;pl2: 120 dB
;pl4: 13C 90 deg

;sp4: 13CA selective 180 deg (23.7*2us @ 600 MHz)
;CPDPRG2: garp (aq C' decoupling)
;pcpd5: C' decoupling (140u or 280u @pl31)
;pl31: C' decoupling power

;15N pulses
;p7 : 90 deg hard 15N pulse @pl7
;p18 : maximum duration of spin-lock; temperature compensation
;pl7 :15N 90 deg
;pl8: 15N spin-lock power
;p30: 90 us 180 deg pulse for cpmg block

; gradients
;p20: 1000u
;p21: 200u
;p22: 300u
;p23: 1000u
;p24: 60.8u Echo/Anti-echo decoding gradient
;p25: 300u Echo/Anti-echo half-encoding gradient

;for z-only gradients
;gpz0: 3%
;gpz1: 2%
;gpz2: 10%
;gpz3: 50%
;gpz4: 33%
;gpz5: -33%
;gpz6: 30%
;gpz7: -50%
;gpz8: 40%

;gpnam2 SINE.10
;gpnam3 SINE.50
;gpnam4 SINE.10
;gpnam5 SINE.10
;gpnam6 SINE.50
;gpnam7 SINE.10
;gpnam8 SINE.10

Curriculum vitae

Personal data

Name: Aldo Román Camacho Zarco
Place of birth: Xochimilco, Mexico City
Date of birth: 17th of November 1981
Nationality: Mexican

Educational qualifications

2010 - 2014 Doctoral student, MPI for Biophysical Chemistry, Göttingen
Graduate School, Georg-August-Universität, Göttingen

2007 - 2009 MSc Biochemistry, Institute of Biotechnology, México

2000 - 2005 BSc Chemical pharmacology, National Autonomous University of Mexico

Professional experience

2009 - 2010 Research assistant, National Laboratory of Genomics for Biodiversity, México

2005 - 2006 Analytical chemist, Schering-Plough Corporation, México

Publications

Camacho-Zarco AR, Munari F, Wegstroth M, Liu MW, Ubbink M, Becker S, Zweckstetter M. Multiple paramagnetic effects through a tagged reporter protein. Angew Chem Int Ed Engl (2014) Oct 7. doi: 10.1002/anie.201408615.

Luz-Madrigal, Asanov A, **Camacho-Zarco AR**, Sampieri A, Vaca L. A cholesterol recognition aminoacid consensus domain in GP64 fusion protein facilitates anchoring of baculovirus to mammalian cells. J Virol 87 (2013) 11894-11907. doi: 10.1128/JVI.01356-13.

Noda-García L, **Camacho-Zarco AR**, Medina-Ruíz S, Gaytán P, Carrillo-Tripp M, Fülöp V, Barona-Gómez F. Evolution of substrate specificity in a recipient's enzyme following horizontal gene transfer. Mol Biol Evol 30 (2013) 2024-2034. doi: 10.1093/molbev/mst115.

Noda-García L, **Camacho-Zarco AR**, Verdel-Aranda K, Wright H, Soberón X, Fülöp V, Barona-Gómez F. Identification and analysis of residues contained on $\beta \to \alpha$ loops of the dual-substrate $(\beta\alpha)_8$ phosphoribosyl isomerase A specific for its phosphoribosyl anthranilate isomerase activity. Protein Sci 19 (2010) 535-543. doi: 10.1002/pro.331.